

# Issues in Active Flow Control: Theory, Control, Simulation, and Experiment\*

**S. Scott Collis<sup>†</sup>**

Sandia National Laboratories<sup>‡</sup> P.O. Box 5800, Albuquerque, NM 87185-0370 USA

**Ronald D. Joslin<sup>§</sup>**

Office of Naval Research, 800 N. Quincy Street, Arlington, VA 22217, USA

**Avi Seifert<sup>¶</sup>**

Faculty of Engineering, Tel-Aviv University, Ramat-Aviv 69978, Israel

**Vassilis Theofilis<sup>||</sup>**

Escuela Tecnica Superior, Universidad Politécnica de Madrid,

Plaza Cardenal Cisneros, 3, E-28040 Madrid, Spain.

May 26, 2004

## Abstract

The goal of this paper is to provide a perspective on the current status and future directions for active flow-control technology with particular emphasis on oscillatory control. This is not a comprehensive review of the literature; rather, certain issues that are often neglected in studies are highlighted showing their importance or impact on the reported observations and targeted outcomes. Feasible routes using flow instability as an efficiency enhancement tool are discussed as an emerging means to explain the physical phenomena of active flow-control and as a tool for control law design and development. Traditional and more recent theoretical approaches to control design are discussed and recommendations are made relevant to numerical complications on the route to design oscillatory flow-control systems. A generic flow control process is put forward and illustrated using experimental examples.

---

\*Distribution Statement A: Approved for public release; distribution is unlimited.

<sup>†</sup>Senior Member of Technical Staff, Optimization and Uncertainty Estimation

<sup>‡</sup>Sandia is a multiprogram laboratory operated by Sandia Corporation, a Lockheed Martin Company, for the United States Department of Energy under contract DE-AC04-94AL85000

<sup>§</sup>Program Officer, Undersea Weapons & Countermeasures

<sup>¶</sup>Senior Lecturer, Department of Fluid Mechanics and Heat Transfer, school of Mechanical Engineering, also visiting scientist, National Institute of Aeronautics, Hampton, VA, USA, Tel. +972 (3) 6405310; fax: +972 (3) 6407334; Email: seifert@eng.tau.ac.il

<sup>||</sup>Ramón y Cajal Research Fellow; also visiting Professor, College of Aeronautics, Cranfield University, UK.

# Contents

<b>1</b>	<b>Introduction</b>	<b>7</b>
<b>2</b>	<b>Utilizing Flow Instabilities for Active Flow Control</b>	<b>9</b>
2.1	Mean turbulent vs. basic laminar flow . . . . .	9
2.2	Local, convective, absolute and BiGlobal instabilities . . . . .	9
2.3	Transient/algebraic growth . . . . .	10
2.4	On control of turbulent flows . . . . .	10
2.5	Eigenmode vs. energy-growth control . . . . .	10
2.6	On the reconstruction of a turbulent flowfield . . . . .	12
2.7	An example: Separated flow . . . . .	13
2.8	Turbulent flow in the wake of a circular cylinder and an airfoil . . . . .	14
2.9	On the relevance of global-flow instability to turbulent flow-control . . . . .	15
<b>3</b>	<b>Control Theory for Active Flow Control</b>	<b>17</b>
3.1	Open-loop control . . . . .	18
3.2	Closed-loop control . . . . .	18
3.2.1	Linear control theory . . . . .	20
3.2.2	Physics based strategies . . . . .	21
3.2.3	Classical control theory . . . . .	22
3.2.4	Modern control theory . . . . .	23
3.2.5	Issues in closed-loop control . . . . .	25
3.3	Optimal control . . . . .	26
3.3.1	Optimal open-loop control . . . . .	26
3.3.2	Issues in optimal control . . . . .	28
3.4	Reduced order modeling . . . . .	29
3.4.1	Physical . . . . .	29
3.4.2	Mathematical . . . . .	31
3.4.3	Data Fitting . . . . .	34
3.4.4	Issues in Reduced Order Modeling . . . . .	34
<b>4</b>	<b>Issues in Computational Fluid Dynamics</b>	<b>35</b>
4.1	Background and current focus . . . . .	35
4.2	Methodology — uncertainty versus reality . . . . .	35
4.3	Governing Equations . . . . .	36
4.3.1	RANS approach . . . . .	37
4.3.2	LES approach . . . . .	38
4.3.3	DNS approach . . . . .	38
4.4	Initial Conditions . . . . .	39
4.4.1	RANS/LES initial conditions . . . . .	39
4.4.2	DNS/LES initial conditions . . . . .	39
4.5	Wall-boundary conditions . . . . .	40
4.6	Free stream conditions . . . . .	40
4.7	Outflow conditions . . . . .	40

4.7.1	RANS outflow conditions . . . . .	40
4.7.2	DNS outflow conditions . . . . .	40
4.8	Actuator modeling . . . . .	41
4.9	Configuration Issues . . . . .	42
4.9.1	Model 1 . . . . .	43
4.9.2	Model 2 . . . . .	44
<b>5</b>	<b>General Concepts with Experimental Notes</b>	<b>47</b>
5.1	A generic process for AFC . . . . .	48
5.2	Generic AFC roadmaps . . . . .	53
5.2.1	Outline for AFC roadmaps . . . . .	53
5.2.2	Separation delay roadmap . . . . .	55
<b>6</b>	<b>Summary</b>	<b>57</b>
	<b>Acknowledgments</b>	<b>58</b>
	<b>References</b>	<b>58</b>

# Nomenclature

## Acronyms

2D	two dimensional
3D	three dimensional
AFC	active flow control
BL	boundary layer
CFD	computational fluid dynamics
dB	decibel
DES	detached eddy simulation
DNS	direct numerical simulation
EFD	experimental fluid dynamics
EVP	Eigenvalue problem
KH	Kelvin–Helmholtz (instability)
IMC	internal model control
LQG	linear-quadratic Gaussian
LPF	low pass filtered
LTR	loop transfer recovery
LST	linear stability theory
LES	large eddy simulation
MAV	micro air vehicle
MEMS	micro-electrical mechanical system
NACA	National Advisory Committee on Aeronautics
OSE	Orr–Sommerfeld equation
PC	personal computer
PI	proportional-integral (control)
PID	proportional-integral-derivative (control)
POD	proper orthogonal decomposition
PSE	parabolized stability equations
QA	quality assurance
R&D	research and development
RANS	Reynolds Averaged Navier-Stokes
RHS	right hand side
RMS	root mean square
ROM	reduced order model
SGS	sub-grid scale
TAU	Tel-Aviv University
TBL	turbulent boundary layer
TKE	turbulent kinetic energy
TRL	technology readiness level
TS	Tollmien-Schlichting (instability)
UAV	unmanned air vehicle

## Notation

$A$	Amplitude
$A, B, C, D$	state-space matrices
$c$	chord length
$c_\mu$	steady momentum coefficient
$C_d$	sectional drag coefficient
$C_l$	sectional lift coefficient
$C_p$	mean pressure coefficient
$C'_p$	root-mean-squared pressure coefficient
$C_\mu$	oscillatory momentum coefficient: $C_\mu \equiv j'/J$
$D$	diameter
$d$	drag
$\Delta t$	time step
$\mathbf{e}$	error vector
$f_e$	frequency of oscillator
$f(x)$	spatial distribution for suction/blowing
$F.M.$	figure of merit (see Eq. (10))
$F^+$	reduced frequency: $F^+ \equiv f_e X / U_\infty$
$H$	slot width or excitation momentum thickness
$\mathcal{H}$	Hardy space
$k_c$	feedback gain
$\mathbf{K}$	feedback kernel
$\hat{i}, \hat{j}, \hat{k}$	unit vectors in $x$ , $y$ , and $z$ directions
$j'$	oscillatory momentum due to excitation, $\rho(u')^2 H$
$J$	reference momentum condition, $1/2(\rho U_\infty^2)$
$k-\omega$	turbulence model
$l$	smallest length scale
$L$	largest length scale
$L_z$	spanwise periodic length scale
$\mathbf{L}$	state estimation feedback matrix
$M$	Mach number
$P$	power provided to actuators
$\mathbf{r}$	calibration control
$R$	Reynolds number
$R_\tau$	Turbulence Reynolds number, $R_\tau \equiv u_\tau \delta / \nu$
$t$	smallest time scale or time
$T$	largest time scale or optimization interval
$T_i$	integral time
$T_d$	rate time
$u$	smallest velocity scale or streamwise perturbation velocity
$u_\tau$	friction velocity, $u_\tau \equiv \sqrt{\tau_w / \rho}$
$\mathbf{u}$	control vector
$U$	largest velocity scale
$U_\infty$	free-stream velocity

$\mathbf{v}$	velocity vector
$v$	normal velocity
$w$	spanwise velocity
$\mathbf{w}$	disturbance vector
$\mathbf{x}$	state vector
$x, X$	streamwise coordinate
$y$	normal coordinate
$\mathbf{y}$	measurement vector
$z$	spanwise coordinate
$\alpha$	angle of attack
$\phi$	angle of injection
$\omega$	frequency (non-dimensional)
$\nu$	kinematic viscosity
$\rho$	density
$\tau_w$	average wall shear-stress

### Subscripts

$d$	drag
$c$	chord
$l$	lift
$s$	sensing plane
$w$	wall
$z$	spanwise
$\tau$	shear stress
$\infty$	infinity

### Superscripts

+	wall variables (inner scaling)
---	--------------------------------

# 1 Introduction

Active flow-control (AFC) is a fast growing multidisciplinary science and technology thrust aimed at altering a natural flow state or development path into a more desired state (or path). Flow control research dates back to the discovery of the boundary layer by Prandtl [1] at the turn of the 20th century. In the period leading up to and during World War II, as well as in the cold war era, flow control was extensively studied and applied, although primarily to military-related flow systems. A comprehensive review and analysis was provided by Lachman [2] and more recently by Gad-el-Hak et al. [3], Gad-el-Hak [4]. All known flow control efforts preceding the pioneering work of Schubauer and Skramstad [5] used steady-state tools and mechanisms for flow management. These are of inherently marginal power efficiency, and therefore limited the implementation of the resulting systems in operational applications. Unsteady flow control using periodic excitation that exploits natural flow instability phenomena (such as control of flow separation [6]) has the potential of overcoming the efficiency barrier (see Section 5). As an example, Seifert et al. [7] showed that separation control using periodic addition of momentum, at a reduced frequency slightly higher than the natural vortex shedding frequency, can save 90-99% of the momentum required to obtain similar gains in performance using steady blowing. The later utilizes the well-known Coanda [8] effect.

The feasibility of increasing the efficiency and simplifying fluid related systems (e.g. high-lift systems) is very appealing if one considers that a one percent saving in world consumption of jet fuel is worth about 1.25 million dollars a day of direct operating costs (in 2002). Likewise, such fuel savings would lead to reduced environmental impact, although such environmental effects are difficult to quantify. The progress in system integration, miniaturization, actuators, sensors and computational techniques enables the utilization of fast-responding, unsteady, flow-control methods into a closed-loop system. However promising the technology might look, significant barriers exist between the capabilities available to the technologist and the successful application. Comprehensive experiments are required to close the gaps between theory, computations, and real-world applications. These experiments are time consuming and expensive and in many occasions do not produce expected nor repeatable results. Furthermore, progress is achieved frequently by innovation, experience and sheer luck (this is why AFC is sometimes referred to as “The ART of Flow Control”). The theory of AFC is of limited scope due to the inherently non-linear nature of the leading physical processes. Still, significant insight can be gained by considering linear stability analysis of simplified problems, as a first order approximation helping identify unstable mechanisms that can enhance performance, isolate optimal leading parameter ranges and increase efficiency. Significant progress has been made in control theory for optimal and automated design of closed-loop controllers that can be applied to AFC systems given a sufficiently accurate and efficient model of the system. Likewise, progress made in computer capabilities (processing speed, memory, storage, and parallel processing) has been accompanied by similar efforts to resolve modeling issues (of turbulence and algorithms) and arrive at efficient and validated numerical tools for unsteady flow computations at relevant Reynolds numbers. However, these efforts are still remote from what the real-world engineering requires, e.g. a trustworthy — at least in terms of providing the right trend — solution of unsteady flow control problems on realistic configurations within thirty minutes and setting up a whole new problem within eight hours of work on a state-of-the-art PC or workstation.

Identifying the above limitations, this manuscript does not attempt to review the state-of-the-art

of flow control. Rather, an attempt is made to identify several key issues and discuss those in a comprehensive manner. These will include discussions of “what did not work” and try to explain why and what could be done in order to resolve these open issues.

The manuscript also includes a generic flow control process chart with examples that will help technologists from industry, academia, and government agencies identify resolved as well as unresolved issues and make logical, knowledge-based, decisions as to the required actions to perform desired tasks. A further objective of the paper is an attempt to establish a generic AFC roadmap (a-la Morkovin [9]) and construct several examples that can assist decision makers and workers in this exciting field understand where we are at present and how to proceed most efficiently.

This manuscript is organized as follows. Section 2 presents a discussion of theoretical issues, with emphasis on the role that global flow instabilities can play in AFC; while Section 3 reviews concepts and issues related to open- and closed-loop control strategies. Section 4 presents numerical aspects of AFC, focusing attention on configuration issues. Section 5 discusses a generic process for constructing AFC systems along with a detailed discussion of experimental issues. Section 5 also advocates the use of roadmaps to guide AFC research along with an example roadmap for AFC applied to boundary layer separation control. The paper closes with a brief summary in Section 6.

## 2 Utilizing Flow Instabilities for Active Flow Control

### 2.1 Mean turbulent vs. basic laminar flow

A single theoretical approach to flow control does not exist, even in the beginning of the 21st century. Instead, several methodologies have been put forward recently, which pursue flow control through control of flow instability. A fundamental question arising in this context concerns the difference between the states that are to be analyzed. From a theoretical or numerical point of view the so-called basic (or base) state must be analytically or numerically provided; examples are Poiseuille flow in channels, the Blasius profile for the flat-plate boundary layer and the two-dimensional steady or time-periodic wake behind a circular cylinder at low Reynolds numbers. Experiments, on the other hand, provide easy access to a statistically averaged mean flow or to an ensemble averaged phase-locked baseline for a time periodic flow. This is different from the corresponding laminar basic state and the different instability properties potentially yielded by the two states at a given point in parameter space have not been reconciled presently. Interestingly, two-dimensional time-periodic basic states may be related with the respective steady laminar basic flow and the most unstable two-dimensional BiGlobal eigenmode [10]. However, considerably more progress has been made on instability analysis of basic states, which is briefly reviewed first.

### 2.2 Local, convective, absolute and BiGlobal instabilities

Strictly, a decomposition of a given solution of the equations of motion into an  $O(1)$  basic and an  $O(\varepsilon) \ll 1$  disturbance state must conform with the equations of motion. The basic state itself is a steady or time-periodic laminar solution of the governing equations, while (on account of neglecting nonlinearity) the disturbance terms are exponentially or algebraically growing/damped solutions of the linear disturbance equations. Since the basic state forms the variable coefficients of the latter equations, its accurate provision is a prerequisite for reliable predictions of stability characteristics.

At this point, the dimensionality of the basic state upon which an instability analysis is performed provides a natural framework to distinguish between convective, absolute and global instabilities. A full discussion of this point may be found in the review of Huerre and Monkewitz [11]. Briefly, flow is convectively unstable when an arbitrary disturbance introduced into the flow is transported by the flow downstream from its point of introduction, albeit amplifying or decaying in the process. A flow is called absolutely unstable when the disturbance remains at or propagates upstream of (as well as downstream from) its point of introduction. Both concepts of convective and absolute instability apply to strictly parallel flows. The term global instability, on the other hand, was originally introduced (and is still in use) to describe absolutely unstable flows whose basic state is weakly nonparallel (e.g. Chomaz et al. [12]). Others have used the term to describe two-dimensional instability of essentially nonparallel two-dimensional basic states (e.g. the 2D basic state in the wake of a circular cylinder [13, 14]) or three-dimensional instability also of essentially nonparallel two-dimensional basic states (e.g. circular cylinder [15], steady 2D lid-driven cavity flow [16]).

Recently [17], the terms BiGlobal and TriGlobal have been introduced to identify instabilities of two- and three-dimensional basic states, respectively, in contrast to those pertinent to weakly nonparallel flows. Interestingly, in two-dimensional basic flows where the assumptions of classic

instability analysis of one-dimensional basic states approximately hold, as the case is in separated boundary layer flow, both classic Kelvin-Helmholtz (KH)/Tollmien-Schlichting (TS)-type and BiGlobal instability are concurrently operative [18, 19]. No *a priori* criteria are presently known to determine which of the physical mechanisms will dominate at a given point in parameter space.

### 2.3 Transient/algebraic growth

In recent years the significance of the non-normality of the linearized Navier-Stokes operator with respect to algebraic/transient growth has been recognized.[20, 21] In this context, linearly damped modes may be introduced into a flow at a given amplitude, such that their combination results in the flow experiencing transient/algebraic growth. Under this scenario, the combined disturbance amplitude can be orders-of-magnitude higher than that of the individual modes at their introduction, before the modes eventually decay as predicted by linear stability theory. If the initial and/or the transiently reached amplitudes are large enough, nonlinearity may take over and lead to turbulence, bypassing the previously discussed linear mechanisms. Transient growth has explained shortcomings of linear stability theory in classic one-dimensional basic flows [22], that illustrates the difficulties in relying upon linear stability analysis in any but the simplest problems.

### 2.4 On control of turbulent flows

Irrespective of the nature of the predominant instability-mechanism, the well-defined instability concepts introduced above can strictly only be applied to low-Reynolds number laminar flows; the ensuing linear, transient or nonlinear instability will result in transition to turbulence. As mentioned, the most readily available quantity, experimentally or numerically, is the mean flow, obtained through statistical averaging of a large number of realizations of the instantaneous turbulent field. Straightforward application of the mean/small-disturbance decomposition concept highlighted earlier is not possible since the interaction (stress) terms are no longer small in magnitude compared to the mean flow itself. Nevertheless, several attempts have been made in this direction, a notable example being the concept of triple decomposition [23], by which a turbulent state is decomposed into a mean time-averaged field, a coherent space-averaged part and small-amplitude stresses. This concept has been utilized for the analysis of inviscidly unstable free-shear layer flows [24].

A different approach has been taken for vortical flows in the wake of commercial aircraft where turbulence has been neglected altogether and an appropriate inviscid instability analysis has been used resulting in the identification of global instabilities in co-rotating [25] and counter-rotating [26] trailing vortex configurations. The most unstable transient instability mechanism was then used to devise an effective flow control strategy leading to the destruction of the wake coherence [27].

### 2.5 Eigenmode vs. energy-growth control

The focus of flow control, through control of flow instability, is on stabilization/reduction of amplification rates of known instability mechanisms of the corresponding laminar flow. Two distinct paths are followed, (nonlinear) modification of the basic state with the resulting modification of its

instability properties, or direct targeting of the instability properties of a given basic state. Early examples of the second approach include the works of Milling [28] who experimentally demonstrated active cancellation of Tollmien-Schlichting waves by a vibrating ribbon and Laurien and Kleiser [29] who used DNS to investigate control of such waves through wall transpiration. More recently, ‘optimal’ control methodologies have been rigorously derived in and applied to the case of two-dimensional wave-cancellation problems; such an effort has been demonstrated by Joslin et al. [30] who used an adjoint formulation of the control problem (see Section 3.3).

On the other hand, wave cancellation techniques cannot be applied for the non-modal optimal perturbations associated with the non-normality of the linearized Navier-Stokes operator (e.g. Reddy and Henningson [31]). As mentioned above, the kinetic energy of non-modal disturbances may grow by several orders of magnitude when selected close to optimal conditions, even (and especially most interesting) in sub-critical flows. A link between the two apparently distinct physical mechanisms can be provided by addressing the initial-value-problem [32].

For non-modal algebraically/transiently growing disturbances, efficient flow control methodologies have been demonstrated by Bewley and Liu [33] and Reddy and Ionannou [34] in laminar and turbulent channel flows, respectively. Both of these examples consider a closed system which has a complete discrete spectrum of eigenvalues. However, eigenspectra of open configurations are composed of both discrete and continuous parts, the latter being harder to resolve numerically and most active in transient growth. Therefore, control of transient growth in open systems remains a fruitful area of research.

For both modal and non-modal linear disturbances, the adjoint formulation of the linearized disturbance equations has received increased attention recently, following the rediscovery of the concept in a fluid dynamics context and its application by Hill to both one-dimensional [35] and two-dimensional [36] basic states. Briefly, while solution of the (standard) linearized disturbance equations permits identification of instability characteristics of eigenmodes of a given basic state, such as amplification rates of most-amplified disturbances alongside their frequencies and spatial structure, solution of the adjoint problem provides information of the spatial location at which introduction of AFC will provide maximum effectiveness in modifying such a basic state. An adjoint approach was proposed for spatially developing boundary layers on the flat-plate boundary layer [37–39] on flat and concave plates including the issue of receptivity [40], Görtler vortices [41], boundary layers subject to pressure gradient [42], and three-dimensional boundary layers [43].

While the issue of efficiency of the adjoint approach will be revisited in Sections 4 and 3, the very ability to perform numerical studies based on the adjoint formulation of the BiGlobal eigenvalue problem, or the respective transient-growth formulation, opens up new avenues for theoretically-founded active flow control methodologies in essentially nonparallel basic states, which naturally arise in complex engineering configurations. One such example is provided by the recent work of Luchini [44], who revisited the BiGlobal instability of the lid-driven cavity and the circular cylinder in an adjoint formulation context. This is perceived by the authors as a potentially promising area for future research, which is expected to be assisted by BiGlobal instability analysis. Indeed, advances in algorithms and the sustained increase in hardware capabilities in recent years permit addressing the instability of essentially nonparallel flows of engineering significance.

By historical analogy with classical linear stability theory, of prime concern in BiGlobal instability analysis is identification of the linear eigenspectrum of flows developing in geometries

of modest complexity which are interesting from an aeronautical engineering point of view, while being tractable numerically. The role that the global eigenspectrum plays in flow control methodologies in complex geometries may be postulated from that of the eigenspectrum in classic flows, the instability of which is governed by the established theories outlined earlier. Following the pace of algorithmic and hardware developments, a small number of essentially nonparallel basic states of relevance to aerodynamics has been analyzed; a review is provided by Theofilis [10]. A case of particular relevance to external aerodynamics, separated flow on a flat surface, will be discussed in some detail in what follows. However, the majority of global eigenspectra for flows in complex configurations are unexplored. Even less research has addressed the issue of non-normality of the BiGlobal linear operator, although evidence exists (e.g. Crouch [25]) that transient growth mechanisms play a central role in instability and control of essentially nonparallel flows.

## 2.6 On the reconstruction of a turbulent flowfield

Some comments are in order at this point on a different methodology relevant to turbulent flow control. Since its relatively recent re-invention in a fluid mechanics context [45] the concept of Karhunen [46] and Loeve [47] decomposition, mostly known as Proper Orthogonal Decomposition (POD), has been widely used in order to reconstruct a flow field at a given point in parameter space, given an accurate space-time field. The methodology proceeds by projecting this field onto an analytically or numerically constructed orthogonal basis, composed of so-called POD modes that contain a decreasing amount of the total flow energy. The same basis is then used at different parameters (e.g. higher Reynolds number) in order to predict and control the flow state at the new parameters. The utility of the methodology lies in the expected small ratio of POD modes to the  $R^{9/4}$  modes necessary to fully resolve three-dimensional, turbulent flows.

A number of issues arise (see also Section 3.4.2). On the feasibility of the approach one notes that the most critical issue in POD is that a solution (or detailed measurement) must exist before the POD concept is applied. Further, the quality of the POD reconstruction depends critically on that of the data provided at one set of parameters. While the POD modes of flows in simple geometries (e.g. flat plate [48]) and low Reynolds numbers are known or easily obtainable, those pertaining to complex engineering configurations must be calculated using data that are in principle inaccessible. Ideally, well-resolved direct numerical simulation (DNS) data would be used, but these cannot be obtained at Reynolds numbers of engineering interest, as discussed in Section 4.2. Using data obtained by large eddy simulation (LES) or Reynolds averaged Navier-Stokes (RANS) confuses the errors attributable to LES/RANS models and those to poor convergence of the POD expansion. A third approach is to use experimental data, which also has limitations as regards accessing flows at parameters of engineering relevance. However, at present the two latter approaches are the only feasible in an engineering sense.

Besides the issue of the predictive capacity of POD, in the absence of an accurate solution at one point in parameter space, realistic flow field configurations exist in which, depending on the level of energy that is deemed necessary to be captured by POD modes, the number of such modes is comparable to those needed to fully resolve the flow [49]. Furthermore, the extent of the parameter space that may be covered by POD, given a solution at one point of this space, is unclear.

Finally, while POD has been applied to turbulent and BiGlobal instability analysis for laminar flows, the relation between the most energetic POD and the least stable BiGlobal eigenmodes

is, in the authors' view, worthy of future investigation. Evidence that such a relation may exist is provided by the qualitatively analogous features of POD and BiGlobal eigenmodes in the few flows for which both types of analysis have been performed [50].

## 2.7 An example: Separated flow

A significant theoretical development, which has recently boosted interest in global linear theory in aeronautics, has been the identification of the potential of a closed laminar separation region to act as a generator of disturbances [51]. Further detailed studies of the phenomenon using two different model flows and different theoretical approaches have been performed independently by Hammond and Redekopp [19] and Theofilis et al. [18]. The latter authors employed analysis based on numerical solutions of the eigenvalue problem described by the Orr-Sommerfeld equation (OSE), the parabolized stability equations (PSE) and the two-dimensional (BiGlobal) eigenvalue problem, to study the instability of incompressible steady laminar boundary-layer flow which encompasses a closed separation bubble. Both stationary and pairs of traveling linear instabilities were discovered, which are distinct from known solutions of the linear OSE or linear PSE instability theories, and can both become unstable at sufficiently high backflow strength.

However, it should be mentioned that at the same parameters that can lead to a BiGlobal instability, KH/TS instability has a wavelength which is an order of magnitude smaller than a typical scale of the latter and growth rates which are approximately two orders of magnitude larger than those of the most unstable BiGlobal eigenmode. A conjecture on the consequence of this disparity in amplification rates of the two instability mechanisms [52] has suggested that, although the classic TS mechanism may act as a catalyst for laminar breakdown, attention must be paid to the control of BiGlobal instability of the flow as a precursor to vortex-shedding and a mechanism relevant to turbulent flow control. In other words, the existence of BiGlobal instability of the separation bubble implies that laminar flow control approaches based on frequency information delivered by either the OSE or the PSE are incomplete as far as traveling disturbances are concerned and inadequate for the BiGlobal stationary disturbances.

The spatial structure of the most unstable BiGlobal eigenmode, recovered by solution of the appropriate two-dimensional eigenvalue problem at  $R \approx 1.7 \times 10^4$ , based on free-stream velocity and a length-scale built with the aid of the free-stream pressure gradient, is shown in Fig. 1. The innocuous nature of the primary separation line alongside the three-dimensionalisation of the primary reattachment region is shown in Fig. 2, where an iso-surface of the disturbance vorticity is shown at an arbitrary level. The primary separation bubble is contained within the dashed lines and paths of particles released in the flow provide a demonstration of the effect of the BiGlobal eigenmode on the closed streamlines of the basic flow.

The recovery of unstable eigenvalues in the problem at hand must be seen in the perspective of the artificial (from a physical point of view) homogeneous Dirichlet inflow boundary conditions. In practice, TS instability in the flow under consideration is orders of magnitude stronger than the BiGlobal mechanism, at least in the bracket of parameters monitored by Theofilis et al. [18] and Theofilis [52]. While it might be expected that recovery of BiGlobal instability should be relatively more straightforward in the course of DNS, the disparity of growth rates could make its experimental isolation difficult and may indeed explain why this mechanism has gone unnoticed despite decades of experimental efforts in this key problem.

Aside from the relevance of the BiGlobal instability to laminar flow control, it has been conjectured by Theofilis [52] that the BiGlobal instability mechanism is related with and sheds light on the phenomenon of vortex-shedding by separation bubbles; the mechanism is also schematically depicted in Fig. 1. In experiments, it is often found that the separation line remains stationary while the reattachment-zone is highly three-dimensional and unsteady, a result that is consistent with BiGlobal analysis. Furthermore, earlier conjectures based on topological arguments regarding the origins of unsteadiness and three-dimensionality in separated flow appear to be substantiated using BiGlobal stability analysis.

A full discussion of both BiGlobal instability of and vortex shedding from a laminar separation bubble may be found in the original reference. However, the existence of global instabilities in separated flow shows that when designing a methodology to attack a new flow instability problem<sup>1</sup> one should refrain from employing simplifications on the grounds of theoretical or numerical feasibility. The risk of such an approach is that potentially existing physical mechanisms go unnoticed on account of such conditioned thinking. Beyond that discussed, examples supporting this assertion are constantly being accumulated (e.g., vortex flow systems [25, 26] attachment-line boundary layer [53]).

## 2.8 Turbulent flow in the wake of a circular cylinder and an airfoil

BiGlobal instability in the wake of a circular cylinder has been discussed by Barkley and Henderson [15] and that in the wake of a NACA 0012 airfoil has recently received attention by Theofilis et al. [53]. The progression from laminar flow on the unswept circular or rectangular cylinder towards flight Reynolds numbers highlights one of the most commonly encountered problems of flow on airfoils at these conditions—that of transitional or turbulent flow separation. Large-scale cellular structures are long known to be associated with this phenomenon [54], which has received a fair amount of attention and interpretations. A qualitative depiction is shown in Figure 3 and a more detailed view, including a sketch of the topological characteristics of one cell, is shown in Figure 4 [55]. Arguments have been put forward in the literature that these cellular structures may be related with end-effects of the measurement section; such arguments can be dismissed on account of the repeatability of the phenomenon shown in Figs. 3 and 4 with varying spanwise extent of the measurement domain, both in the case of the cylinder and that of the airfoil. One conjecture was put forward by Goelling [55] on the basis of his experimental results on the cylinder; namely, these structures point to a BiGlobal instability mechanism.

Experimental findings in support of this conjecture are the following. On a qualitative level, the two-dimensional closed separation bubble on the unswept cylinder first becomes spanwise unsteady with increasing Reynolds number value; the related spanwise periodic vortical cellular structure appearing as a result is shown in Fig. 4. Associated is the formation of Karman-like vortices, having their axes parallel to the generator of the cylinder, while up to this point the same qualitative scenario is followed on the airfoil. The topological description of one of the spanwise periodic cells at the upper side of the cylinder is shown in the lower part of Fig. 4; a pair of streamwise vortices separates from one of these cells, either from the cylinder or from the airfoil at comparable flow parameters.

---

<sup>1</sup>In the authors' view, most flow instability problems for flows in complex geometries should be treated as being new, although isolated regions may exist in which approximations may simplify the instability problem.

On a quantitative level Humphreys [54] has argued that the spanwise periodicity length  $L_z$  of the structures on the circular cylinder scales with its diameter  $D$ . In flow visualizations he found  $L_z \approx D \in [1.7, 2.4]$ . In recent experiments, Goelling [55] confirmed this bracket at corresponding Reynolds number values and showed that an increase in Reynolds number decreases the spanwise periodicity length to  $L_z \approx D$ . Interestingly, this progression is not continuous; this is interpreted as a hint of amplification of different BiGlobal eigenmodes as  $R$  increases. The link to a BiGlobal instability scenario on bluff bodies is provided by the shear-layer that engulfs the wake-region within which the unstable BiGlobal “B” mode develops.

With increasing Reynolds number the laminar shear-layer emanating from the cylinder surface becomes unstable and turbulent, whereby transition is associated with the appearance of small-scale streamwise-oriented turbulent vortices [56, 57]. The transition point moves upstream as the Reynolds number increases above  $R \approx 5 \times 10^3$ . It has been conjectured [55] that the interaction of the laminar boundary-layer at the cylinder surface with the unsteady flow field in the near-wake is the reason for the appearance (through a BiGlobal instability mechanism) of the large-scale spanwise periodic structures on the cylinder surface itself. Such structures have also been observed by Schewe [58, 59] on his generic airfoil experiment, with periodicity lengths similar to that found on circular cylinders at comparable conditions, as shown in Fig. 4.

Whether this mechanism can be described in the framework of a BiGlobal linear instability of separated flow or bluff-body instability deserves further investigation. In case of the absence of a steady or time-periodic laminar two-dimensional basic state underlying a BiGlobal instability analysis for the problem at hand, one may employ the triple-decomposition methodology discussed earlier. The connection of the topological features in the present flow with those in the BiGlobally unstable laminar separation bubble on an airfoil, discussed earlier, including mechanisms for vortex shedding from cylinders and airfoils also deserves investigation in the framework of the present theory.

## 2.9 On the relevance of global-flow instability to turbulent flow-control

The scope of the previous discussion can be naturally broadened to incorporate the broader field of turbulent separated flow control. The reader is referred to the recent milestone review of this problem by Greenblatt and Wygnanski [6] who highlighted the potential of periodic excitation, i.e. oscillatory momentum injection, as an effective and efficient means of flow control, irrespective of whether the base flow is laminar, transitional or turbulent. Based on overwhelming amounts of experimental information, Wygnanski and co-workers [7, 60–62] arrived at the conclusion that periodic excitation can be more efficient for certain airfoil applications than classic boundary-layer control methodologies based on steady momentum injection and at least as effective as slot suction.

Wygnanski and co-workers provide two key parameters to quantify their excitation: a momentum coefficient and reduced frequency. The level of oscillatory injected momentum was referred to free-stream conditions to arrive at the momentum coefficient (in parallel to the classic definition of steady momentum injection, e.g. Lachman [2])

$$C_\mu \equiv \frac{j'}{J} \quad (1)$$

where  $j'$  denotes oscillatory momentum due to the excitation, and  $J$ , a reference momentum injection velocity in a flow configuration of  $L = O(1)$  length,  $L$  denoting the length of the separation

region, for simplicity taken to be the chord length of an airfoil [62]. The actuation frequency is characterized by a reduced frequency  $F^+ = f_e X / U_\infty$  where  $X$  is a distance from the location on the body surface at which excitation is provided (optimally the baseline separation region, in most applications the excitation would be significantly attenuated otherwise) to the end of the body (or the natural reattachment point) in question and  $f_e$  is the excitation frequency.

The underlying theme of the experimental work in this group is that efforts must be directed toward utilizing inherent flow instabilities, enhanced by periodic addition of momentum at the appropriate location, magnitude and frequency to interact with the large-scale coherent structures of a flow. In the case of turbulent flow, it is found that the most effective oscillation frequencies of the periodic forcing are widely disparate from those of the energy containing scales of the turbulence itself. To isolate the dependence of the reduced frequency from the momentum coefficient, Wygnanski and co-workers proposed a generic deflected flap configuration, shown in Fig. 6, as an example for which the controlling parameters could be varied independently. For this configuration, they discovered that  $F^+ \approx 1$  is the optimum reduced frequency for control of turbulent separated flow, independent of Reynolds number and the level of free-stream turbulence [7, 61]. This suggests that structures scale with the separation bubble length itself (or even with the distance between the actuator and the trailing edge, in the case of an open bubble), and not the order-of-magnitude smaller TS/KH-wavelengths associated with shear-layer instability. The optimal reduced frequency  $F^+ \approx 1$ , points to the importance of the BiGlobal eigenmodes shown in Fig. 1 and  $F^+ = O(1)$  has been corroborated in a multitude of turbulent separated flow control experiments [6]. The possible existence of a feed-back mechanism between the separation and unsteady reattachment regions indicates a potential association with a generic BiGlobal instability mechanism that is worthy of further investigation.

It is the authors' view that information on flow instability mechanisms enhances the ability to control a flow successfully and efficiently and we expect further progress in the area of active flow control to be achieved by cross-fertilization between the fields of flow instability and flow control (which are currently developing nearly independently). In this respect, we next discuss flow control in a broader theoretical context, starting from first principles.

### 3 Control Theory for Active Flow Control

The goal of flow-control is to achieve some desired objective as a function of time and space by application of an appropriate actuator. The objectives may include drag reduction, separation control, enhanced mixing, noise suppression, change of a surface property, etc. Not surprisingly, many approaches to flow control have been proposed and several recent reviews Gad-el-Hak [4], Moin and Bewley [63], Lumley and Blossey [64], Bewley [65] attempt to categorize the wide range of possible flow-control strategies. For our purposes, we categorize control strategies in two ways: 1) based on the type of actuation — either passive or active, and 2) based on the means by which the actuation changes in response to changes in the flow — open-loop, closed-loop, or optimal control.

Passive actuation includes such devices as vortex generators, riblets, and steady suction or blowing, just to name a few. The primary advantage of passive control is simplicity. Passive control techniques tend to be lighter, less expensive to design and manufacture, and easier to maintain than active control thereby making passive control more likely to be used in real-world applications. On the downside, passive controls may only be effective over a limited range of operating conditions and there may even be conditions for which a passive control degrades system performance. Likewise, since most engineering flows contain complex unsteady motions (instabilities, turbulence) the ability of a passive (steady) device to control these unsteady motions is inherently limited. A dramatic example is the case of riblets [66] used for drag reduction in turbulent boundary layers. Experimentally [66] and verified by careful DNS [67–70], riblets yield approximately 5–9% drag reduction depending on their detailed geometric configuration. Even very simple active-control strategies (discussed below) are able to achieve 15–25% drag reduction under similar conditions.

Consider, as an example, controlling the transition from laminar to turbulent flow. As discussed in Section 2, one means of altering the transition process is by modifying the basic flow state upon which instabilities grow. Passive techniques, such as distributed suction, do exactly this by modifying the base flow making it more stable and thereby reducing the growth of instabilities. Of course, care must be taken to make sure that the control itself does not initiate new instabilities. Likewise, there is often a trade-off between stability and receptivity. The more stable a flow typically the more receptive [39] it is to disturbances, although, such changes in receptivity are often small compared with the change in amplitude due to altering the exponential growth-rate of a disturbance. The bottom line is that passive controls that target the mean flow may require more energy than an active control that targets the small disturbances directly. Likewise, active controls can exploit the inherent instability mechanisms in a flow (see Section 2.5) thereby using the flow as an *amplifier* to achieve a global-effect due to a very small (and often localized) control input and this is the primary focus of this paper (see Section 2.9). As a caveat, there are flows that are unstable to stationary disturbances, such as crossflow and Görtler instabilities, so that passive techniques can directly target instabilities in these flows [71].

Active control includes, in general, all types of unsteady actuators where oscillatory momentum injection for separation control (mentioned in Section 2.9) is a typical example. While passive control is inherently open-loop (it cannot respond to changes in the flow state), active control offers significantly more flexibility. In the following, we discuss different strategies for incorporating *active control* into a flow control system including: open-loop, closed-loop (i.e. feedback), and optimal control strategies.

Although the majority of the discussion in this paper is focused on oscillatory excitation for

separation control, in this section we also discuss flow-control strategies in the context of near-wall turbulence-control. In some ways, this problem is more challenging than many other flow-control problems in that the spatial and temporal scales of near-wall turbulence are much smaller than that of the relatively large-scale structures commonly found in free-shear flows (mixing layers, jets, wakes, etc.). The primary motivation for including a discussion of near-wall turbulence-control strategies is that there are a wide range of examples of different types of control strategies as applied to this flow. Issues associated with application of similar approaches to other flow-control problems, in particular separation control, will be discussed.

### 3.1 Open-loop control

In open-loop control, the either steady (passive) or unsteady (active) actuator parameters are set at the design stage and remain fixed regardless of changes in the state of the flow. As mentioned above, all passive controls are effectively open-loop. Conversely, open-loop active control is clearly an under-utilization of the potential of active control to respond to changes in the flow. Having said this, to date, most computational and experimental flow-control studies have been conducted in an open-loop manner where actuation was accomplished through a variation of the actuator parameters and the resulting control was monitored, usually in an integral manner (e.g. lift and/or drag). At first this may seem surprising, but in control theory one needs to have a good understanding of open-loop dynamics before proceeding with closed-loop studies. As such, open-loop studies have typically focused on improving understanding of flow physics and on actuator development and testing. While these early studies have focused more on proof-of-concept demonstration than development of production flow-control systems, they provide the foundation and motivation for future closed-loop studies. This is particularly true given the success of open-loop oscillatory control for separation control where it is demonstrated that small, localized controls can have a global influence on a flow (see, e.g., [6, 7]). Of course, there are a number of shortcomings of open-loop flow control with perhaps the most important being what happens in off-design conditions.

### 3.2 Closed-loop control

In closed-loop flow-control, one utilizes measurements of the current flow state along with a model of the state to devise a new control that alters the system state in the desired direction such that it gets closer to the target state. Thus, closed-loop control requires that both actuators and sensors be designed and utilized in an effective way. Two key concepts in linear control theory that are related to the design and use of actuators and sensors are *controllability* and *observability*. While these concepts have well-defined mathematical definitions in the context of linear control theory (see, e.g., Zhou and Doyle [72]), they also are important in nonlinear systems (and their linearization) common in fluid dynamics. In lieu of providing precise mathematical definitions, we instead discuss these concepts from a more physically intuitive perspective as a means of identifying important issues that must be considered in the design of closed-loop controllers for active flow-control.

*Controllability* is a property of both the actuator system and the state that determines whether all the state modes can be arbitrarily influenced by the control actuator(s). Controllability obviously depends on the appropriateness of a particular actuator system. For example, if an actuator

only generates irrotational disturbances (i.e. sound waves) then it may be quite difficult to effectively control a flow dominated by vortical flow features. Controllability is intimately related to the concept of linear receptivity in fluid mechanics [9]. In receptivity analysis, one determines the amplitude of certain natural modes of the state due to different disturbance (i.e. control) inputs. This type of input/output framework for receptivity analysis has been explored by [35, 73] for parallel boundary layers based on an adjoint analysis of the Orr–Sommerfeld equation. For nonparallel flows, approaches based on both the adjoint parabolized stability equations (PSE) [37, 39, 74–77] and full adjoint Navier–Stokes equations [39, 74, 75] have been performed both for two- and three-dimensional boundary layers. An important outcome of these studies is that stable modes are often significantly more receptive to excitation than unstable modes [39, 75] which along with the discussion in Section 2.3 again suggests the potential importance of transient growth of linearly stable modes. In related work, initial conditions or inflow profiles that lead to the largest energy growth have been an area of significant recent research [20–22, 33, 78]. A weaker version of controllability is *output controllability* where, instead of requiring complete control of the state of the system, we may be content to control the measured output. Output controllability is the ability to construct a control that takes any initial output to a desired output. Unlike controllability, output controllability depends not only on the actuator and state but also on the sensor system used.

*Observability* is related to the ability of a particular sensor system to reliably measure changes in the state. More precisely, a system is observable if the initial state can be determined from the values measured by the sensors along with known control inputs. Observability obviously depends on the quality, number, and placement of the sensor system used. But, observability also depends more subtly on the nature of the state. For example, if a sensor is constructed that only measures vortical disturbances then it would be completely insensitive to irrotational disturbances, like acoustic waves, and could never tell if the initial state contained acoustic disturbances. Likewise, with only a limited number of sensors, one might not be able to distinguish between two different modes and this would also limit observability.

Of course, in these examples concerning acoustic and vortical disturbances, there are physical mechanisms that allow the conversion of irrotational disturbances to rotational disturbances (e.g. leading-edge receptivity) and vice versa (e.g. turbulence-induced sound) so that the degree of controllability and observability in these examples depends strongly on the role of such conversion mechanisms in a given flow system. Boundary conditions and geometric features (e.g. leading and trailing edges, and localized roughness) often play an important role in such conversion processes.

Another concept from linear control theory that is also useful in the context of flow control is the idea of *stabilizability*. A combination of state and control is stabilizable if all unstable modes are controllable. This is obviously a less stringent condition than controllability and for some flow control problems (e.g. transition dominated by linear eigenmode growth) this may be all that is required. However, as discussed in Section 2.3, stable modes can play a very important role in the transient response of some flow systems so that stabilizability may not be sufficient. Recent work of Lauga and Bewley [79] highlights the role of stabilizability for the complex Ginzburg–Landau equation which serves as a model for inhomogeneous weakly non-parallel flows such as wakes. The main conclusion of this study is that the system is increasingly more difficult to stabilize using a single actuator as a Reynolds number like parameter is increased. While, theoretically the system is stabilizable at all conditions, practically speaking the system becomes uncontrollable with a single point source actuator at finite “Reynolds” numbers. The loss of controllability of the unstable modes is found to be related to non-normality of the closed-loop system where the shapes of the

two most unstable open-loop eigenfunctions become increasingly similar as the Reynolds number is increased. *Non-normality* of both open- and closed-loop modes in fluid dynamics systems is now known to commonly occur in fluid flows [20–22, 33, 78] so that similar effects may happen in physically realistic flows. However, it is important to emphasize that controllability and stabilizability depend both on the system dynamics *and* the control mechanism. In their study, Lauga and Bewley [79] limited their control input to a single point source. Thus, another interpretation of their result is that as Reynolds number increases, one must also increase control authority by including multiple actuators or perhaps incorporating some type of distributed control mechanism and these are interesting directions for further research.

When considering closed-loop control one needs to somehow convert the values measured by the sensors into changes in the parameters that are appropriate to be used as input to the actuators. The conversion of some measured quantity to a control input is accomplished by the *controller* as shown in the simple closed-loop block diagram in Fig. 7. In the following, we will focus on three approaches to controller design: physics-based control, classical control, and modern control. An illustrative comparison of classical and modern control theories can be found in [80]. An important property of a closed loop control system is its *robustness* to unknown environmental disturbances or uncertainties in the models used to design the controller. The prevalence of environmental disturbances in flow control systems (e.g. freestream turbulence, sound, and vibrations) combined with the fact that most of the models we use to predict fluid flows are approximate, makes the issue of robust control design of particular importance.

### 3.2.1 Linear control theory

To set the stage for a discussion of linear control theory, it is useful to introduce simple notation that allows a discussion of particular aspects of control design using the language common in control theory. In linear control theory, the state equation in state-space form is written as

$$\dot{\mathbf{x}} = \mathbf{A}\mathbf{x} + \mathbf{B}\mathbf{u} + \mathbf{D}\mathbf{w} \quad (2)$$

where the measurements are given by

$$\mathbf{y} = \mathbf{C}\mathbf{x} \quad (3)$$

and the control is

$$\mathbf{u} = \mathbf{K}\mathbf{y}. \quad (4)$$

In the above expressions  $\mathbf{x}$  is the state vector,  $\mathbf{u}$  is the control-input vector,  $\mathbf{w}$  are external disturbances, and  $\mathbf{y}$  is the output (i.e. measurements) where  $\mathbf{A}$ ,  $\mathbf{B}$ ,  $\mathbf{C}$ , and  $\mathbf{D}$  are the state-space matrices for the system and  $\mathbf{K}$  is the feedback-control kernel.

In the context of flow-control, one can think of Eq. (2) as the spatially discretized, linearized Navier–Stokes equations with boundary conditions included. As pointed out by Joshi et al. [81] and reiterated in Bewley [65], care is required in selecting the spatial discretization as certain choices may lead to much simpler interpretations of the state-vector  $\mathbf{x}$ . For example, in homogeneous, constant-coefficient systems, a Fourier series discretization leads to a decoupling of different Fourier modes that can simplify both analysis and design of a control system. Using this notation, the design of the controller requires selecting an appropriate feedback kernel  $\mathbf{K}$  given particular actuators and sensors, described by  $\mathbf{B}$  and  $\mathbf{C}$ , respectively. The controllability of a system is a property of  $\mathbf{A}$  and  $\mathbf{B}$ , while the observability is a property of  $\mathbf{A}$  and  $\mathbf{C}$  (see, e.g., [72, 82]).

### 3.2.2 Physics based strategies

Perhaps the simplest type of feedback control is when the controller in Fig. 7 is a simple unity gain multiplying some measured physical value. For such a strategy to be successful, the measured quantity and control actuation have to be closely related and directly applicable (in the sense of controllability and observability) to the physical phenomena one wishes to control. In other words, the selection of both the measured flow quantity and the control rely on a clear understanding of the underlying physics of the problem. In practice, it may be quite difficult to find such a clear correspondence between a measurable quantity and a control variable and this is a significant limitation of the approach.

A classic example of such a physics-based (or intuitive) feedback-control strategy is opposition control (also called “out-of-phase” control) [4, 83] for drag-reduction of wall-bounded turbulence. Opposition control is a conceptually simple feedback control strategy that introduces control in the form of distributed suction and blowing at the wall surface in an attempt to oppose the motion of near-wall turbulent structures. Near-wall turbulent structures generally take the form of streamwise oriented counter-rotating vortices (see, e.g., Clark and Markland [84], Jimenez and Moin [85], Jeong et al. [86]). By sensing the vertical component of velocity at a sensing plane located a distance  $y_s^+$  (in wall units) from the wall and using suction/blowing in opposition to the measured velocity, one hopes to attenuate the motion of turbulent structures thereby reducing the transport of high momentum fluid toward the wall and eventually reducing skin-friction drag.

The first simulations demonstrating this method are those of Choi et al. [83] who used DNS at a turbulence Reynolds number,  $R_\tau = 180$ , reporting about 20% drag reduction when the sensing plane is located at  $y_s^+ = 10$ . The more recent DNS by Hammond et al. [87] shows that, again for  $R_\tau = 180$ , the optimal sensing plane location is  $y_s^+ = 15$  which gives about 25% drag reduction. Both studies reveal that drag increases when the control is set to counter motions too far from the wall, say at  $y_s^+ > 25$  [83, 87]. These DNS studies serve to demonstrate the effectiveness of opposition control as well as identify likely mechanisms for drag reduction when using opposition control. In doing so, they spurred on a number of other investigations that built on the idea of opposition control in a variety of ways. However, the applicability and net efficiency of the above ideas are still an open question.

Lee et al. [88] developed neural network controllers that effectively correlate spanwise wall shear-stress with the off-wall normal velocity used in opposition control. Koumoutsakos [89] devised a method based on the relation between wall pressure-gradient and wall vorticity-flux which is used to determine wall-normal velocity control and this is shown to yield drag reductions similar to or better than opposition control [90]. Building on the idea of opposition control, Kang and Choi [91] investigated the effect of using active wall-motion instead of wall-normal transpiration as the control actuator within an opposition control strategy and they obtain 17% drag reduction at  $R_\tau = 140$  with  $y_s^+ = 10$ . A similar approach is reported by Kellogg [92] who used an immersed boundary method to simulate the moving wall as opposed to the more computationally expensive mesh-moving method of Kang and Choi [91]. At  $R_\tau = 100$  with  $y_s^+ = 16$ , Kellogg [92] reports a 14% drag reduction — a value that is strongly influenced by the allowable degree of wall-deformation which may explain the reduced effectiveness of wall motion compared to traditional wall-transpiration. Clearly wall motion is more technically challenging than wall transpiration.

Opposition control has also played an important role in helping to explain the physics of near-wall turbulence. Farrell and Ioannou [93] applied opposition control to the linear, non-normal

evolution of optimal roll and oblique disturbances in channel flow and these results compared favorably to the nonlinear turbulent opposition control simulations of Choi et al. [83]. In related work, Jiménez and Pinelli [94] performed studies where terms related to the generation of near-wall streaks were damped leading to a laminarization of low Reynolds number turbulent channel flows and they hypothesize that this is a likely mechanism for drag reduction due to opposition control. More recently, the role of linear processes in nonlinear turbulent flows has been further explored by Kim and Lim [95] who showed that when the linear coupling term between wall-normal velocity and wall-normal vorticity is artificially removed in DNS at  $R_\tau = 100$ , turbulence decays and they related the linear coupling term to opposition control.

The success of opposition control for near-wall turbulence control suggests that physics based approaches may be useful for other classes of flow control problems. While this may be true, there are a number of potential challenges with a physics-based strategy, including: limitations in physical insight, inability to handle off-design conditions, and difficulties in extending to coupled complex-physics systems. Likewise, there may be practical issues that prevent one from directly measuring or controlling the physical quantities needed in a physics based approach and such an approach does not directly account for the dynamics of the sensor/actuator combination. Finally, a physics based design does not provide any clear indication of whether the resulting closed-loop system is robust to external disturbances. For these reasons and others, more systematic methods for closed-loop control design are typically preferred although it is certainly advantageous if these approaches are based upon a strong physical foundation.

### 3.2.3 Classical control theory

In classical linear control theory (see, e.g., Franklin et al. [96]), the determination of a control,  $\mathbf{u}(t)$ , from some error value,  $\mathbf{e}(t)$ , is often accomplished using a proportional-integral (PI) controller of the form

$$\mathbf{u}(t) = \mathbf{r} + k_c \left[ \mathbf{e}(t) + \frac{1}{T_i} \int \mathbf{e}(t) dt \right] \quad (5)$$

where  $k_c$  is the gain,  $T_i$  is the integral-time of the controller,  $\mathbf{e}(t) = \widehat{\mathbf{y}}(t) - \mathbf{y}(t)$  is the deviation of (or error in) the state measurement  $\mathbf{y}$  from some desired or reference value  $\widehat{\mathbf{y}}(t)$ , and  $\mathbf{r}$  is used to calibrate the control so that at zero error the desired set-point  $\widehat{\mathbf{y}}$  is obtained. While the vector notation for the control and output was retained, in practice one would likely use different gains and integral-times for each control loop. The design of effective PI controllers for multiple-input/multiple-output systems is challenging due to potential interaction between the multiple control loops. Finally, we remark that the robustness of classical feedback control systems to external disturbances is provided by ensuring sufficient gain and stability margins and these must be evaluated and validated for each control-system design.

Returning briefly to the idea of opposition control introduced above, we see that it is a simple proportional control rule for a single-input/single-output system where the input is the vertical velocity measured a distance  $y_s^+$  above the actuator, while the output (control) is the local value of wall-transpiration velocity and the gain,  $k_c = -1$ .

An example of PI control applied to a flow-control problem is the work of Joshi et al. [81] who show that both linear and finite-amplitude disturbances can be stabilized using linear PI control in plane Poiseuille flow. An important issue identified in this work is that when control is turned on, energy can be fed into modes during the transient such that their amplitude reaches nonlinear

levels thereby violating the assumptions of linear control theory and possibly triggering transition to turbulence. In their simulations, Joshi et al. [81] observe such a transient response for a mode that was unobservable by their wall-mounted shear-stress sensors. The key point is that the startup of a control system may generate transients that are more difficult to control than the original open-loop problem and this issue potentially pertains to other flow control systems.

Another example of closed-loop classical control is the work of Rapoport et al. [97, 98] who applied closed-loop feedback control for vectoring of a turbulent jet. The motivation for closed-loop control in this case was to enable fast and smooth transitions between different stationary deflection angles while maintaining desired jet deflections under varying environmental conditions. They explored both proportional-integral derivative (PID) control [98] and internal model control (IMC) [97]. PID control is similar to PI control but, in an effort to improve the dynamic response of the closed-loop system, a term proportional to the time-derivative of the error is also included

$$\mathbf{u}(t) = \mathbf{r} + k_c \left[ \mathbf{e}(t) + \frac{1}{T_i} \int \mathbf{e}(t) dt + T_d \frac{d\mathbf{e}(t)}{dt} \right] \quad (6)$$

where  $T_d$  is called the ‘rate-time’ and in PID there are three parameters ( $k_c$ ,  $T_i$ ,  $T_d$ ) that must be tuned. Conversely, IMC is a model-based feedback control approach where the inverse transfer function of a (hopefully simple) model of the system is multiplied by additional poles at  $-1/\lambda$  where  $\lambda$  is the time-constant of the IMC controller that must be tuned to achieve good response. In order to account for errors present in the simplified model of the system used for the controller, the feedback signal in IMC is the difference between the measured response of the real system and the response predicted by the model. In the case of jet vectoring control, Rapoport et al. [97] developed a model of the system experimentally by fitting the measured transfer function to an appropriate rational polynomial. After doing so, Rapoport et al. [97] conclude that the resulting IMC controller is simpler than PID control with fewer parameters (1 versus 3) that must be tuned while both controllers have equivalent performance. Thus, the advantage of IMC, and model-based control in general, is that by capturing some of the relevant physics within a model, a simpler controller design with fewer unknown parameters results. Classical feedback control has also recently been applied to control acoustic noise from cavity flows [99, 100] yielding a 7dB noise reduction of the primary resonant mode. Model based control for cavities is also underway with both physics-based [101] and experimentally based [100] models under construction.

In model-based control, one leverages knowledge of the physics of a system, in the form of a model, in order to simplify controller design. This philosophy can be taken to the limit where an optimal controller is constructed that fully exploits the physics encoded in a model and this is the approach taken in *modern control theory*.

### 3.2.4 Modern control theory

Modern control theory is distinguished from classical control theory in that it provides a systematic means of constructing (or synthesizing) closed-loop feedback control laws for multiple-input/multiple-output systems that explicitly account for both model uncertainty and external disturbances. An essential ingredient in modern control theory is the use of a model that serves to estimate the state of the system (i.e. the *estimator* shown in Fig. 8) given limited measurements. A control is then determined from this estimated state which is then fed back to the system. The combination of the *estimator* and *controller* yields the *compensator* as shown in Fig. 8. Ideally,

one would like the compensator to perform well even when the system is subjected to external disturbances, shown as  $\mathbf{w}(t)$  in Fig. 8. One of the most useful results of modern control theory for linear systems is that for a given model (estimator) one can *synthesize* a controller that has desirable physical properties (e.g. minimizes drag or unsteadiness) even in the presence of external disturbances,  $\mathbf{w}$ , that excite the closed-loop system.

The system model for the estimator can be written as

$$\begin{aligned}\dot{\hat{\mathbf{x}}} &= \hat{\mathbf{A}}\hat{\mathbf{x}} + \hat{\mathbf{B}}\mathbf{u} + \hat{\mathbf{D}}\mathbf{w} - \mathbf{L}(\mathbf{y} - \hat{\mathbf{y}}) \\ \hat{\mathbf{y}} &= \hat{\mathbf{C}}\hat{\mathbf{x}}\end{aligned}$$

where the quantity  $\mathbf{y} - \hat{\mathbf{y}}$  drives the estimated state measurement,  $\hat{\mathbf{y}}$ , to match the actual state measurement,  $\mathbf{y}$ . The control is then based on feedback of the state estimate

$$\mathbf{u} = \mathbf{K}\hat{\mathbf{x}}$$

where  $\mathbf{K}$  is the controller feedback matrix and  $\mathbf{L}$  is the state-estimation feedback matrix. The goals of modern control theory are to find  $\mathbf{K}$  and  $\mathbf{L}$  such that the estimator feedback drives the estimated state close to the actual state and the controller feedback drives the actual state to a desired condition. When the disturbances  $\mathbf{w}$  are taken to be worst-case disturbances then the approach is referred to as  $\mathcal{H}_\infty$  control design and the interested reader should consult [72, 82, 102] to learn more about the theory of  $\mathcal{H}_\infty$  control. In principle,  $\mathcal{H}_\infty$  control provides means of accounting both for uncertainties in the model of the system as well as unknown environmental disturbances. Bewley [65] provides a comprehensive review of  $\mathcal{H}_\infty$  control design in the context of transition and turbulence control in the planar channel, while Bewley and Liu [33] present in-depth results for a transitional flow problem. This work has recently been extended by converting the feedback and estimation matrices from frequency space to physical space leading to spatially localized convolution kernels that may play an important role in design of distributed control systems [103].

A special case of  $\mathcal{H}_\infty$  control occurs when the external disturbances are assumed to be Gaussian white noise and the result is referred to as  $\mathcal{H}_2$  control, also called linear-quadratic Gaussian (LQG) control [104]. Unfortunately, with LQG control there are no guarantees that the resulting controller will be stable for all possible external disturbances [72]. In practice, when using LQG control design, one needs to ensure that adequate gain and phase margins are available. A technique to overcome this limitation of LQG control has been developed called LQG/loop transfer recovery (LQG/LTR) [72]. LQG/LTR is similar to  $\mathcal{H}_\infty$  in that one simultaneously designs both an estimator feedback matrix and a control feedback kernel such that the resulting controller approximates the properties of full-state feedback using linear-quadratic regulation (LQR) [72]. LQR with full-state feedback provides well known stability margins therefore providing a degree of robustness that, under certain conditions, can also be achieved using LQG/LTR. LQG/LTR control synthesis has been successfully applied by Cortezzi and Speyer [105] to control transient growth in two-dimensional transitional channel flow. Likewise, Lee et al. [106] applied LQG/LTR control synthesis, based on reduced-order model of the linearized Navier–Stokes equations for Poiseuille flow, to turbulent channel flow at  $R_\tau = 100$  and drag reductions in the range of 10–17% were obtained.

### 3.2.5 Issues in closed-loop control

For all of the control system design strategies considered so far, an essential ingredient for success of a control system is the availability of an appropriate model of the state. In the case of heuristic control, this model may just be a intuitive idea of how the flow behaves without requiring a concrete mathematical model. At the other extreme, modern control theory requires a mathematical model of the state for use in the estimator. Of course, any model used within a control system typically must be significantly less expensive to solve than the full-state equations while still providing reasonably accurate predictions. Such reduced-order-models (ROM) are of particular importance in flow-control systems since fluid flows tend to be high-dimensional and highly nonlinear. A number of approaches to ROM for problems in fluid systems have been explored and these are discussed in more detail in Section 3.4. The formulation of ROM and accounting for errors associated with model reduction remain active areas of research.

Another important issue in formulating closed-loop control for active flow control is in accounting for the effect of transient growth of stable modes. As mentioned above, Joshi et al. [81], in their application of PI control to transitional channel flow, found that the transient associated with the startup of control led to an unobservable transient response that could grow large enough to trigger turbulence. Since flows can be very receptive to transient disturbances [74], it remains a challenge in control system design to ensure that the control itself does not initiate new, undesirable flow states. This is particularly true in the context of classical control theory which, since devised in the frequency domain, focuses on the time asymptotic response of a system with the transient response verified (and possibly tuned) a posteriori. On the other hand, modern control theory directly accounts for transient effects due to eigenmode non-normality by working with norms of transfer functions and the recent work of Bewley and Liu [33] and Lee et al. [106] demonstrates that transient growth can be controlled with modern control designs. Because of the importance of non-modal, transient growth in fluid systems it seems likely that modern control theory will continue to be an active area of research for active flow control design.

Related to this is the issue of robust control. In traditional control design, robustness is determined after the fact by verifying that there are adequate stability margins. Modern control, either  $\mathcal{H}_\infty$  or LQG/LTR, have built in robustness properties that not only account for unknown environmental disturbances but also for uncertainties and errors in the models used to estimate the state dynamics and both of these issues are of particular importance to active flow control systems. Flow control systems will be subjected to freestream turbulence, surface roughness, acoustic disturbances, etc. Likewise, mathematical models of fluid systems are often highly truncated so that the effect of unresolved scales must be approximated through models of the Reynolds or subgrid-scale stresses and the errors and uncertainty in these models must be accounted for. Again, modern control theory ( $\mathcal{H}_\infty$ ) is attractive from this point of view in that it provides direct means of incorporating model uncertainty. Of course, this does not come for free — modern control synthesis is expensive to perform and techniques to improve the efficiency of modern control synthesis for large-scale problems are desirable.

A final issue that needs to be addressed is the role of nonlinearity and its impact on a feedback control system. All of the approaches we have discussed so far are designed specifically for linear problems, although in practice such linear control rules are often successfully applied to nonlinear problems. A common example is that of an airplane autopilot. Airplane dynamics are governed by a six degree of freedom coupled system of nonlinear ordinary differential equations. However,

autopilots are routinely designed and successfully executed based solely on linear control theory. One common justification for this is that it is desirable for safety, comfort, and performance if the aircraft remains in smooth flight so that deviations from smooth flight should be small. Of course in practice there may be situations where large disturbances are unavoidable (such as a thunderstorm) so that another control system (the pilot) may be required.

While smooth flight is fortunately the norm for aircraft, smooth flow (i.e. laminar flow) is quite uncommon in fluid systems. In fact, most engineering flows are turbulent and it is not clear to what degree such an inherently nonlinear process like turbulence can, in general, be controlled using linear control theory. While there has been success in using linear control for wall bounded turbulence ranging from simple opposition control [83, 87, 107] to modern control theories [103, 106], it seems likely that this success is due, in part, to the importance of linear processes in the near-wall region [94, 95]. Whether linear processes play an equally important role in other turbulent flows, such as jets and wakes, is an open issue. Fortunately, the design of control systems directly for nonlinear systems is an active area of research. While the authors are unaware of such nonlinear control theory applied to flow control problems, a control approach that can and has been applied directly to nonlinear problems is that of optimal control.

### 3.3 Optimal control

The previous section focused exclusively on linear feedback control. Here, optimal control as a general framework for flow control of nonlinear systems is considered. Not only can optimal control be used to construct locally optimal open-loop control distributions for the full nonlinear equations of motion, but optimization can potentially also be used for the optimal design of practical feedback control systems, even in the nonlinear setting. For linear problems, LQG [104] and  $\mathcal{H}_\infty$  [82] control design are both based on the solution of specific linear-quadratic optimization problems.

#### 3.3.1 Optimal open-loop control

The most common application of optimal control theory to flow control problems is to find optimal open-loop controls that minimize a specified objective functional. Optimal control methodologies have been applied to a variety of steady or simplified flow control problems involving drag reduction, flow and temperature matching to provide more sophisticated flow control strategies in engineering applications. The papers [108–115] represent a small sample of the work on adjoint methods for the optimization of unsteady flows and the reader is referred to the introduction in [116] for a brief review of some of the recent work in this area as well as a discussion of some of the important issues that arise when applying optimal control to unsteady flows. The mathematical nature of optimal control theory makes it amenable to the derivation of mathematical theorems related to existence of solutions and well-posedness of the problem. However, only partial results of this type are possible in three-dimensions since, in this case, the Navier-Stokes equations themselves do not enjoy a full theoretical foundation; in two-dimensions, a complete theory is available for incompressible flow. The reader is referred to references on optimal control theory [108, 117–120] for details.

In optimal control, one begins by postulating a family of desired controls and an objective functional (e.g., stress over a region of an airfoil). Then, through a formal minimization process, one

derives a set of differential equations, and their adjoints, whose solution produces the optimal actuator profile (among the specified set). This procedure is referred to as the optimize-then-discretize approach. A second approach, called discretize-then-optimize, involves first discretizing the original state equations and objective functional and then performing the minimization procedure at the discrete level. In general, these two approaches lead to different results (see, e.g., Nadarajah and Jameson [121], Gunzburger [122]) and both approaches have been used in the literature. Further research is required to provide guidance as to which approach is better and to ensure that solutions, using either approach, converge to the solution of the original infinite dimensional problem as the discretization is refined. Since the state equations for flow control problems are typically nonlinear, the solution to the full optimality system (state and adjoint equations) is accomplished using some form of iterative gradient-descent method such as the nonlinear conjugate gradient algorithm. The performance of such algorithms depends on the inner-products used to define the adjoint equations which effectively serve as preconditioners and further details can be found in Collis et al. [116]. Another important, and related, topic is the selection of an appropriate family (or space) of controls and the enforcement of sufficient regularity (i.e. smoothness) of the control in the objective function. Control regularity can impact both the ability to solve the optimal control problem as well as the physical realizability of the resulting control distributions [110, 116]. Finally, it is important to emphasize that gradient-descent algorithms only converge to *local* minima that depend on their initial starting point. Thus, there is no guarantee of finding a globally optimal solution using these approaches. In an engineering application this may not be of paramount importance as long as the performance (i.e. reduction in the objective functional) is sufficient at the local minima.

The optimal control technique described above provides a locally optimal open-loop control that minimizes the prescribed objective functional. As such, it does not directly provide the real-time control that is ultimately of interest for engineering applications. However, by systematically computing an optimal control within specified tolerances, for a given objective function, it is possible to use such results to guide the development of control strategies (active or passive). Optimal control allows a determination of the benefits of different objective functionals (which guides sensor system design) and provides insight into the spatio/temporal structure of the control (which can guide actuator design). Likewise, this coupling between input and control provided by optimal control theory can be built into a neural network, or other type of self-learning system, to allow effective control over a wide range of input parameters.

An early example of optimal control applied to unsteady flows is the work of Joslin et al. [30, 123] on boundary layer transition suppression. Joslin et al. [30] coupled the time-dependent incompressible Navier–Stokes system with the adjoint Navier–Stokes system and optimality conditions from which optimal states (i.e., unsteady flow fields and controls) were determined. Although the approach is sufficiently generalized so that separation control or other problems of interest may be solved, Joslin et al. [30, 123] focus on boundary layer transition suppression.

Others have used a similar methodology for drag reduction in planar turbulent channel flow [65, 124, 125] using DNS. Similar results have been also been obtained using LES with the dynamic subgrid-scale model by Collis et al. [126], Chang and Collis [127], Chang [128] and both the evolution of drag and turbulent kinetic energy from this study are shown in Fig. 9. At this low turbulence Reynolds number, optimal control is able to return the flow to the laminar state for sufficient large optimization intervals,  $T$ . This is to be compared with opposition control (see Section 3.2.2) where only a 26% drag reduction is obtained [107]. The use of LES versus DNS to model the state for this problem led to factor of 5-10 savings over the DNS study of [125] with

no significant change in the performance or spatio/temporal structure of the control. An important element in the success of LES in predicting this controlled flow is that the dynamic subgrid-scale model can adapt to changes in the flow due to the presence of control. Referring to Fig. 9 for  $T^+ > 25$  the control effectively suppresses the turbulence and the dynamic model automatically turns off as laminar flow is approached. An important issue for reduced-order models for use in controlled flows is that such models must be able to adapt to changes in the flow dynamics due to the action of control. The work of Collis et al. [126] highlights both the potential for and important issues associated with reduced-order modeling (and LES in particular) for use in optimal control and this is discussed in more detail in Section 3.4.

### 3.3.2 Issues in optimal control

There are a number of formulation and implementational issues that must be addressed when performing optimal control including boundary conditions, gradient accuracy, and computational expense.

Care must be exercised in the implementation of the coupled state and adjoint equations, especially with regard to boundary conditions. Figure 10 summarizes the issues pictorially for a spatially evolving flow like that studied in [30, 123]. The coupled system involves the Navier-Stokes equations which are solved forward in time and the adjoint Navier-Stokes equations that are solved backward in time. The actuator introduces control authority (suction/blowing velocities) and sensor assesses the state of the control in the Navier-Stokes equations. These roles are reversed for the adjoint system. In Section 4.7 considerable discussion is focused on outflow conditions because wave reflections can easily occur with improper implementation of the boundary conditions. This issue is compounded now that the problem deals with inflow and outflow conditions for both the state and adjoint systems, and appropriate non-reflecting conditions must be used for each. In [30] the need for non-reflecting outflow conditions was avoided by selecting the time-interval short enough to prevent waves from reaching the outflow boundary. Recently, Dobrinsky and Collis [39] formulate and implement appropriate buffer conditions for use as outflow conditions for both the state and adjoint Navier–Stokes equations with good results obtained.

Challenges associated with boundary conditions for the state and adjoint equations are exacerbated in the context of optimal control of unsteady compressible flows where acoustic waves (and adjoint acoustic waves) can easily be reflected and even created by inexact boundary conditions. Nonreflecting boundary conditions based on both characteristic decompositions and sponge regions have been applied with success for both discretize-then-optimize [116] and optimize-then-discretize [129] adjoint formulations. Not only are far-field nonreflecting conditions important, but one must also implement stable and accurate near-field boundary treatments for use in modeling the control and Collis et al. [129, 129] present an approach suitable for use in high-order accurate, central-difference discretizations of the compressible Euler equations. Based on the formulation and implementation presented in [110, 116, 129, 129], Collis et al. [130] have successfully applied optimal control to reduce the sound generated by a model blade-vortex interaction and a 13db reduction is obtained over the spatial region of interest. This work represents the first use of optimal control applied to unsteady compressible flows. The application of control (whether optimal or feedback) to unsteady compressible flows is a ripe area for future research.

As a final point on the use of optimal control, it is important to note that such capability does not come without cost. From an implementation viewpoint, the coupled system can be quite

challenging to solve for three-dimensional large-time horizon problems. The adjoint system requires that the velocity field obtained from the Navier-Stokes equations be known in the computational domain for all time. For large three-dimensional problems these storage requirements can quickly become prohibitive and sophisticated storage management techniques must be utilized [109, 112, 131]. Given the large spatial domains for three-dimensional problems, it is also likely that the length of time over-which one optimizes may have to be artificially truncated in order to make the problem tractable. In this suboptimal control setting, one typically solves multiple optimization problems in a sequential manner in time. This, in fact, is the approach used by Bewley et al. [125] and Collis et al. [126] for the channel flow problem discussed above where the optimization interval is  $T^+$  as shown in Fig. 9. In some cases this approach has been taken to an extreme where the optimization interval is exactly one time-step of the numerical simulation [132, 133] and this is sometimes referred to as instantaneous control. Recently, Heinkenschloss [134] has shown that instantaneous control can be thought of as one pass of a Gauss-Seidel method for a large-time linear-quadratic control problem. This opens the door to new optimization algorithms where instantaneous control serves as a preconditioner to more efficiently solve the original large-time optimization problem. Such research holds promise for future applications of optimal control to large-scale flow control problems.

It is also important to point out that most if not all current research on optimal control theory applied to flow control has been performed numerically. While the examples discussed above went to great lengths (either DNS or well-resolved LES along with extensive grid refinement studies) to ensure the fidelity of their predictions, nevertheless, experimental validation is lacking and extension of these approaches to the laboratory setting remains a significant research challenge.

### 3.4 Reduced order modeling

In all of the control strategies discussed above, some form of model or surrogate of the system to be controlled is required. In the case of heuristic control, this model may just be a intuitive idea of how the flow behaves without requiring a concrete mathematical model. Conversely, optimal control requires a full mathematical model of the system while feedback control requires something in between. Clearly, if one's eventual goal is the real-time control of a fluid system then very simple models will be required as real-time solution of the Navier–Stokes equations is untenable for the foreseeable future (see Section 4.2). Thus, the objective of a *reduced-order model* (ROM) is to capture the essential physics of the flow under control while reducing the expense associated with solving the model.

For fluid systems there are a variety of approaches that can be taken to construct ROMs and they can be broadly categorized as being based on either: physics, mathematics, or data fitting. Of course, in practice a ROM may be a hybrid of one or more of these approaches.

#### 3.4.1 Physical

Physics based approaches to reduced order modeling include many of the techniques for modeling and simplification commonly used in fluid dynamics analysis. A hierarchy of such models can be made (roughly in order from low to high fidelity): potential flow analysis, vortex methods, boundary layer equations, parabolized stability equations, Euler equations, harmonic linearized Navier–Stokes equations, RANS, detached eddy simulation (DES), and LES. Each of these are approxi-

mations to the full Navier–Stokes equations and each can serve as effective reduced-order models under appropriate conditions. Other common reduced physics models include: incompressible versus compressible flow, two-dimensional versus three-dimensional flow, inviscid versus viscous flow.

The model reduction in physics based ROM is accomplished by neglecting certain physical processes that can potentially occur but are thought not to be important for the system under consideration. Selecting an appropriate physics based model requires careful consideration of the relevant physical processes active in a given flow and for a complex engineering flow, this may be very difficult. If an inappropriate model is selected, there is typically no easy way to bring in additional physics. For example, if a boundary layer separates the boundary layer equations become ill-posed and one cannot correct the situation without returning back to the full Navier–Stokes equations in the vicinity of the separation. On the positive side, physics based ROMs can be very efficient to solve (vortex methods, parabolized stability equations, etc.) so that there is some chance that they could be used in near real-time control applications.

A nice application of physics-based modeling to a relevant flow-control applications is the work of Rowley et al. [101] who developed a physics based model of sound generation in cavity flows using linear stability theory and simple wave propagation. Feedback control of this model demonstrated the same peak splitting phenomena observed in experiments [100, 101].

On the other end of the fidelity spectrum is the use of large eddy simulation (LES) as a reduced-order model [126, 128, 135]. Typically, in a well-resolved LES one expects about an order of magnitude reduction in computation expense compared to DNS. While this reduction is nowhere near sufficient to make LES available as a real-time model (see Section 4.2), it does, however, make LES advantageous as a reduced-order model for control system design including optimal control/design. In 1998, Collis and Chang [136] pioneered, to the best knowledge of the authors, the use of LES based on the dynamic subgrid scale model as a tool for flow control simulations. Subsequent publications [126, 128, 135] validated LES for control of near-wall turbulence as well as significantly extended the range of Reynolds numbers for which turbulence control simulation had been performed [107]. A key observation of this research has been that any turbulence model applied to a controlled flow must respond in a reasonable way as the flow is modified by the action of the control. For this purpose, Collis and Chang [136] used the dynamic model and found that it successfully responds to changes in the flow due to control. Collis et al. [126] provide a review of LES as a reduced-order model for both a simple feedback control strategy (opposition control) as well as optimal control. Results for optimal control using LES were presented in Fig. 9 where LES is used exclusively, both as the state model, and in computing the control through the adjoint of the LES equations. Whenever using a model within the context of optimization, one must make sure that the resulting control is viable for the full state model. Fig. 11 shows the drag and turbulent kinetic energy histories for optimal control using DNS, LES and a hybrid of LES and DNS. In the hybrid approach, all optimization is performed on the LES model. Once the optimal control is computed on a given time horizon, the flow is then advanced using DNS with that control input. In this context, LES serves as a reduced-order model for use in optimization. As seen from the results in Fig. 11, the hybrid LES/DNS results are nearly identical to optimizing the full state model (DNS).

Taking advantage of the added efficiency of LES, Chang et al. [107] studied opposition control in a planar channel flow for Reynolds numbers up to  $R_\tau = 720$  which is 4 times higher than available DNS results [83, 87] and is large enough to be free of the most obvious low Reynolds

number effects [137]. Results from this investigation are given in Fig. 12 which shows the computed drag reduction for opposition control with changes in both the sensing plane location,  $y_s^+$ , and turbulence Reynolds number,  $R_\tau$ . The main conclusion is that as Reynolds number increases from  $R_\tau = 100$  to 720, drag reduction for the controlled flows drops from 26% to 19% indicating that opposition control is less effective at higher Reynolds numbers. To make matters worse, Fig. 13 plots the ratio of power saved, due to drag reduction, to power input to perform the control. Regardless of which measure of the power input [107], the ratio of power saved to power input reduces by a factor of 5 when  $R_\tau$  is increased from 100 to 720 making the conservative estimate of the power-saved to power-input only 10 at the highest Reynolds number. All additional loss mechanisms (mechanical and electrical) must still be accounted for. This example provides a good reminder that caution must be used in developing flow control strategies using low Reynolds number DNS while also indicating the important role of high-fidelity reduced order models, such as LES for flow control research. We expect LES, DES, and potentially hybrid LES/URANS (see Section 4.3.2) to play an even more important role as reduced-order models in free-shear flows where the distinction between large and small scales is greater.

### 3.4.2 Mathematical

Mathematical approaches to constructing ROM typically begin by selecting an appropriate set of basis functions. The flow-field is then formally represented by a linear combination of these basis functions and a Galerkin projection of the governing equations (e.g., the Navier–Stokes equations) for a truncated set of these basis functions is performed (see e.g., Holmes et al. [138]). In most cases, the basis functions only represent the spatial structure of the flow so that the Galerkin projection results in a set of coupled, nonlinear ordinary differential equations that must be solved for the temporal amplitude functions corresponding to each basis function. However, one can also envision circumstances where the basis functions may also include the temporal structure of the flow [e.g. Fourier modes for a (nearly) periodic flow] which would result in a coupled system of nonlinear algebraic equations.

It is important to realize that the steps outlined here are exactly the same as those typically done for many numerical discretizations of PDE’s including spectral methods and finite elements. As such, many of the same issues discussed in Section 4 including nonreflecting boundary conditions, turbulence (subgrid-scale) models, and small-scale actuator modeling must also be addressed in this context.

The key difference between traditional Galerkin discretizations and Galerkin ROM’s is in the selection of the basis functions. In a discretization method, the basis functions are typically chosen *a priori* such that the resulting numerical method has a desirable compromise between accuracy, numerical efficiency, and geometric flexibility. Conversely, basis functions for ROM are typically chosen *a posteriori* based on prior experimental or numerical data. The overriding goal in selecting a basis for ROM is to capture the relevant physics of a flow using the fewest number of basis functions thus leading to the greatest reduction in model size (i.e. the fewest number of equations and unknowns).

Before discussing specific examples, there are several key issues/questions that should be kept in mind: 1) How does one intelligently select a basis that captures *just* the important physics, 2) How should the influence of neglected scales/physics be accounted for, 3) How can a basis/model be adapted to account for changes in physics as a flow is controlled.

A classic example of a mathematical technique for ROM is the Karhunen–Loeve [46, 47] expansion or Proper Orthogonal Decomposition (POD) [45] as it is more commonly referred to in the fluid-mechanics community (see also Section 2.6). The POD constructs an orthogonal basis (often called POD modes) that are optimal in an energy ( $L_2$ ) norm. In other words, the POD modes can be ordered in terms of energy content, where the first POD mode contains more energy than any other mode and so on. The first few POD basis functions often capture a significant percentage of the flow energetics thus suggesting that a truncated POD basis may be a promising approach to constructing reduced-order models.

In the context of simple laminar flows, there have been several successful applications of POD based reduced-order models for flow control [139–141]. However, in these investigations the dimension of the original system was small so that a highly truncated POD basis was successful. For turbulent flows, where the inherent dimensionality of the system is large, the potential of POD for constructing reduced-order models is not as clear. However, the work of Lumley and colleagues [142] provides a link between low-dimensional dynamical systems and the dynamics of coherent structures, including bursts and sweeps in near-wall turbulent flows. The success of POD in representing the dynamics of near-wall flows has prompted the development of POD based reduced-order models (see *e.g.*, ref. [142–148]) that could be used in the context of turbulence control [64, 149].

One of the potential limitations of POD (and other related methods for ROM) is that the basis functions are intrinsic to a particular flow so that as a flow is modified by the action of control, the POD basis (and the ROM based on that POD) must also change. Thus, a reduced-order model constructed from a subset of POD basis functions for one particular flow, often taken to be the uncontrolled flow, would certainly not be optimal and may not even successfully represent the dynamics of the controlled flow under some circumstances [139, 140, 149–151]. This in turn calls for an adaptive POD basis for use in reduced-order models to prevent reductions in model effectiveness.

The recent work of Prabhu et al. [151] highlights the influence of two wall-boundary control strategies [opposition control ( $y_s^+ = 16$ ) which results in a 25% drag reduction and optimal control with ( $T^+ = 36$ ) which yields 40% drag reduction] on the POD basis for turbulent channel flow. Results from this study are given in Figure 14 which shows a highly energetic POD “roll” mode that is related to the counter-rotating streamwise vortical structures commonly observed in near-wall turbulence. Although the POD modes are, in general, complex valued, for roll modes the streamwise and wall normal components are purely real whereas the spanwise component is purely imaginary. For the roll-mode shown in Figure 14, the peak of the streamwise component occurs at around  $y^+ \approx 20$  for the no-control and  $y^+ \approx 30$  and  $y^+ \approx 43$  for the opposition control and optimal control flows respectively. This upward shift corresponds to the development of a so-called “virtual wall” in the controlled flows that is more clearly seen in Figure 15 which shows velocity vectors for the same POD mode in a crossflow plane for all three cases. A solid horizontal line is used to highlight the location of the “virtual wall” for the two controlled flows. While the large-scale features of the roll-mode shown in Figure 15 are unchanged by the presence of control, a close comparison does reveal subtle changes in the vector fields near the wall and these small changes are responsible for the drag reduction obtained for the two controlled flows [151].

The primary conclusion of Prabhu et al. [151] is that efforts to construct low-dimensional models based on POD are hindered by the fact that a POD basis is intrinsic to a given flow. For flows that employ less effective control strategies (such as opposition control), a low dimensional model

based on the no-control POD basis may perform adequately for small number of modes although model errors increase with increasing number of modes. Since POD captures the energetic structures pertaining to a given flow and control strategies either directly or indirectly manipulate such structures, the basis sets for each of the flows considered differ in the location and energy of the dominant structures. Hence, constructing reliable low-dimensional models for controlled flows by employing no-control POD eigenfunctions will require some form of augmentation to include the effects of the control. Further research is required to establish automated means of augmenting or altering no-control POD bases to use as ROM's for controlled flows. One such approach is based on an iterative improvement in the POD basis using the method of snapshots [139].

Recently, Du et al. [152] have begun work on centroidal Voronoi tessellations (CVT) which, similar to POD, can be used to construct an "optimal" reduced basis for use in ROM. While POD requires the solution of an eigenvalue problem the size of the number of samples in the reference database, CVT does not, making it potentially more tractable for large systems. Likewise, CVT is more amenable to adaptively changing the reduced basis which, as discussed above, is critical for flow control applications. Finally, CVT can be combined with POD and this appears to be an interesting research direction [153].

We conclude by returning to the key issues in ROM construction mentioned above. Selecting a suitable basis that somehow captures the important physics of a flow, while neglecting everything else, is a critical step. Proper orthogonal decomposition provides one means of doing so that is optimal in the energy norm. However, for many flows this may not provide sufficient model reduction. For example, to capture 65% of the kinetic energy in turbulent channel flows requires 500 POD modes [151]. Although this is a dramatic reduction in the total dimension of the system (an LES of this flow typically uses  $\approx 150,000$  degrees of freedom), it is difficult to build an efficient reduced order model based on global POD eigenfunctions that captures a significant fraction of the energetics for wall-bounded turbulence. Omurtag and Sirovich [154] have developed models for channel flow based on several hundred POD modes that do exhibit reasonable quantitative predictions of near wall dynamics but the size of these models still limits their use for real-time predictive control. Likewise, it is not clear that kinetic energy is the best (or only) measure that should be used to identify physically important modes in a flow. The BiGlobal instability modes discussed in Section 2.2 may provide a closer coupling to important physics in a flow. Likewise, bases derived for other norms (such as enstrophy) or local bases (constructed over a limited spatial region of a larger flow [151, 155]) may prove more useful in flow control applications.

Although we have already discussed the key issue of adaptive basis selection, an issue that we have not yet discussed is that of modeling neglected scales. The key idea of ROM is that one only explicitly carries important scales, which, of course, implies that many other scales of motion are neglected. While neglected scales may not directly contribute to physical processes (e.g., drag, mixing, and sound production) they indirectly influence these quantities through nonlinear interactions. This issue is at the heart of the classic turbulence closure problem and is the impetus for turbulence models in RANS and LES. When one uses a (highly) truncated bases for a ROM of a turbulent fluid flow, some form of model *must* be incorporated to account for the indirect influence of neglected scales. Unfortunately, much of the work in POD based ROM has not included a model for neglected scales and the ability of such approaches for large space-time domains is questionable. However, a promising approach to incorporating such models within a mathematical ROM approach is the variational multi-scale method originated by Hughes et al. [156, 157]. This approach naturally allows for separate models to be incorporated at different scales [158] and

preliminary applications to controlled turbulent flows have been promising [159].

### 3.4.3 Data Fitting

This final category for ROM's includes all methods that are constructed as "fits" to a high fidelity model<sup>2</sup>, be it an experiment or numerical simulation. Such methods are particularly attractive for applications with relatively few control variables, problems involving non-smooth dependence of the flow on control parameters (e.g., phase changes, shocks, and jumps to different attractors), and problems where physical models are unknown or unavailable.

A detailed review of all the possible data fit approaches is beyond the scope of this discussion. However, some examples of this approach applied to flow control systems include:

- System identification for transfer function estimation: Rapoport et al. [97, 98], Rowley et al. [101];
- Neural networks: Lee et al. [88], Faller et al. [160], Narayanan et al. [161], Faller and Schreck [162]; and
- Evolutionary algorithms: Koumoutsakos and Moin [163], Milano et al. [164].

Other types of data fitting methods include response surface construction using Taylor series, polynomial and spline interpolants/regression, and Kriging interpolation and these techniques have been used successfully in the context of ROM for engineering optimization [165].

### 3.4.4 Issues in Reduced Order Modeling

Regardless of the approach used to construct a ROM, a key issue is to strike an appropriate balance between model complexity and accuracy. This tradeoff often depends on the context in which a ROM is to be used. For example, one may accept a more complicated yet more accurate ROM for use in optimal design of a control system while a ROM for use in a real-time feedback control system will likely have to sacrifice accuracy for efficiency.

In many control applications, one can make use of a hierarchy of ROM's of varying accuracy/complexity with most predictions done using low fidelity models with infrequent "truth" evaluations with a high fidelity model. The use of a higher fidelity "truth" model is crucial to ensure that a control does not exploit a weakness in a low fidelity model. Rigorous techniques for using model hierarchies are available in the context of engineering optimization [166], and as such, are also available for optimal design of active flow controllers and this is an important area for future research.

Finally, for nonlinear systems, care must be taken to ensure that physical processes that are "approximated away" in a ROM are appropriately modeled. It may not be sufficient to naively truncate a representation (such as a POD basis) without modeling the indirect influence of neglected scales/physics.

---

<sup>2</sup>Statisticians refer to data-fit methods as "emulators."

## 4 Issues in Computational Fluid Dynamics

This section focuses on numerical issues (including discretization, boundary conditions, and modeling) associated with both baseline no-control and active flow-control configurations.

### 4.1 Background and current focus

In 1976, Chapman [167] showed a progression of Computational Fluid Dynamics (CFD) capability with time (Table 1). Using computer-speed forecasts, viscous time-averaged and time-dependent CFD were projected to be possible during the late-1970s and mid-1980s, pending the resolution of the noted limitations. More than 25 years after Chapman's projections, accurate time-dependent viscous calculations are possible only at low Reynolds numbers and on somewhat simplified configurations [168, 169]. At high Reynolds numbers, turbulence models are still required and some controversy surrounds accuracy and interpretation of the results in time-dependent flows in lieu of the inherent assumptions in the various turbulence models. Significant experience is required to obtain and interpret the CFD solutions, lending to the assumptions and limitations of any given code and methodology.

The challenge of CFD is now compounded with the introduction of active flow control technologies, whereby local (often large amplitude) actuation is employed for control. However, experimental data suggests that revolutionary performance improvements are feasible with time-dependent (often periodic) actuation. The potential of periodic actuation offers hope that current tools (with some further development) can be used to predict the performance benefits of active flow-control in the near term. In the long run, design tools will require time-dependent optimization capabilities to extend active flow control to complex engineering applications (see Section 3.3).

The design approaches that have led to the most common operational applications (e.g., aircraft) have coupled CFD analysis/design tools with considerable experimentation. Such empirical designs are extremely expensive, but have been necessary, given the inherent limitations of current computational tools. If active flow control technologies are to be applied to engineering applications, then design and analysis tools must be reliable, robust, and accurately capture the physics of the actuator-induced flow phenomena. Because of the inherent complexity of active flow control, some of what is discussed below is conjecture, based on experience, and will hopefully lead to some constructive discussions and useful guidelines for future active flow control activities. Some factual results are discussed for configuration-type issues in Section 4.9. Re-iterating from the introduction, this paper is not a review of all of many important contributions involving CFD and active flow control but rather an attempt to focus on several isolated issues in a rather comprehensive manner.

### 4.2 Methodology — uncertainty versus reality

Rarely are the Navier-Stokes equations directly solved but rather they are numerically modeled. It is the fidelity of this modeling that leads to the various high-level categories of tools for baseline analysis and for potential use in design and analysis of active flow-control. These categories include Reynolds Averaged Navier Stokes (RANS) equations, Large-Eddy Simulation (LES), Direct

Numerical Simulation (DNS). Recent investigations by Spalart [170], Israel and Fasel [171], Piomelli and Balaras [172] (to name only a few) clearly show that these distinct categories are beginning to merge into tools that take advantage of the merits of each category. Such tools are sometimes termed hybrid methods.

Whereas limitations of RANS reside in the turbulence modeling, one can easily show that DNS is currently limited to low Reynolds number flows and to a simple geometries. These limitations arise for two different but related reasons. By definition, DNS implies that all relevant time and space scales in the flow should be resolved. Turbulent flows have a range of scales that depend on the Reynolds number. If  $[U, L, T]$  represent the largest velocity, length, and time scales and  $[u, l, t]$  are the smallest scales, then the relationship [173] between the smallest to largest scales is

$$l = LR^{-3/4}, \quad t = TR^{-1/2} \quad \text{and} \quad u = UR^{-1/4} \quad (7)$$

The number of grid points (coupled with the choice of numerical method) typically dictates the computer memory required for DNS, where one can assume that the smallest scales can be represented with two grid points. The length scale in Eq. (7) refers to one-dimensional problems. Therefore, for the three-dimensional problems of interest in most applications, the grid would involve order  $R^{9/4}$  grid points. Even if/when the issue of complex geometry finds an acceptable working solution, the above Reynolds-number scaling remains the main obstacle, since DNS often involves unattainable memory and computational speed requirements. Concerning memory, 3D simulations of solar convection, for example, could require on the order of  $10^{30}$  grid points [174]. Concerning performance, some studies suggest that DNS could be attainable for flow past an airfoil ( $R \approx 10^8$ ) if Teraflop ( $10^{12}$  flops) performance is available and around a complete aircraft (in theory) if Exaflop ( $10^{18}$  flops) performance is available for the computation [174]. However, the simple estimation of computer requirements to solve all scales in a relevant turbulent boundary layer tends to suggest DNS will not be available (in the near term) for full configuration analysis [169]. Likewise, understanding the reliability and interpretation of such massive calculations remains a significant challenge even if one could run them.

Clearly, DNS is not currently practical at high Reynolds numbers and on full configurations. So active flow control computations must rely on various levels of CFD fidelity/modeling, depending on the physical phenomena of interest and may also require additional modeling and empiricism to achieve accurate active flow-control solutions.

### 4.3 Governing Equations

In the following, we focus on incompressible flows as a starting point for discussions related to active flow control. Of course, active flow control for high-speed, compressible flows; chemically reacting flows; and even flows of complex fluids is certainly of interest in engineering applications. However, many of the key issues in modeling active flow-control systems can be discussed in the simpler setting of low-speed, incompressible flow of Newtonian fluids and, where appropriate, we comment on issues related to more complex flow systems.

The incompressible Navier-Stokes equations can be written with the primitive variables (velocity and pressure), velocity and vorticity, streamfunctions and vorticity, or streamfunctions. As such, the number of unknowns equals the number of equations and the posed equations can be solved in either a deterministic or a non-deterministic manner. The equations can be spatially

averaged to decrease computational cost, yet the averaging process yields a system with more unknowns than equations. Hence, the unclosed system requires a model (e.g., turbulence, or subgrid scale) to make the problem well posed. Such models are used in Reynolds Averaged Navier-Stokes (RANS) and Large-Eddy Simulation (LES) approaches to CFD.

### 4.3.1 RANS approach

Typically, the closure problem is mitigated using zero, one or two equation models for the Reynolds or turbulence stress terms in the equations. Many productive models are available and are required for production-type CFD applications (e.g., automotive, aircraft, engine, etc. analysis). These models are validated, or rather calibrated, for specific classes of flow problems and typically are deficient when the flow conditions are outside the range of calibration. Further, significant scatter in the various turbulence models occurs and is problem dependent; significant variation in the computational cost for the various turbulence model occurs because of the model cost, numerical instability, and complexities in the application (flow fields) [175]. However, in all fairness to the turbulence models, implementations, coding, grid quality/density, and evaluation practices add to potential uncertainties in the RANS approach [176].

Taking active flow control into account, many additional issues arise that have not yet been fully addressed. Some of these include:

- Must higher-order moment terms be modeled and used for closure for separated flows? Slomski et al. [177] have shown that full Reynolds stress transport models are required to match experimental trends for the relatively simple application of steady-blowing Coanda circulation-control. Two-equation models (perhaps serendipitously) provided proper trends with low blowing mass coefficients ( $C_\mu < 0.1$ ), but drastically failed with moderate to high blowing coefficients ( $C_\mu > 0.1$ ). Presumably, the allowance for anisotropic stresses in the full Reynolds stress transport equations enabled a reasonable agreement in the trends with experiments. However, this presumption has not been verified by analyzing the stresses.
- Typically, 2nd order spatial and 1st or 2nd order temporal methods are employed. Are 4th or higher-order spatial methods and 2nd or 3rd order temporal methods required for the practical simulation of dynamic, time-dependent flows given current computational resources? Carpenter et al. [178] did a thorough analysis of the order of numerical schemes toward unsteady CFD and flow control. Higher than 2nd order methods were clearly argued as necessary to achieve the Reynolds numbers of interest to most applications and to accomplish the computations within a reasonable wall-clock time budget.
- Is local automatic grid adaptation effective to resolve the time-dependent dynamics in the flow in an efficient way? With vortices being shed in a dynamic manner from the configuration or actuation system, some grid manipulation would most likely be required when three-dimensional configurations are being considered. This adaptation figures into cost effectiveness issue in active flow control.
- Should the current numerical methods be abandoned in lieu of alternative approaches (e.g., vortex methods, if all above issues are answered positively)? This is a controversial question with strong opinions in the various groups on this issue. Likely a hierarchy of methods

is required with design/optimization performed on low fidelity models and relatively few evaluations of high fidelity models which serve as "truth" models. See Sections 3.4 for further discussions along these lines.

Two attractive elements of the RANS approach include: (1) many production-type codes exist within the various applications industries and (2) solutions of (even unsteady) cases can be cost-effective. But the key open issue remains: do current implementations of the RANS approach work for AFC?

### 4.3.2 LES approach

For LES, the governing equations involve spatially filtered variables instead of the temporally averaged dependent variables commonly used in RANS. As such, the solution strategy seeks to resolve the unsteady large-scale "structures" of the flow and model the small-scale Reynolds stresses with a subgrid scale (SGS) model. A variety of different models exist and the reader can refer to Piomelli [67] for a discussion of LES and SGS models. These models have been used to varying degrees of success for many applications. However, there are many unresolved questions concerning the LES approach:

- Will grid resolution near the actuator approach DNS?
- Many codes use 2nd order spatial methods for discretization. Are 4th or higher order spatial discretization effective for efficient simulation of active flow control given limited computational resources?
- Are hybrid LES/RANS methods useful to achieve affordable solutions whereby hybrid suggests some portion of the flow uses LES and some portion uses RANS? The transition from LES to RANS methodologies is currently under development and Spalart [170], Israel and Fasel [171], Piomelli [179] discuss hybrid approaches. This hybrid approach would typically use RANS or a wall function near the wall and LES to capture some desired unsteady structures away from the wall (e.g., wakes or vortex shedding). However, this concept seems to contradict an inception goal of LES. Namely, LES was "sold" to remove RANS limitations near the wall so that near-wall unsteady physics could be computed. Such is particularly important for studies of acoustical (noise) source prediction in the near-field of a configuration. Furthermore, linking the LES-RANS interface is non-trivial. For example, transitioning a RANS region to a LES region in a boundary layer in a wall-normal plane is as yet unproven. Essentially, the RANS serves as an inflow boundary condition to the LES region.

### 4.3.3 DNS approach

The direct numerical simulation (DNS) method denotes solutions of the Navier-Stokes equations with all space-time scales resolved. For linear hydrodynamic instability studies, there might be only a few scales of interest whereas, for the nonlinear transitional regime and fully turbulent flows, there are many orders of magnitude difference in the scales. Joslin [168] highlighted the many issues that may impact DNS for active flow control of transitional boundary layers. Most of the covered issues, including boundary conditions, numerical issues, and active flow control approaches, apply directly to the current discussion. Some of these issues include:

- Are full or disturbance equations formulations “better?”
- Should rotational, divergence, skew-symmetric, or convective forms of the equations be used?
- What order of numerical approximation is sufficient to capture the necessary features of the flow?
- Is it rational to use a temporal DNS approach for active flow control when an actuator is involved in the control?
- Can dissipative (i.e. upwind or stabilized) methods be used, or must numerical methods achieve exact, discrete kinetic energy conservation?

*We conjecture:* Probably 4th order spatial accuracy with 3rd or 4th order time-marching methods in a spatial DNS approach will be required to capture sufficient physical phenomena of the flow control problem given current computational capabilities. The temporal approach will have little utility in oscillatory control problems where the spatial and temporal content are both important near the actuator location.

## 4.4 Initial Conditions

In this section, initial conditions are discussed for RANS, LES, and DNS. Typically, there are two forms of initial conditions for simulations of active flow control studies. The first involves initializing the base flow to an equilibrium condition while the second initiates the actuator for control and both are discussed below.

### 4.4.1 RANS/LES initial conditions

For RANS and LES methodologies used for full configuration flow fields (albeit at different Reynolds numbers), the initial (pre-actuation) conditions can be a variety of free-stream like conditions. The codes are then run until an equilibrium flow state is reached and the residuals of the equations drop several orders of magnitude. The steady or statistically stationary flow-state then serves as the initial conditions for active flow control simulations. The alternate is starting from  $t = 0$ , prescribed free-stream conditions are set as the initial condition for active flow control simulations. Currently, no study suggests converged solutions are obtained “quicker” in one set of conditions over the other. Here attention of the reader must be drawn to the related issue of the role of the BiGlobal/TriGlobal eigenspectrum in recovering steady or stationary basic states [180]. Furthermore, the transients are likely very different in the two different simulated flows.

### 4.4.2 DNS/LES initial conditions

The simulation can begin at time  $t = 0$  with no initial condition or an analytical approximation to the steady-state solution. Then at time  $t = t + \Delta t$ , disturbances can be forced at the inflow.

Care must be taken so that the actuators are not located too close to the inflow boundary to prevent unwanted interaction between the actuator input and the inflow boundary conditions. For

example, one (unpublished) study attempted to investigate an actuator-induced flow with oscillatory excitation. Because the actuator was too close to the upstream inflow, an unphysical interaction between the actuator and the inflow led to spurious disturbances far from the wall, yet near the inflow. These numerical disturbances then evolved in the flow as though they were physical. Care must be taken in the selection of inflow and actuator locations as well as the imposed conditions.

## 4.5 Wall-boundary conditions

The boundary conditions for RANS/LES/DNS applications most often used at the wall are

$$u, v, w = 0 \quad \text{at} \quad y = 0 \quad (8)$$

In theory this ensures a no-slip condition on a wall; however, in practice it can be quite difficult to ensure a divergence-free flow and no-slip on the wall simultaneously, as such a slip velocity may develop for some time-marching algorithms. For DNS/LES, using a Taylor series correction technique [181], this slip velocity can be minimized (or reduced). For actuator-induced boundary conditions, the order of accuracy may no longer be higher order, unless some corrective technique is introduced for the actuator models.

## 4.6 Free stream conditions

The far-field computational boundary must be sufficiently far from the wall so that free stream conditions can be enforced without artificially contaminating the solution within the domain for all three methods and their hybrids.

## 4.7 Outflow conditions

The rational use of outflow treatment differs between RANS and DNS/LES and each are considered individually below.

### 4.7.1 RANS outflow conditions

For RANS, the grids traditionally extend many body lengths downstream, with ever expanding grid sizes. With the current lower order methods and large grid spacing, excess dissipation exists to suppress the flow structures near the outflow boundary.

### 4.7.2 DNS outflow conditions

Joslin [168] highlighted a host of outflow boundary conditions that have been used with DNS/LES, so this discussion will not be repeated here. Summarizing, typically a buffer or sponge region is appended to the physical region of interest and disturbances are “prevented” from reflecting off the outflow location [168]. With care, such conditions are quite effective for most problems of interest. With the introduction of actuator-induced effects, there is no reason to doubt that these outflow treatments will be other than satisfactory.

## 4.8 Actuator modeling

Aerodynamic design and integration have a whole new set of challenges with the introduction of unsteady flow control. One of these challenges is modeling the actuator-induced flows for implementation as simplified boundary conditions. The alternative would be coupling a structural finite-element model of the actuator to the CFD code or fluid model [182].

Consistent with oscillatory actuation, unsteady suction and blowing through the wall can be modeled as a simple analytic function. Often, this approach is used as a harmonic-source generator. An equal amount of mass injected by blowing can be extracted by suction so that no net mass is added. Although the disturbances may be generated by random frequency input, disturbances of interest can also be forced with known frequencies. Essentially, this disturbance generator is a modification to the no-slip boundary conditions that are conventionally used for the wall condition in viscous flow problems. An example of a simple boundary condition is

$$\mathbf{v}_w = A \sin(\omega t) f(x) \left( \sin(\phi) \hat{i} + \cos(\phi) \hat{j} \right) \quad (9)$$

where  $\mathbf{v}_w$  is the velocity vector at the wall,  $\omega$  is the frequency of the disturbance of interest,  $\phi$  is the angle of injection, and  $f(x)$  is the spatial profile. In early studies,  $f(x)$  was assumed to be a half-period sine wave with a shallow injection angle used to generate an oscillatory wall-jet with only one temporal frequency forced. Although these choices are somewhat arbitrary, in practice they seemed to work rather well. In three-dimensional simulations, the spanwise extent of actuation may be an infinite slot/strip or a fixed length actuator [183]. For small amplitude forcing, this velocity forcing can mimic the motion of a physical diaphragm [184]. However, the often used Neumann boundary conditions for pressure may require modification on the actuator region due to the unsteady imposed velocity conditions.

For oscillatory control, Kral et al. [185] have shown that a turbulent-like jet can be induced using such simplified boundary conditions. By replacing the no-slip condition on the actuator region with an analytical boundary condition, the RANS solution showed a good match with experiments and suggested a first order suitability for zero-net-mass oscillatory excitation and synthetic jets.

One might expect from looking at the many design parameters of oscillatory actuators, that the flow exiting the actuator opening (slot or hole) could be much more complicated than Eq. (9). A more recent study [186] clearly shows that the velocity profile induced with these types of actuators is a function of the actuator operating parameters and configuration parameters. The profiles can be very different than a simple half-sine profile but the *major* change occurs due to the interaction of the actuator-induced flow with the external flow; this case has not yet been thoroughly documented experimentally nor its importance on differences between experiments and computations. For example, shown in Fig. 16 are exit peak velocity profiles with varied lip thickness for a particular actuator concept. Some questions that need to be answered for active flow actuator-induced flows include:

- Can the actuator modeling be decoupled from the CFD analysis? Specifically, can mathematical models for actuators be developed using bench-top laboratory experiments and introduced as boundary conditions or source terms for the CFD? Or, is the actuator-induced/boundary layer fluid coupling required to capture the flow phenomena? The RANS results given by Joslin et al. [187] serve to provide some evidence that neglecting some seemingly insignificant features of the application (i.e., experiment) can lead to irresolvable discrepancies in CFD/EFD comparisons.

- What are the CFD requirements for oscillatory flow control? This was addressed (yet not resolved) in Section 4.2.
- What exit velocity profiles lead to optimal performance benefits (e.g. profile, time variation, non-zero mass flux as well)?
- Can analytical or empirical boundary conditions be “designed” for simple CFD implementation (or what minimum actuator parameters are required for CFD)? More specifically, do we know sufficient information about the many types of oscillatory actuators to determine the common important parameter selection? Some of the more obvious parameters include mass flow coefficient, angle of injection, and injection/free stream velocity ratio. However, what are the optimum injector lip shape characteristics, does the driving mechanism (e.g., mechanical vs electromaterial) change the observed induced flow, can different induced vibration or acoustics impact the flow, etc.?
- Are the optimal parameters (e.g. lip thickness) common to all oscillatory actuators? For example, is it clear that thicker lips generate more developed velocity profiles for all actuator designs?
- Must the exit be an adjustable opening (size, shape, angle, etc)? Namely, can the actuator be designed for primarily point-design operational conditions? The answer is probably application dependent but would, in most cases, require adjustable opening capability.

In addition to questions concerning the zero-mass-flux oscillatory momentum generator, one should also question the functionality required in a numerical fluid solver. Unsteady actuation assumes time-resolution in the numerical schemes. Even though Kral et al. [185] showed that the actuator-induced flow using RANS was in good agreement with experimental data for mean flows, one cannot assume that the RANS methodology will be adequate for oscillatory control. Specifically if the dynamics of the boundary-layer/actuator-induced flows is dominated by the turbulence and not an instability mechanism, then either RANS will not achieve the prediction correctly, the results will be happenstance, or the modeling parameters will need to be adjusted to account for the new turbulence characteristics.

## 4.9 Configuration Issues

In this section, we focus on the issue of configuration fidelity. This topic is common to DNS, LES, and RANS and therefore, we simply address the topic without subsections. Furthermore, this section is relevant to any comparison between experimental and computational solutions.

Specifically, how well does the computational model of the configuration of interest mimic the model used in the experiments? Broadly speaking, how well does the entire computational approach mimic the experiment? This question is the crux of whether the computed baseline (no control) analysis matches (or fails to match) the experimental data; therefore, a considerable portion of this discussion will be devoted to this subject. Issues to consider include:

- fidelity of model geometry
- fidelity of wind tunnel geometry

- flow tripping (transition)
- model surface roughness, waviness, discontinuities (transition and separation)
- free-stream turbulence levels
- pressure gradients
- turbulence models

A significant effort was expended on resolving the above issues [187, 188] comparing RANS solutions with the two Seifert and Pack [189] experimental data sets. In this section, we summarize the key findings of those studies concerning configuration fidelity in the absence of control.

#### 4.9.1 Model 1

Figure 17 shows the leading edge and trailing edge regions of the configurations used in the Joslin and Viken [188] study. The mid-chord regions for all airfoils are the same and therefore not shown in Fig. 17. A NACA0015 airfoil is used in the study to provide reference point results. The finite thick trailing edge of the NACA0015 airfoil matches the TAU0015. The TAU0015 airfoil model was tested in a low-speed wind tunnel at Tel-Aviv University (TAU). The model is a NACA0015 airfoil modified in the leading-edge region to accommodate an actuation slot. The airfoil had an additional slot at the flap shoulder,  $x/c = 0.75$ . Hence, the airfoil configuration is referred to as the TAU0015 airfoil. The TAU0015 model had a 0.3645 m chord, a 0.3% thick blunt trailing edge, and a 0.4% chord thick notch at 76.6% chord that results from the flap/main element connection used in a different experiment. The actuation slot for the TAU0015 tests was located at the leading edge and results in a 0.3% chord discontinuity (shown as a straight horizontal line region in Fig. 17). The modified TAU0015 (or TAU0015m) airfoil neglects the mid-chord notch and smooths the discontinuity at the actuator so that a structured-grid solver can be used for the analysis [190, 191].

The Full Unstructured Navier-Stokes Two-dimensional RANS code (FUN2D) [192, 193] was used with the Spalart-Allmaras (SA) turbulence model [194] and fully turbulent flow. The unstructured grids were generated using advancing-front point-placement with iterative local re-meshing for grid quality improvement [195, 196]. A fine grid was first used to determine the effect of the geometric discontinuities on the aerodynamic performance. The internal actuator cavity was not considered for this study. The experimental conditions have Mach number  $M = 0.15$  and chord Reynolds numbers of  $R = 1.2 \times 10^6$ .

Figure 18 shows the computed lift coefficient ( $C_l$ ) with variation in angle of attack ( $\alpha$ ) for the NACA0015, TAU0015, and TAU0015m airfoils compared with the experimental data. For the NACA0015, the maximum  $C_l$  and stall angle are 30% and  $4^\circ$  higher than the experimental data, respectively. For the TAU0015m airfoil, the maximum  $C_l$  and stall angle are 23% and  $2^\circ$  higher than the experiments. These over-predictions for the TAU0015m airfoil are consistent with earlier studies [141, 190] that used the same airfoil but a structured grid and two different RANS codes. In closer agreement, the computed results for the TAU0015 airfoil approach the experimental results, overestimating the stall angle by  $2^\circ$  and the maximum  $C_l$  by 9%. So the subtle differences in geometry for the NACA0015, TAU0015m and TAU0015 airfoils lead to large differences in the computed stall  $\alpha$  and maximum  $C_l$ .

No pressure spikes were measured in the wind-tunnel experiments because no taps could be positioned on the actuator. Therefore, the experiments could not capture the additional pressure spike predicted in the computations. Based on this understanding of the experimental data, the computed  $C_l$  were calculated by integrating the pressure over the TAU0015 airfoil at points consistent with the experimental pressure tap measurements. Only the contribution from the leading-edge actuator discontinuity is excluded in this recalculated  $C_l$ . The latter  $C_l$ - $\alpha$  curves are compared with experimental data in Fig. 19. The computed maximum  $C_l$  is now over-predicted by 2% compared with the experimental data and the stall  $\alpha$ 's are in agreement at  $12^\circ$ .

A comparison of the results from the various airfoil configurations suggest that the mid-chord discontinuity does not affect the aerodynamics of the wing in a meaningful manner and can be ignored for more efficient computations. Based on the later analysis of Joslin et al. [187] discussed hereafter, the mid-chord discontinuity is probably important when the separation point starts from the trailing edge and approaches this region. The leading-edge discontinuity significantly affects the maximum lift performance; hence, the integrity of the leading-edge notch discontinuity must be maintained in the computations to achieve a good match with the experimental data.

The analysis of computed performance versus experimental data for the TAU0015 airfoil demonstrated that consistency in determining lift and drag coefficient quantities was important to achieve quantitative agreement. The integration of computed pressure should be constrained to regions of the airfoil consistent with the pressure taps.

#### 4.9.2 Model 2

Using a different configuration (shown in Fig. 20) described by Seifert and Pack [189], Joslin et al. [187] used single-block, multi-block, and Chimera structured and unstructured Reynolds-Averaged Navier-Stokes solvers and various turbulence models to compare computed results with the baseline and flow controlled experimental results. The results clearly showed that the fidelity of the complete experimental setup and numerical model are important in order to reproduce the experimental results. In this section, most of the results are new and were not included in the previous study by Hammond and Redekopp [19]. All the current results use the compressible CFL3D [197] RANS code with the Mach number fixed at  $M = 0.2$  to approximate an incompressible flow. Initial comparisons use the Spalart-Allmaras turbulence model with second-order time advancement and second-order spatial discretization.

For the initial analysis, the NACA/flap configuration was studied in a free stream environment using a single-block grid that extended 10 chord lengths around the airfoil. Figure 21 shows the total and near-airfoil region of the grid. For this C-grid, two grids were used to assess grid invariant solutions. First, 197 nodes around the airfoil and 81 nodes in the normal direction were used for the computations. Then, a  $385 \times 161$  grid was used. The coarse grid was insufficient to resolve the flow and only the fine-grid results are presented here. It is recognized that the trailing edge and actuator region may be under-resolved; however, part of the goal of this study is to assess minimum grid resolution requirements for both the baseline (no control) and flow control cases.

Figure 22 shows the variation of the lift coefficient as the number of iterations in the flow solver increases for  $R = 8 \times 10^6$ . The solutions quickly converge to equilibrium oscillatory states. The timestep was set sufficiently small so that over 80 time steps per period resulted; hence, the time evolution of any unsteadiness of the shedding process was resolved. The experimental measurements showed that the flow was unsteady on the airfoil as well, but there were no dynamic

balance measurements to directly compare this unsteady behavior.

Finally, pressure coefficients are compared in Fig. 23 for  $\alpha = -4^\circ$ . Surprisingly and quite happenstance, the computed baseline pressures are in close agreement with the oscillatory control results. This comparison leads to some questions and some observations. The computations must then under-predict the separation point because the affect of control is to suppress/delay this separation. Missing the separation point dramatically impacts the incorrectly computed global pressure field and subsequent enhanced lift and circulation. For the experiments, oscillatory injection caused a spike in the pressure (as one might envision). Could neglecting the actuator cavity in the computations lead to this spike in the baseline (no control) computations?

Next, a multi-block grid treatment is used with local enrichment where high-gradient flow conditions exist and the configuration is placed in the tunnel as in the experiment. Inviscid conditions are enforced on the walls of the tunnel and constant enthalpy and entropy are forced as inflow conditions. Figure 24 shows the multiple blocks configured in the tunnel with attention paid to the key geometric features (actuator, hinge, and trailing edge) and Table 2 lists the grid density in each block.

For  $\alpha = 0^\circ$ , residual history and lift coefficient convergence are shown in Fig. 25 for  $R = 17 \times 10^6$  and  $R = 28 \times 10^6$ . The lift is principally independent of Reynolds number in the simulations and a steady flow field is observed. Although the experiments found such Reynolds number independence, the experimental measurements found that the flow was highly unsteady. In retrospect, perhaps viscous boundary-conditions are required on the wind tunnel walls, or numerical dissipation suppressed the unsteadiness, or the inflow/outflow boundary conditions may not properly capture the unsteady flow phenomena for this compressible flow.

Figure 26 shows, using streamwise velocity contours, that the upper surface of the airfoil configuration is impacted by the close proximity of the wind tunnel wall. An increase/decrease in angle of attack would have more coupling to the wind tunnel walls. The flow separates over the flap region. So the flow features look qualitatively realistic, as expected.

Figure 27 shows a comparison of airfoil pressures distributions using the Spalart-Allmaras [194], Baldwin-Lomax [198], and  $k-\omega$  [199] turbulence models. As anticipated, the computed solutions show only small variance with the choice of turbulence model (and Reynolds number [188]) and do not resolve the discrepancy between the computational and experimental results, similar to a previous study [175] for a wing configuration.

The computed baseline results were in poor agreement with the experimental results. As indicated above, issues like tunnel walls and turbulence models were considered and found to have small impact on the computational results. The most likely cause for this disagreement is associated with differences in the process of flow separation on the flap, significantly impacting performance due to a global change in the pressure field and circulation. Very high grid resolution is required near the airfoil/flap junctures points and at the trailing edge region to resolve the separated and wake flow regimes. To further study this issue, the unstructured approach [192, 193] was used to explore the issue of configuration fidelity.

The original geometry for the NACA0015/flap configuration had a small discontinuity at the airfoil/flap juncture associated with the actuator. To simplify the structured grids, this discontinuity was “faired over.” However, because the unstructured approach can easily resolve discontinuities, the analysis was repeated to examine the impact of this discontinuity on the flow.

Figure 28 shows the flap region of the mesh with the discontinuity evident at the airfoil/flap juncture on the top of the configuration. An additional 11,000 nodes are introduced because of the

inclusion of the juncture discontinuity. The notch geometry was constructed from actual model QA measurements. In retrospect (again), this notch does not truly represent the actual geometry as discussed later. Here, we simply attempt to gain an understanding of the importance of a discontinuity on the separating flow properties, noting that all existing high lift system posses certain similar discontinuities.

Streamwise velocity contours are shown in Fig. 29 with and without the juncture (notch) discontinuity. Without the notch, the flow separates from the flap at 86% chord and a re-circulation region is observed. By resolving the flow with the notch at the airfoil/flap juncture, the flow is significantly affected by this notch with separation now occurring at 73% chord. However, a comparison of the pressure coefficients in Fig. 30 suggests that the changes in the flow field resulting from the notch cannot fully explain the significant differences between the computational and experimental results.

The notch at the airfoil/flap junction changes the separation point by over 10% of the chord length. This suggests that some portion of the actuator must be accounted for in the CFD analysis. As per the actuator questions in Section 4.8, how much of the actuator geometry is required for an accurate analysis? This answer has not been fully resolved in this discussion. The final RANS analysis involves changing the actuator characteristics to create a channel into the airfoil, in an attempt to come closer to the experimental configuration. Streamwise velocity contours are shown in Fig. 31 for this configuration. Clearly, the separation process has changed considerably compared with Fig. 29. Based on results of Lee and Goldstein [186], we now clearly know that more details of the actuator must be carefully included in the computational analysis. In retrospect, detailed measurements of the model and interior actuator geometry are likely required to develop adequate computational models for active flow control configurations.

## 5 General Concepts with Experimental Notes

This section of the paper discusses several issues related to active flow control (AFC), with emphasis on experimental issues, including two generalized approaches, e.g. a generic AFC process and an AFC roadmap, with detailed illustrative examples. Naturally and conveniently, the majority of the experimental examples originate from the authors' work to facilitate the discussion of key issues.

Active flow control with specific emphasis on utilizing flow instability to enhance effectiveness, could lead to significant advantages over traditional, steady state, design methods (see e.g., [7]) and reduced emissions. The latter are hard to quantify economically, but the environmental impact is qualitatively clear. McLean et al. [200] evaluated different AFC concepts and candidate applications were considered for civil jet transports. The simplification of conventional high-lift systems by AFC was identified as a prime candidate, possibly providing 0.3% airplane cost reduction, up to 2% weight reduction and about 3% cruise drag reduction (the added 1% was due to the elimination of the large, drag producing external flap hinges and positioning actuators). This systems study was conducted with retrofit as a means to apply AFC; whereas the maximum benefits come from system integration of AFC during the design phase of an application. Experimental work on these benefits is on-going [201].

The low end of the Reynolds number range also provides opportunity for the utilization of AFC. Lifting surfaces perform very poorly below a chord Reynolds number of  $10^5$ , where natural transition does not take place and cannot be utilized to maintain an attached boundary layer at high incidence. Periodic excitation was demonstrated to be extremely effective at maintaining attached boundary layer flow on the flap and therefore in generating high-lift as the Reynolds number decreased [7]. Its effectiveness was compared to boundary layer tripping by roughness, placed close to the deflected flap leading edge (as shown in Fig. 32). Boundary layer tripping was found to be effective only at a very narrow range of Reynolds numbers, while AFC effectiveness was not reduced at a flap-based Reynolds number of  $R = 0.35 \times 10^5$  (the flap chord was 25% of the airfoil). AFC can also provide flight control and propulsion at low Reynolds numbers, eliminating the need for any movable parts in a Miniature UAV (MAV) [202].

In the following sections, a generic flow control process for AFC will be discussed where the objective is to alter a flow state to achieve a more desirable state. A detailed discussion and examples of the uncontrolled flow state, actuation, receptivity, instability, interaction, sensing and control mechanism will be provided.

A generic AFC roadmap (a-la Morkovin [9]) will be suggested and a preliminary roadmap for delay of boundary layer separation will be presented and discussed. All roadmaps should include a clear target, in flow physical terms; concrete methods to obtain the task; tools needed to enable progress along each route; and an indication of the Technology Readiness Level TRL for each tool along each route. Researchers are encouraged to construct and publish roadmaps for their applications which should prove helpful for industry, funding agencies, and academic activities, each with its special needs and interests. The identification of fundamental scientific and technological challenges is essential for the effective performance of AFC Research and Development (R&D), as is the identification and indication of resolved issues. A helpful roadmap should identify the critical path for each route and the easiest route to obtain the target, at a given point in time, and should be updated periodically.

An attempt should be made to present and discuss limitations and report "what did not work"

and preferably why (where understanding exists), since the reporting of “failures” (i.e. when the researcher did it all “right” but the system did not respond as expected) is where the community can learn, perhaps more than from the so often reported “successes.”

## 5.1 A generic process for AFC

A suggestion for the structure of a generic process for AFC is shown in Fig. 33 and will be discussed in this section. Every flow control process is initiated at a certain flow state. The state could include an undesired steady state or a development path the technologist would attempt altering. Knowledge must exist about the state of the system prior to even deciding if, what and certainly how anything should be altered. The system state, either using local indicators or global parameters should be evaluated using sensors. Inherent uncertainty always exists in the “knowledge” of the system state. Once the state is “known” decisions must be made as to what needs to be altered. The “how” and “where” comes next. Imagine we are equipped with a complete spectrum of actuators, with sufficient control authority and the ability to place the actuators everywhere — we are in a limbo. Guidance could come from techniques such as optimal control theory (Section 3.3) with proper human input, but the computational cost of such an approach is high and considerable research is required to extend optimal control theory to relevant conditions. However, it is often the case that the researcher has an actuator that barely performs under certain limited operating conditions, it is so large it can fit only in one location in a model and the expected control authority is marginal. Still it “has” to work! If not for such determined individuals and milestone demonstrations, AFC would have not become as highly studied and as close to being applied as it is today. The typical situation is somewhere in between these two extremes.

Once the setup (experimental or numerical) is ready, and the baseline flow is known, the actuator can be turned on. The choice of the frequency, amplitude, phase, waveform and 3D distribution of these parameters will be discussed later. Many types of actuators exist, and for any type, it is crucial to evaluate the actuator’s performance without the presence of the baseline flow and later to quantify the effect of the external/core flow on the actuator’s performance. Figure 34 presents results from a numerical simulation of the interaction of a boundary layer with an oscillatory momentum generator [203]. The calculation included the external and cavity flows and concluded that the interaction between the two is crucial to accurately model the system.

Surface mounted, mechanical actuators, rely on the interaction with the incoming boundary layer to generate the excitation. An experiment utilizing ten, segmented Piezo benders (i.e. cantilevered plates) across the 609mm span of an IAI Pr8-SE airfoil (Fig. 35) was performed and reported by Seifert et al. [204]. The amplitude and phase of the benders was individually controlled, and a cross section and top view of the installation is shown in Fig. 36. Several points are worth mentioning. The fluidic outcome of the mechanical actuator, interacting with an incoming turbulent boundary layer is limited by the available reservoir (i.e. the mean shear). The peak actuator tip velocity is negligible compared to the fluidic velocities required for flow control. Figure 37 demonstrates that the peak RMS velocity fluctuations close to the wall is about 20% when the actuator’s tip amplitude was about 3mm, spanning the entire high shear region of the incoming TBL. An interesting feature that was utilized in the course of the latter investigation was the operation of the actuators out of phase (i.e. 180 degrees apart from each other). This mode of operation was found to consume only 25% of the power required to operate all actuators “in phase,” presumably due to compression of the cavity air under the actuators (Fig. 36) that assists the upwards

motion of every second actuator as its neighbors are moving down. The resulting lift-drag ratios are presented in Fig. 38, showing that the two-dimensional (2D) mode is slightly superior to the three-dimensional (3D) mode (i.e. operation in 180 degrees phase shift) in terms of aerodynamic performance. However, the fact that the generation of the 3D mode consumed only 25% of the power, led to an earlier achievement of larger than unity “Figure of merit”

$$F.M. \equiv \left[ \frac{LU_\infty}{DU_\infty + P} \right] / \left[ \frac{L}{D} \right]_{\text{Baseline}}, \quad (10)$$

where  $P$  is the power provided to the actuators (see Fig. 39). A value of  $F.M. > 1$  indicates that it is more energy efficient to introduce power to the actuator than to the powerplant. Besides the important applicability aspect, the fundamental nature of the 3D interaction between the multiple modes of excitation resulting from the complex actuator motion indicates the importance and relevance of studying 3D modes of instability to enhance AFC effectiveness and efficiency. Margalit et al. [205] also cites  $F.M. > 1$  data using Piezo actuators applied to control the flow over a delta wing at high incidence.

The process in which the actuator’s fluidic, acoustic and/or mechanical output is translated into flow properties at a certain downstream distance (that is difficult to determine in general) from the actuator is termed *receptivity*. (When comparing experimental results to linear stability theory calculations this determination seems easier, since the end of the receptivity dominated region would be the beginning of the good agreement to LST). The desire is to replace the actuator by a “black box,” both in space and in action, that could be modeled and later plugged into a low-order model for further analysis (be it theoretical, numerical or experimental). The linear receptivity of a boundary layer to a wide range of input disturbances was and still is extensively studied (see e.g. [206, 207]). The issue under discussion here is more complex because the input amplitudes are order 0.1 to 1 (with respect to a typical undisturbed base velocity), and therefore nonlinearity may play an essential role. (Earlier work that relied on receptivity of acoustic excitation for the control of separated flow is discussed by Greenblatt and Wygnanski [6] and Halfon et al. [208]). However, appropriate linear theory can still be extremely helpful in identifying the most receptive location in the flow and the mode(s) the flow is most receptive to.

Caution should be exercised when characterizing the actuators output, which serves as input to the receptivity process. There exists a range of options for characterization of the oscillatory momentum input to the boundary layer.

In the following example, Nishri [209] demonstrated that neither the wall normal distribution or the RMS of the imposed excitation are sufficient to describe the excitation. Instead, one should study the spectra, even in the case of harmonic excitation, due to inherent nonlinearities. A comprehensive set of experiments was performed on a “generic flap” (Fig. 40a). This set-up consisted of a flat plate on which a tripped turbulent boundary layer developed. A hinged flap allowed imposing a controlled adverse pressure gradient and introducing periodic excitation, using either mechanical or fluidic excitation, at the flap hinge. Figure 40b presents the minimum momentum coefficient  $C_\mu$  required to reattach the separated flow over the “generic flap” experiment, using either fluidic or mechanical excitation with the same integral  $C_\mu$ . The results shown in Fig. 40b indicate that the minimum  $C_\mu$  is identical but the most effective  $F^+$  is significantly lower for the mechanical excitation. A careful evaluation of the mechanical versus the fluidic excitation spectral content (Fig. 40c) at the harmonic ( $2F$ ) of the excitation frequency reveals that the mechanical disturbance

has an order of magnitude higher activity at  $2F$ . This could partly explain why the mechanical excitation is effective at roughly half the threshold frequency compared to the fluidic excitation.

After *receptivity*, the next phase in transition is typically *instability* and we will make two points with regard to flow instability. First, linear stability theory (LST) may have a role to play in identifying instability modes of the modified state as well. Incorporating an LST analyzer in the 'black-box' system, to perform real-time analysis/control, might look appealing. However, one may want to think whether such an analyzer can cope with the frequency of the basic/mean flow changes. Second, the discussion in Section 2 of mean (i.e. time-averaged) versus instantaneous (steady) basic or time-periodic basic flow is relevant here as well. If one wants to follow the first path, there may be some hope that the LST analyzer part of the "black-box" can cope with the flow changes. The same is possibly true for the case where a time-periodic basic state is to be analyzed. However, it is the viewpoint of the authors that it is not realistic to analyze the instantaneous basic field. It could be highly speculative to draw conclusions on the behavior of a flow system based on knowledge of the instability characteristics of parts or regions of the flow. Several examples exist to support this assertion (e.g. instability characteristics of isolated versus systems of (Batchelor) vortices [210], monitoring TS waves while optimal perturbations are more dangerous, etc.) It is proposed that global linear theory via solution of multidimensional eigenvalue problems (EVP), i.e. 2D EVPs in case a substantial portion of the flow can be identified in which variation of the (mean/basic) flow in one spatial direction is negligible compared with that in the other two, and 3D EVPs otherwise should be used (see Section 2).

Once the actuator's output has been translated to flow properties that are independent of the actuator's details, the instability characteristics of the flow (e.g. the shear layer shown in Fig. 33) come into play. To be efficient, AFC should be applied at the lowest input level that would trigger instability, which in turn would draw energy from the external or core flow and redistribute it to perform the required action, rather than provide the "brute force" action using the actuator as a generator and not as a trigger. Again, appropriate LST, taking advantage of all known principles (i.e., convective, absolute, algebraic and global),<sup>3</sup> should be used but the leading mechanism is again nonlinear.

Experimental evidence exists which shows that the effective frequencies for separation control are affected by the excitation momentum, as expected from a nonlinear system. Figure 41 presents the minimum  $C_\mu$  required to shorten a large separation bubble with excitation frequency (in the form of  $F^+$  based on the flap chord and free stream velocity). It can be seen that the range of effective  $F^+$  widens as the magnitude of the excitation increases. It should be noted that the spectral content of the measured disturbances in the boundary layer is amplitude dependent. A similar observation is shown in Fig. 42 [6] in which data is presented on using periodic excitation to alleviate leading-edge separation off a NACA0015 airfoil. The range of effective frequencies (as quantified by the lift increment) widens as the excitation oscillatory momentum increases. A practical observation from these findings is that one should perform frequency scans at the lowest effective  $C_\mu$  that generates a measurable effect.

In some flow control applications, it is possible that the base flow may not be sufficiently receptive (sensitive) to the proposed actuator. In this case, stability modifiers could be used to locally or globally alter the base flow in order to be more receptive to the excitation. Two examples

---

<sup>3</sup>For example, classic Orr-Sommerfeld-based analysis can be used for control of Tollmien-Schlichting waves [28] while BiGlobal analysis is required for separated flows [23]

that illustrate this approach, based on a high Reynolds number separation control experiment [211], are now discussed.

It is well known that distributed suction alters the instability characteristics of laminar boundary layers, such that transition can be significantly delayed. It is also known that a velocity profile can be turned absolutely unstable if the reverse velocity close to the wall exceeds roughly 30% of the external velocity [14]. A high Reynolds number experiment was conducted by Seifert and Pack [211] on a wall mounted “Hump” (see Fig. 43a) to explore the effect of periodic excitation on a turbulent separation bubble. Zero mass flux periodic excitation was shown to be very effective in shortening the bubble (compare triangles to asterisks in Fig. 43b). Minute levels of steady mass-flux (denoted by  $c_\mu \neq 0$ ) were superimposed on the periodic excitation in an attempt to alter the receptivity and instability characteristics of the separated shear layer. The effect of steady blowing ( $c_\mu > 0$ ) was shown to be detrimental while steady suction ( $c_\mu < 0$ ), superimposed on the periodic excitation, proved beneficial in generating a healthier pressure recovery (compare squares to circles in Fig. 43b). The amplitudes of the surface pressure fluctuations at the fundamental excitation frequency ( $F$ ) and its harmonic ( $2F$ ) corresponding to the data of Fig. 43b are plotted in Fig. 43c, in order to search for a possible explanation to the observations of the mean pressure coefficient ( $C_p$ ) alternation. Note that fluctuating pressure coefficient ( $C'_p$ ) for the superimposed suction was increased while added blowing reduced  $C'_p$  downstream of the excitation slot (located at  $x/c = 0.64$ , Fig. 43a,  $C'_p$  is the RHS ordinate in Fig. 43b). The amplitudes at  $F$  and  $2F$  of Fig. 43c were normalized by the corresponding amplitudes of the zero-mass-flux excitation. The data indicates that suction enhances the receptivity of the separated shear layer to  $F$  while blowing does the opposite. However, the instability characteristics of the flow were not significantly altered due to the added mass transfer, since the  $F$  and  $2F$  data sets remained parallel further downstream. Steady blowing has a favorable effect on the receptivity of  $2F$ . Similar observations were made and reported at the same time by Greenblatt et al. [212]. These results are also consistent with the receptivity studies of Dobrinsky and Collis [39] (discussed in Section 3.2) which demonstrate that there is a trade-off between instability and receptivity — modifying a flow to make it less stable typically makes it more receptive.

After receptivity and linear instability, the next physical stage in the flow response process is *nonlinear interaction*. As in any nonlinear process, the interaction (Fig. 33) can be of wave-wave and/or wave-mean flow types. Wave-wave interactions, typically involve lower (sub-) and higher (super-) harmonics of the fundamental excitation frequency, that do not necessarily coincide with the most unstable frequency of the excited flow. Moreover, it was noted in the discussion of *instability*, that the nonlinear interaction between high amplitude waves and the mean flow changes the mean flow and its associated receptivity and instability characteristics. In that respect, the simplest way to trigger any flow instability would be to excite a full spectrum (in both space and time, e.g. Gaster’s wave packet, [51] and references therein) and let the flow select and amplify the most-unstable frequencies and wave numbers. Once these are identified, they could hopefully be triggered (actuator dependent) artificially at a higher and controllable magnitude, if deemed necessary.

As an example of the latter, one can consider the work on a delta wing at high incidence [205], in which a low duty-cycle, pulsed excitation was used and proved extremely effective for improved performance. Fundamental studies of nonlinear interactions in a plane mixing layer [213] provide an inspiration and guidelines to application of similar ideas to a separated mixing layer above an airfoil, several of which are on-going. However, the difficulties in applying these ideas to a

turbulent reattaching boundary layer are twofold. As seen before, when the excitation becomes effective, the boundary layer reattaches, the excitation decays and attenuates, possibly to below an effective level needed downstream, once the flow will tend to separate again. First, the excitation may lose coherence [208] as it evolves downstream so that the potential for nonlinear interaction may be lost. Second, once the excitation becomes effective, the boundary layer will reattach. However, the excitation may subsequently decay to an ineffective level so that the boundary layer may tend to separate again downstream. An example of this second scenario will now be discussed.

It should be mentioned that once an effective periodic excitation is applied to a highly receptive flow in the right location, it will alter the flow through nonlinear interaction. Consequently the stability characteristics of the reattaching shear layer are altered, and no longer amplify the excitation. This is a desirable effect that could partly be explained by a return to an equilibrium state of the controlled flow. Figure 44 shows mean and fluctuating wall pressures measured on the “Hump” model [211] using three excitation frequencies. The  $C'_p$  at  $x/c = 0.67$  indicates that the receptivity for all frequencies is similar (as inferred from the RMS of the surface pressure fluctuations, RHS in Fig. 44a), while Fig. 44b shows that it is actually lower for  $F^+ = 0.4$ , based on the spectral component at the excitation frequency alone. While  $F^+ = 0.4$  and  $0.8$  amplify at least for a certain distance over the bubble,  $C'_p$  at  $F^+ = 1.6$  decays immediately downstream of the slot. Interestingly,  $F^+ = 1.6$  is the most effective for separation control since it leads to the best pressure recovery as shown in Fig. 44a.

*Sensing* could be applied at any stage (i.e. *actuation, receptivity, instability and interaction*, see Fig. 33) to evaluate the baseline flow, to monitor the “health” of an actuator, to measure the resulting boundary layer oscillations in space and time, to identify the amplification of introduced or nonlinearly generated wave components and to monitor the resulting modification of the mean (base) flow. However, there are few studies that demonstrate such extensive use of sensors. Sensor devices and techniques are an open research area limited only by human imagination that utilizes the emerging MEMS technology [214]. A simple sensor (e.g. load cell or accelerometer) or arrays of networked surface mounted “glue on” flexible sheets of pressure or skin friction sensors could be used to evaluate the flow state. Every effort should be made to use simple approaches and a small number of sensors for identifying the flow state before one constructs and integrates arrays of sensors and develops logic that is based on cross correlating multi-sensor (in time and/or space) derivative information. Indicators should be sought that provide robust information for the system state, possibly using multiple sensors for redundancy [98]. An effective means of assessing an actuator’s performance may be a pressure sensor located within the actuator cavity while simple “health” monitoring could be provided by utilizing a part of a Piezo actuator as a sensor. Using an “on actuator” sensor can also enable the construction of a self-locking operation to the actuator’s resonance frequency regardless of the operational and environmental conditions and verify optimal, energy efficient operation [215].

Interestingly, a single sensor within the actuator cavity could also be used as a flow-state sensor for measurement and for closing the loop. An example of the latter approach was recently provided by Rapoport et al. [98]. Jet vectoring was achieved by adding a short, wide angle diffuser at the jet exit and introducing periodic excitation over a quarter of the circumference of the diffuser inlet [216]. Figure 45 shows the experimental set-up for AFC vectoring. Figures 46 and 47 show the baseline and vectored jets, respectively (Seifert, 1996, unpublished). Figure 48 shows how the jet deflection angle varies with the magnitude of the oscillatory control input, while Figure 49 shows

how the diffuser-wall and actuator-cavity mean-pressures vary as the level of the cavity pressure fluctuations increase and the jet is vectored. It was noted [98] that a single sensor located at the actuator cavity (Fig. 45), can provide health monitoring, a measure of the control authority (“input”) on the flow in the form of cavity pressure fluctuations (that drive the oscillatory momentum out of the actuator slot) and also serve as an indicator for the jet deflection angle (using its low-pass-filtered signal, since the flow turning angle induces low pressure at the jet-diffuser corner). A system identification study was conducted, for this jet vectoring system, to build the transfer function and design a closed-loop controller. Figure 50a shows the low frequency signal provided to modulate the amplitude of the actuator resonance frequency. Fig. 50b presents the resulting cavity pressure, showing an offset as the envelope magnitude increases. Also shown in Fig. 50b is the low pass filtered (LPF) cavity pressure, shown in gray with the right-hand side (RHS) ordinate, which indicates that the jet deflects to a larger angle as the magnitude of the cavity pressure fluctuations increase as a result of the actuator action. For low frequency modulation, the cavity pressure is opposite in phase from the signal read by a hot-wire (Fig. 50c) located in the excited shear layer. This is a result of the fact that as the jet is vectored, the shear velocity increases while the suction level at the actuator slot decreases, due to enhanced acceleration around the “corner.” This example demonstrates that a single sensor, located within the actuator cavity, can be used as a “health” monitor, system input indicator, and system output indicator — depending on which part of the measured spectrum is considered.

Once the system flow-state is known, a *closed-loop control* methodology (Fig. 33) can be applied to close the loop and achieve the AFC target in an automatic and robust manner. The motivation for closed-loop flow-control could be as simple as eliminating steady-state errors and achieving fast and smooth transition between flow states, or could be more complicated, such as altering heat transfer to protect certain critical components in an electronic circuit. *Closed-loop control* methodologies can range from simple (e.g. PID for linear deterministic systems) to elaborate (e.g. Fuzzy logic for nonlinear stochastic systems) and Section 3 contains a discussion of the various approaches. Specific uncertain, complex systems might require auto-tuning via real-time identification processes, but, every attempt should be made to utilize the simplest possible controller design.

## 5.2 Generic AFC roadmaps

Roadmaps were introduced into fluid mechanics research by Morkovin [9] in 1969 in the context of laminar to turbulent transition. For more than 20 years, these roadmaps were developed and tuned by Morkovin, Reshotko, and the fluid mechanics community to help identify what was known on boundary layer transition and to identify gaps in physical understanding. These maps were instrumental in generating a common knowledge base, documenting the state-of-the-art and in assisting researchers and funding agencies in making informed decisions based on collective knowledge. However, it is critical that areas of controversy be marked on these roadmaps to indicate where future research is required.

### 5.2.1 Outline for AFC roadmaps

An outline for a generic AFC roadmap will now be discussed. Every roadmap should have a *target*, described in terms of flow physics (e.g. lift enhancement is not a valid AFC *target*, rather it is a

result of several physical processes like delay of BL separation, reattachment of separated BL, vortex capture, delay of vortex breakdown, etc.).

Likewise, a hypothesized *mechanism* should be cited whenever possible. While this is not a crucial component in a roadmap, it is nevertheless highly desirable as it helps to clarify physical understanding. Places where the *mechanism* is unknown or poorly understood should be highlighted as areas in need of fundamental research.

*Methods* (at least one) should be described to achieve the *target*. The available, validated and proposed methods should be organized logically and evolutionarily (i.e. in the order in which every component of a certain method comes to play) in terms of the obstacles they are supposed to overcome. Every method included in a roadmap should be applicable or as least deemed as such and required *enabling capabilities* should be listed for each application. Methods that are known to be inapplicable should (obviously) not be included, however this requires a renewed emphasis and commitment within the scientific community to publish not only what works, but also what does not work. Roadmaps must also clearly indicated areas that require further study and development including estimates of the Technology Readiness Level (TRL) of each of the existing or missing enabling capabilities. Footnotes should be used to identify strengths and weaknesses of any stage in the roadmap, as these are directions for future research.

A *critical path* should be identified for every method — nothing should be on the map that is not connected to at least two components and be part of a path or road leading from a target to its realization. An attempt should be made to identify the most efficient and highest TRL routes. For otherwise promising paths that are "blocked" by a low TRL item, researchers will tend to look for better, alternative enabling-technologies, or perhaps suggest altogether new routes. The Morkovin [9] roadmap for boundary layer transition clearly follows these guidelines.

Topics in AFC are significantly more diverse than the laminar-turbulent transition issues the Morkovin-Reshotko roadmap(s) deal with. Targeted AFC roadmaps include, but are not limited to:

1. Separation
  - (a) Delay
  - (b) Reattachment and manipulation
  - (c) Stabilization (shear layer, wake, unsteady flow-surface interaction: buffet, bubbles, . . .)
2. Transition
  - (a) Delay
  - (b) Promote
  - (c) Regulate
3. Jet
  - (a) Spreading
  - (b) Vectoring
  - (c) Acoustics
4. Drag Reduction
  - (a) Laminar skin friction
  - (b) Turbulent shaping (Stratford, riblets, . . .)
  - (c) Additives (polymers, surfactants, . . .)

- (d) Separation control
- 5. Thermal management
  - (a) Cooling, heating
  - (b) Reduced signature
- 6. Guidance, Propulsion and Control
  - (a) Hingeless maneuvering
  - (b) Gust alleviation
  - (c) Thrust generation
- 7. Vortex Dominated Flows
  - (a) Delta wings
  - (b) Tip vortices
  - (c) Forebody vortex asymmetry
  - (d) Flap, aileron, edge tone
- 8. Combustion, Turbomachinery
  - (a) Inlets (separation, distortion)
  - (b) Low Reynolds numbers stators, rotors and diffusers
- 9. Cavity
  - (a) Noise
  - (b) Vibration
  - (c) Optical distortion

The following section provides a draft roadmap for the delay of boundary layer separation. This is by no means more than a draft that should be critically evaluated and updated. The community is encouraged to generate and publish roadmaps for all possible AFC applications.

### **5.2.2 Separation delay roadmap**

Separation delay of a nominally two-dimensional attached boundary layer could be achieved by enhancing the averaged skin friction upstream of the mean separation region. Typically, simply and most effectively, increased skin friction could be achieved by enhanced near wall-outer/core flow (for external and internal flows, respectively) momentum transfer, but many other methods exist, and some would be discussed presently. The separation delay roadmap should include, as a minimum and according to Sec. 5.2, the following components:

Target: Delay (turbulent) boundary layer separation.

Mechanism: Enhance skin friction upstream of the baseline-mean flow separation region.

Methods: At least three known methods exist to enhance near wall streamwise momentum: (1) add (high momentum fluid), (2) remove (low momentum fluid) or (3) re-distribute (momentum across the boundary layer). Emphasis should be placed on minimum energy expenditure in order to re-distribute momentum. Introduction of oscillatory momentum that is coupled with flow instability is typically one to two orders of magnitude more efficient than steady momentum addition

for separation control (Fig. 51 and [7]). Even intermittent momentum addition, at intervals that are smaller than the typical flow response time is significantly more effective than steady momentum injection. An inherent difficulty arises immediately when searching for high efficiency in maintaining attached turbulent boundary layers that are stable to all known perturbations, with the possible exception of steady streamwise vortices of selected scales. This is a missing *enabling technology*, identifying and utilizing unstable/least stable modes of an attached turbulent base flow.

The following is a partial list of known separation delay techniques. A detailed discussion can be found in Gad-el-Hak et al. [3]. Proper aerodynamic shaping can allow the tailoring of gradual favorable streamwise pressure gradient for laminar-turbulent transition delay. The use of this approach however, is limited by the need to close the aft-body, accompanied by the associated adverse pressure gradient. It is always desirable to tailor the geometry and the pressure gradient such that transition will take place just upstream of the natural mean separation location (in the absence of transition) or at least promote/control transition and enhanced mixing above the separation bubble.

Shaping, transpiration, slot suction, wall-jets, heat transfer and moving walls are just a partial list of proven methods for separation delay. All methods mentioned above rely on enhanced near-wall momentum (see e.g., Lachman [2], Gad-el-Hak et al. [3] and Gad-el-Hak [4]).

Local or distributed steady suction is a well-known and effective method for separation delay, especially when the flow related aspect is of prime importance. However, if overall efficiency and maintenance issues are included in the decision making process, the appeal of steady suction is lowered [2]. Other techniques include vortex generators (mechanical, pop-out, fluidic, and zero-mass-flux) which are effective streamwise vorticity generators that, in turn, mix across the boundary layer and delay separation. Periodic excitation could also be used to enhance skin friction, but 3D unstable modes should be sought to perform this task as 2D excitation is significantly attenuated in zero and slightly adverse pressure-gradient turbulent boundary layers (see e.g., Seifert and Pack [211]).

*Enabling Technologies* that can assist in enhancing skin friction should provide order 0.1 to 1.0 velocity ratio effectors (i.e. actuators with sufficient control authority). The search for low penalty methods (i.e. methods that cause little or no disturbance while inactive, but with sufficient control authority and low energy consumption) could be combined with working on the verge of separation (i.e. skin friction approaching zero) [217].

Separation delay might require distributed sensing, as incipient separation is a local phenomenon. The actuators selected to achieve the desired target, the required power and the control logic are all open issues. Again, effectiveness could be greatly enhanced if flow instability is used to mix across the boundary layer to enhance skin friction.

## **6 Summary**

Theoretical, numerical and experimental issues in active flow control (AFC) with special emphasis on utilizing flow instability were discussed. Issues in control theory were presented including model based, optimal and robust feedback control design with emphasis on the important role of reduced order models. A generic flow control process was presented and relevant experimental examples were highlighted. The need to establish, update, and publish “Morkovin style” roadmaps was emphasized. The relevance of global flow instabilities and the crucial importance of geometric fidelity were identified as important theoretical and numerical aspects of AFC, respectively.

## Acknowledgments

The collaboration and assistance of students and co-workers of the four co-authors is greatly appreciated. V. Theofilis acknowledges support by a Ramón y Cajal research fellowship of the Spanish Ministry of Science and Technology and the Window on Science programme of the European Office of Aerospace Research and Development and the United States Air Force Research Laboratory. The work of V. Theofilis was partly supported by Grants No. F49620-03-1-0295, monitored by Dr. T. Beutner (AFOSR) and FA8655-02-13059, monitored by Dr. J. Schmisser (AFOSR) and Mr. W. Donaldson (EOARD). The views of R.D. Joslin expressed in this article do not necessarily represent those of the Office of Naval Research or the United States Department of Defense. The work of S.S. Collis was supported in part by Texas ATP grants 003604-0011-2001 and 003604-017-1997; NSF grants DMS-0075731 and MRI-0116289; and the Department of Energy. The authors are grateful for the helpful comments of Tim Trucano of Sandia National Laboratories.

## References

- [1] Prandtl L. Uber Flussigkeitsbewegung bei sehr kleiner Reibung. In: Proceedings of the Third International Mathematics Congress, Heidelberg, 1904. p. 484–491.
- [2] Lachman G, editor. Boundary Layer and Flow Control. Vol. 1 and 2. Pergamon Press, 1961.
- [3] Gad-el-Hak M, Pollard A, Bonnet J, editors. Flow Control: Fundamentals and Practices, Springer, 1998.
- [4] Gad-el-Hak M. Introduction to flow control. In: Gad-el-Hak M, Pollard A, Bonnet J, editors. Flow Control: Fundamentals and Practices, Springer, 1998. p. 199–273.
- [5] Schubauer GB, Skramstad HK. Laminar boundary layer oscillations and transitions on a flat plate. *J Aero Sci*, 1947;14:69–79.
- [6] Greenblatt D, Wagnanski IJ. The control of flow separation by periodic excitation. *Prog Aero Sci*, 2000;36(7):487–545.
- [7] Seifert A, Darabi A, Wagnanski I. Delay of airfoil stall by periodic excitation. *J Aircraft*, 1996;33:691–698.
- [8] Newman BG. The deflection of plane jets by adjacent boundaries – Coanda effect. In: Lachman GV, editor. Boundary Layer and Flow Control, Pergamon Press, 1961.
- [9] Morkovin MV. On the many faces of transition. In: Wells CS, editor. Viscous Drag Reduction, New York, 1969. Plenum Press, p. 1–32.
- [10] Theofilis V. Advances in global linear instability of nonparallel and three-dimensional flows. *Prog Aero Sci*, 2004;to appear.
- [11] Huerre P, Monkewitz P. Local and global instabilities in spatial developing flows. *Ann Rev Fluid Mech*, 1990;22:473–537.

- [12] Chomaz JM, Huerre P, Redekopp L. Bifurcations to local and global modes in spatially developing flows. *Phys Rev Lett*, 1988;60:25–28.
- [13] Morzynski M, Thiele F. Numerical stability analysis of flow about a cylinder. *ZAAM*, 1991;71:T424–T428.
- [14] Morzynski M, Afanasiev K, Thiele F. Solution of the eigenvalue problems resulting from global nonparallel flow stability analysis. *Comp Meth Appl Mech Eng*, 1999;169:161–176.
- [15] Barkley D, Henderson R. Three-dimensional Floquet analysis of the wake of a circular cylinder. *J Fluid Mech*, 1996;322:215–241.
- [16] Theofilis V. Globally unstable flows in open cavities. AIAA Paper 2000-1965, 2000.
- [17] Theofilis V, Colonius T, Seifert A. A position paper on global flow instability and control. In: Proceedings of the 1st and 2nd global flow instability and control symposia, Crete, Greece, 2004. (to appear as DLR Mitteilung).
- [18] Theofilis V, Hein S, Dallmann U. On the origins of unsteadiness and three-dimensionality in a laminar separation bubble. *Proc Royal Soc Lon A*, 2000;358:3229–3246.
- [19] Hammond DA, Redekopp L. Local and global instability properties of laminar separation bubbles. *Euro J Mech B/Fluids*, 1998;17:145–164.
- [20] Butler K, Farrell BF. Three-dimensional optimal perturbations in viscous shear flow. *Phys Fluids*, 1992;4(8):1637–1650.
- [21] Trefethen LN, Trefethan AE, Reddy SC, Driscoll TA. Hydrodynamic stability without eigenvalues. *Science*, 1993;261:578–584.
- [22] Schmid P, Henningson D. *Stability and Transition in Shear Flows*. Springer-Verlag, 2001.
- [23] Reynolds WC, Hussain AKMF. The mechanics of an organized wake in turbulent flow. Part 3. Theoretical models and comparisons with experiments. *J Fluid Mech*, 1972;54:263–288.
- [24] Reau N, Tumin A. On harmonic perturbations in turbulent shear flows. In: *Advances in Turbulence VIII*, 2000. p. 209–212.
- [25] Crouch JD. Instability and transient growth of two trailing-vortex pairs. *J Fluid Mech*, 1997;350:311–330.
- [26] Fabre D, Jacquin L. Stability of a four-vortex aircraft model. *Phys Fluids*, 2000;2:1–6.
- [27] Crouch JD, Spalart PR. Active system for early destruction of trailing vortices. U.S. Patent 6082679, 2000.
- [28] Milling RW. Tollmien–Schlichting wave cancellation. *Phys Fluids*, 1981;24(5):979–981.
- [29] Laurien E, Kleiser L. Numerical simulation of boundary-layer transition and transition control. *J Fluid Mech*, 1989;199:403–440.

- [30] Joslin RD, Gunzburger MD, Nicolaides RA, Erlebacher G, Hussaini MY. Self-contained automated methodology for optimal flow control. *AIAA J*, 1997;35(5):816–824.
- [31] Reddy SC, Henningson D. Energy growth in viscous channel flows. *J Fluid Mech*, 1993;252:2009–238.
- [32] Lasseigne DG, Joslin RD, Jackson TL, Criminale WO. The transient period of boundary layer disturbances. *J Fluid Mech*, 1999;381:89–119.
- [33] Bewley T, Liu S. Optimal and robust control and estimation of linear paths to transition. *J Fluid Mech*, 1998;365:305–349.
- [34] Reddy SC, Ionannou PJ. Energy transfer analysis of turbulent plane Couette flow. In: Saric W, Fasel H, editors. *Proceedings of the IUTAM Laminar-Turbulent Symposium V*, Sedona, AZ, USA, 2000. p. 211–216.
- [35] Hill DC. Adjoint systems and their role in the receptivity problem for boundary layers. *J Fluid Mech*, 1995;292:183–204.
- [36] Hill DC. A theoretical approach to analyzing the restabilization of wakes. *AIAA Paper 92-0067*, 1992.
- [37] Collis SS, Dobrinsky A. Evaluation of adjoint based methods for the prediction of linear and nonlinear receptivity. In: Fasel H, Saric W, editors. *Proceedings of the 5th IUTAM Symposium on Laminar-Turbulent Transition*. Springer Verlag, 1999. p. 111–116.
- [38] Luchini P. Reynolds-number independent instability of the boundary layer over a flat surface: optimal perturbations. *J Fluid Mech*, 2000;404:289–309.
- [39] Dobrinsky A, Collis SS. Adjoint parabolized stability equations for receptivity prediction. *AIAA Paper 2000-2651*, 2000.
- [40] Cathalifaud P, Luchini P. Optimal control by blowing and suction at the wall of algebraically growing boundary layer disturbances. In: Saric W, Fasel H, editors. *Proceedings of the IUTAM Laminar-Turbulent Symposium V*, Sedona, AZ, USA, 2000. p. 307–312.
- [41] Luchini P, Bottaro A. Gortler vortices: a backward-in-time approach to the receptivity problem. *J Fluid Mech*, 1998;363:1–23.
- [42] Corbett P, Bottaro A. Optimal perturbations for boundary layers. *Phys Fluids*, 2000;12(1): 120–130.
- [43] Corbett P. *Non-Modal Growth in Boundary Layers and its Optimal Control*. PhD thesis, EPF Lausanne, 2000.
- [44] Luchini P. Adjoint methods in transient growth, global instabilities and turbulence control. In: *Proceedings of the 1st and 2nd global flow instability and control symposia*, Crete, Greece, 2004. (to appear as DLR Mitteilung).

- [45] Lumley JL. The structure of inhomogeneous turbulent flow. In: Yaglom AM, Tatarski VI, editors. Atmospheric Turbulence and Radio Wave Propagation, Nauko, Moscow, 1967. p. 160–178.
- [46] Karhunen K. Zur spektraltheorie stochastischer prozesse: Ueber lineare methoden in der wahrscheinlichkeitsrechnung. *Annales Academiae Scientiarum Fennicae, Series A1: Mathematica-Physica*, 1947;37:3–79.
- [47] Loeve MM. Fonctions aleatoires de second ordre. *Comptes Rendus Acad. Sci. Paris*, 1945;220.
- [48] Rempfer D, Fasel H. Evolution of three-dimensional structures in a flat-plate boundary layer. *J Fluid Mech*, 1994;260:351–375.
- [49] Lerche T. Experimental investigation of turbulent separated flow on an airfoil. DLR Institute of Fluid Mechanics, 1996.
- [50] Colonius T. An overview of simulation, modeling, and active control of flow/acoustic resonance in open cavities. *AIAA Paper 2001-0076*, 2001.
- [51] Gaster M. Stability of velocity profiles with reverse flow. In: Hussaini MY, Streett CL, editors. *Instability, Transition and Turbulence*, 1992. p. 212–215.
- [52] Theofilis V. Global linear instability in laminar separated boundary layer flow. In: Saric W, Fasel H, editors. *Proceedings of the IUTAM Laminar-Turbulent Symposium V*, Sedona, AZ, USA, 2000. p. 663–668.
- [53] Theofilis V, Barkley D, Sherwin S. Spectral/hp element technology for global flow instability and control. *Aero. J.*, 2002;106(1065):619–625.
- [54] Humphreys JS. On a circular cylinder in a steady wind. *J Fluid Mech*, 1960;12:123–130.
- [55] Goelling B. Experimentelle Untersuchungen des laminaren-turbulenten Ueberganges der Zylindergrenzschichtstroemung. PhD thesis, DLR Institute of Aerodynamics and Flow Technology, 2001.
- [56] Schiller L, Linke W. Druck- und reibungswiderstand des zylinders bei Reynoldszahlen 5000 bis 40000. *Zeit Flug Motorluft*, 1933;24:193–198.
- [57] Zdravkovich MM. *Flow Around a Circular Cylinder, Vol. I*. Oxford University Press, 1997.
- [58] Schewe G. Sensitivity of transition phenomena to small perturbations in flow around a circular cylinder. *J Fluid Mech*, 1986;172:33–46.
- [59] Schewe G. Reynolds-number effects in flow around more-or-less bluff bodies. *J Wind Eng Ind Aero*, 2001;8:1267–1289.
- [60] Seifert A, Bachar T, Koss D, Shepshelovich M, Wygnanski I. Oscillatory blowing: A tool to delay boundary-layer separation. *AIAA J*, 1993;31:2052–2060.

- [61] Nishri B, Seifert A, Wygnanski I. Active control of a transitional separation bubble at low Reynolds number and elevated free-stream turbulence. Technical Report CP-2001-210888, NASA, 2001.
- [62] Darabi A, Lourenco L, Wygnanski I. On flow reattachment by periodic excitation. In: *Advances in Turbulence VIII, European Turbulence Conference VIII, 2000*. p. 201–204.
- [63] Moin P, Bewley T. Feedback control of turbulence. *Appl Mech Rev*, 1994;47(6-2):S3–S13.
- [64] Lumley J, Blossey P. Control of turbulence. *Ann Rev Fluid Mech*, 1998;30:311–327.
- [65] Bewley TR. Flow control: New challenges for a new renaissance. *Prog Aero Sci*, 2001;37: 21–58.
- [66] Bechert DW, Bartenwerfer M. The viscous flow on surfaces with longitudinal ribs. *J Fluid Mech*, 1989;206:105–129.
- [67] Chu D, Henderson R, Karniadakis GE. Parallel spectral-element-Fourier simulation of turbulent flow over riblet-mounted surfaces. *Theor Comp Fluid Dyn*, 1992;3(4):219–29.
- [68] Goldstein D, Handler R, Sirovich L. Modeling a no-slip flow boundary with an external force field. *J Comp Phys*, 1993;105:354–366.
- [69] Choi H, Moin P, Kim J. Direct numerical simulation of turbulent flow over riblets. *J Fluid Mech*, 1993;255:503–539.
- [70] Goldstein D, Handler R, Sirovich L. Direct numerical simulation of turbulent flow over a modeled riblet covered surface. *J Fluid Mech*, 1995;302:333–376.
- [71] Abegg C, Bippes H, Janke E. Stabilization of boundary-layer flows subject to crossflow instability with the aid of suction. In: Fasel H, Saric W, editors. *Laminar-Turbulent Transition*. Springer, 2000. p. 607–612.
- [72] Zhou K, Doyle JC. *Essentials of Robust Control*. Prentice Hall, 1998.
- [73] Tumin A. Application of biorthogonal eigenfunction system to receptivity problems and to multimode decomposition. *ERCOFTAC Workshop on adjoint systems, Toulouse France, 1999*.
- [74] Dobrinsky A, Collis SS. Adjoint analysis for receptivity prediction. Technical Report FPS-3, Flow Physics and Simulation Group, Rice University, 2002. [mems.rice.edu/~collis/papers](http://mems.rice.edu/~collis/papers).
- [75] Dobrinsky A, Collis SS. Adjoint methods for receptivity prediction in nonparallel flows. (submitted), 2003.
- [76] Airiau C, Walther S, Bottaro A. Nonparallel receptivity and the adjoint PSE. In: Fasel H, Saric W, editors. *Proceedings of the 5th IUTAM Symposium on Laminar-Turbulent Transition*. Springer Verlag, 1999. p. 57–62.

- [77] Pralits J, Airiau C, Hanifi A, Henningson D. Sensitivity analysis using adjoint parabolized stability equations for compressible flows. *Flow Turb Comb*, 2001.
- [78] Bamieh R, Dahleh M. Energy amplification in channel flows with stochastic excitation. *Phys Fluids*, 2001;13(11):3258–3269.
- [79] Lauga E, Bewley TR. The decay of stabilizability with Reynolds number in a linear model of spatially developing flows. *Proc Royal Soc Lon A*, 2003. (to appear).
- [80] Lewis F. *Modern Control Theory*. Prentice-Hall, 1992.
- [81] Joshi SS, Speyer JL, Kim J. A systems theory approach to the feedback stabilization of infinitesimal and finite-amplitude disturbances in plane Poiseuille flow. *J Fluid Mech*, 1997;332:157–184.
- [82] Doyle JC, Glover K, Khargonekar PP, Francis BA. State-space solutions to standard  $\mathcal{H}_2$  and  $\mathcal{H}_\infty$  control problems. *ICC Trans Automat Control*, 1989;34(8):831–847.
- [83] Choi H, Moin P, Kim J. Active turbulence control for drag reduction in wall-bounded flows. *J Fluid Mech*, 1994;262(75):75–110.
- [84] Clark JA, Markland E. Flow visualization in turbulent boundary layers. *ASCE Journal of the Hydraulics Division*, 1971;87:1635–1664.
- [85] Jimenez J, Moin P. The minimal flow unit in near wall turbulence. *J Fluid Mech*, 1991;225:221–240.
- [86] Jeong J, Hussain F, Schoppa W, Kim J. Coherent structures near the wall in a turbulent channel flow. *J Fluid Mech*, 1997;332:185–214.
- [87] Hammond EP, Bewley TR, Moin P. Observed mechanisms for turbulence attenuation and enhancement in opposition-controlled wall-bounded flows. *Phys Fluids*, 1998;10(9):2421–2423.
- [88] Lee C, Kim J, Babcock D, Goodman R. Application of neural networks to turbulence control for drag reduction. *Phys Fluids*, 1997;9(6):1740–1747.
- [89] Koumoutsakos P. Active control of vortex-wall interactions. *Phys Fluids*, 1997;9(12):3808.
- [90] Koumoutsakos P. Vorticity flux control for a turbulent channel flow. *Phys Fluids*, 1999;11(2):248–250.
- [91] Kang S, Choi H. Active wall motions for skin-friction drag reduction. *Phys Fluids*, 2000;12(12):3301–3304.
- [92] Kellogg SM. Immersed boundary methods with applications to flow control. Master’s thesis, Rice University, Mechanical Engineering and Materials Science, 2000.
- [93] Farrell BF, Ioannou PJ. Turbulence suppression by active control. *Phys Fluids*, 1996;8(5):1257–1268.

- [94] Jiménez J, Pinelli A. The autonomous cycle of near-wall turbulence. *J Fluid Mech*, 1999;389:335–59.
- [95] Kim J, Lim J. A linear process in wall-bounded turbulent shear flows. *Phys Fluids*, 2000;12(8).
- [96] Franklin G, Powell JD, Emami-Naeini A. *Feedback Control of Dynamic Systems*. Addison-Wesley, 1988.
- [97] Rapoport D, Fono I, Cohen K, Seifert A. Closed-loop vectoring control of a turbulent jet using periodic excitation. *J Prop Power*, 2003;19(4):646–654.
- [98] Rapoport D, Fono I, Cohen K, Seifert A. Closed-loop vectoring control of a turbulent jet using periodic excitation. *AIAA Paper 2002-3073*, 2002.
- [99] Williams D, Fabris D, Morrow J. Experiments on controlling multiple acoustic modes in cavities. *AIAA Paper 2000-1903*, 2000.
- [100] Williams D, Rowley C, Colonius T, Murray R, MacMartin D, Fabris D, Albertson J. Model-based control of cavity oscillations — Part I: Experiments. *AIAA Paper 2002-0971*, 2002.
- [101] Rowley C, Williams D, Colonius T, Murray R, MacMartin D, Fabris D. Model-based control of cavity oscillations — Part II: System identification and analysis. *AIAA Paper 2002-0972*, 2002.
- [102] Zhou K, Doyle JC, Glover K. *Robust and Optimal Control*. Prentice-Hall, 1996.
- [103] Hogberg M, Bewley TR, Henningson DS. Linear feedback control and estimation of transition in plane channel flow. *J Fluid Mech*, 2003. (to appear).
- [104] Athans M. The role and use of the stochastic linear-quadratic-Gaussian problem in control system design. *IEEE Trans Automat Contr*, 1971;AC-16:529–552.
- [105] Cortelezzi L, Speyer JL. Robust reduced-order controller of laminar boundary layer transitions. *Physical Review E*, 1998;58(2):1906–1910.
- [106] Lee KH, Cortelezzi L, Kim J, Speyer J. Application of reduced-order controller to turbulent flows for drag reduction. *Phys Fluids*, 2001;13(5):1321–1330.
- [107] Chang Y, Collis SS, Ramakrishnan S. Viscous effects in control of near-wall turbulence. *Phys Fluids*, 2002;14(11):4069–4080.
- [108] Abergel F, Temam R. On some control problems in fluid mechanics. *Theor Comp Fluid Dyn*, 1990;1:303–325.
- [109] Berggren M. Numerical solution of a flow-control problem: Vorticity reduction by dynamic boundary action. *SIAM J Sci Comp*, 1998;19:829–860.
- [110] Collis SS, Ghayour K, Heinkenschloss M, Ulbrich M, Ulbrich S. Towards adjoint-based methods for aeroacoustic control. *AIAA Paper 2001-0821*, 2001.

- [111] Collis SS, Ghayour K, Heinkenschloss M, Ulbrich M, Ulbrich S. Numerical solution of optimal control problems governed by the compressible Navier–Stokes equations. In: International Series of Numerical Mathematics, volume 139. Birkhäuser Verlag, 2001. p. 43–55.
- [112] He JW, Glowinski R, Metcalfe R, Nordlander A, Periaux J. Active control and drag optimization for flow past a circular cylinder. I. oscillatory cylinder rotation. *J Comp Phys*, 2000;163:83–117.
- [113] Fursikov AV, Gunzburger MD, Hou LS. Boundary value problems and optimal boundary control for the Navier–Stokes systems: The two–dimensional case. *SIAM J Cont Opt*, 1998;36:852–894.
- [114] Gunzburger MD, Manservigi S. The velocity tracking problem for Navier–Stokes flows with boundary control. *SIAM J Cont Opt*, 2000;39:594–634.
- [115] He H, Ghattas O, Antaki JF. Computational strategies for shape optimization of time–dependent Navier–Stokes flows. Technical Report CMU-CML–97–102, Engineering Design Research Center, Carnegie Mellon University, 1997. <http://www.cs.cmu.edu/~oghattas/>.
- [116] Collis SS, Ghayour K, Heinkenschloss M, Ulbrich M, Ulbrich S. Optimal control of unsteady compressible viscous flows. *Inter J Num Meth Fluids*, 2002;40:1401–1429.
- [117] Gunzburger MD, editor. *Flow Control*. Springer-Verlag, New York, 1995.
- [118] Borggaard J, Burkardt J, Gunzburger M, Peterson J. *Optimal Design and Control*. Birkhauser, Boston, 1995.
- [119] Gruver WA, Sachs E. *Algorithmic Methods in Optimal Control*. Pitman Advanced Publishing, Boston, 1980.
- [120] Burghes DN, Graham A. *Introduction to Control Theory Including Optimal Control*. John Wiley and Sons, New York, 1980.
- [121] Nadarajah SK, Jameson A. A comparison of the continuous and discrete adjoint approach to automatic aerodynamic optimization. AIAA Paper 2000-0667, 2000.
- [122] Gunzburger M. Adjoint equation-based methods for control problems in incompressible, viscous flows. *Flow Turb Comb*, 2000;65(3-4):249–272.
- [123] Joslin RD, Gunzburger MD, Nicolaidis RA, Erlebacher G, Hussaini MY. A self-contained automated methodology for optimal flow control validated for transition delay. NASA Contractor Report 198215, 1995;ICASE 95-64.
- [124] Bewley T, Moin P, Teman R. Optimal and robust approaches for linear and nonlinear regulation problems in fluid mechanics. AIAA Paper 97-1872, 1997.
- [125] Bewley TR, Moin P, Teman R. DNS-based predictive control of turbulence: an optimal target for feedback algorithms. *J Fluid Mech*, 2001;447:179–225.

- [126] Collis SS, Chang Y, Kellogg S, Prabhu RD. Large eddy simulation and turbulence control. AIAA Paper 2000-2564, 2000.
- [127] Chang Y, Collis SS. Active control of turbulent channel flows based on large eddy simulation. ASME Paper No. FEDSM-99-6929, 1999.
- [128] Chang Y. Reduced Order Methods for Optimal Control of Turbulence. PhD thesis, Rice University, Mechanical Engineering and Materials Science, 2000.
- [129] Collis SS, Ghayour K, Heinkenschloss M. Optimal control of aeroacoustics: Transpiration boundary control. AIAA J, 2003;41(7).
- [130] Collis SS, Ghayour K, Heinkenschloss M. Optimal control of aeroacoustic noise generated by cylinder vortex interaction. Int J Aero, 2002;1(2):97–114.
- [131] Restrepo JM, Leaf GK, Griewank A. Circumventing storage limitations in variational data assimilation studies. SIAM J Sci Comp, 1998;19:1586–1605.
- [132] Lee C, Kim J, Choi H. Suboptimal control of turbulent channel flow for drag reduction. J Fluid Mech, 1998;358:245–258.
- [133] Hinze M, Kunisch K. Suboptimal control strategies for backward facing step flows. In: Sydow A, editor. Scientific Computing, volume 3, IMACS / North–Holland, Amsterdam, New York, Oxford, Tokyo, 1997. p. 53–58.
- [134] Heinkenschloss M. From suboptimal to optimal control. NSF Workshop on Control of Flows, 1999.
- [135] Collis SS, Chang Y. On the use of LES with a dynamic subgrid scale model for the optimal control of wall bounded turbulence. In: Knight D, Sakell L, editors. Recent Advances in DNS and LES. Kluwer Academic Publishers, 1999. p. 99–110.
- [136] Collis SS, Chang Y. Computer simulation of active control in complex turbulent flows. In: Atluri, O’Donoghue, editors. Modeling and Simulation Based Engineering, volume I. Tech Science Press, 1998. p. 851–856.
- [137] Moser RD, Kim J, Mansour NN. Direct numerical simulation of turbulent channel flow up to  $Re_\tau = 590$ . Phys Fluids, 1999;11:943.
- [138] Holmes P, Lumley JL, Berkooz G. Turbulence, Coherent Structures, Dynamical Systems and Symmetry. Cambridge University Press, 1996.
- [139] Afanasiev K, Hinze M. Adaptive control of a wake flow using proper orthogonal decomposition. In: Dekker M, editor. Shape Optimization and Optimal Design: Proceedings of the IFIP Conference, Lecture Notes in Pure and Applied Mathematics, 2000.
- [140] Kunisch K, Volkwein S. Control of Burger’s equation by a reduced order approach using proper orthogonal decomposition. J Opt Theor App, 1999;102(2):345–371.

- [141] Ravindran SS. Proper orthogonal decomposition in optimal control of fluids. NASA/TM-1999-209113, 1999.
- [142] Aubry N, Holmes P, Lumley J, Stone E. The dynamics of coherent structures in the wall region of a turbulent boundary layer. *J Fluid Mech*, 1988;192:115–173.
- [143] Zhou X, L.Sirovich. Coherence and chaos in a model of turbulent boundary layer. *Phys Fluids A*, 1992;4(12):2855–74.
- [144] Rempfer D. On the structure of dynamical systems describing the evolution of coherent structures in a convective boundary layer. *Phys Fluids*, 1994;6(3):1402.
- [145] Rempfer D. Investigations of boundary layer transition via Galerkin projections on empirical eigenfunctions. *Phys Fluids*, 1996;8(1):175.
- [146] Bloch AM, Marsden JE. Controlling homoclinic orbits. *Theor Comp Fluid Dyn*, 1989;1:179–190.
- [147] Collier BD, Holmes P, Lumley JL. Control of bursting in boundary layer models. *Appl Mech Rev*, 1994;6(2):S139–S143.
- [148] Podvin B, Lumley J. Reconstructing the flow in the wall region from wall sensors. *Phys Fluids*, 1998;10(5):1182–1190.
- [149] Blossey PN. Drag Reduction in near wall turbulent flow. PhD thesis, Cornell University, 1999.
- [150] Delville J, Cordier L, Bonnet J. Large-scale-structure identification and control in turbulent shear flows. In: Gad-el-Hak M, Pollard A, Bonnet J, editors. *Flow Control: Fundamentals and Practices*, Springer, 1998. p. 199–273.
- [151] Prabhu RD, Collis SS, Chang Y. The influence of control on proper orthogonal decomposition of wall-bounded turbulent flows. *Phys Fluids*, 2001;13(2):520–537.
- [152] Du Q, Faber V, Gunzburger M. Centroidal Voronoi tessellations: applications and algorithms. *SIAM Rev*, 1999;p. 637–676.
- [153] Gunzburger M. Centroidal voronoi tessellations. *CCS-2/CNLS Seminar*, Los Alamos National Laboratory, 2003.
- [154] Omurtag A, Sirovich L. On low-dimensional modeling of channel turbulence. *Theor Comp Fluid Dyn*, 1999;13(2):115–27.
- [155] Moin P, Moser RD. Characteristic-eddy decomposition of turbulence in a channel. *J Fluid Mech*, 1989;200:471–509.
- [156] Hughes TJR, Feijoo GR, Mazzei L, Quincy JB. The variational multiscale method – a paradigm for computational mechanics. *Comp Meth Appl Mech Eng*, 1998;166(1–2):3–24.

- [157] Hughes TJR, Mazzei L, Jansen KE. Large eddy simulation and the variational multiscale method. *Comp Vis Sci*, 2000;3:47–59.
- [158] Collis SS. Monitoring unresolved scales in multiscale turbulence modeling. *Phys Fluids*, 2001;13(6):1800–1806.
- [159] Ramakrishnan S, Collis SS. Turbulence control simulations using the variational multiscale method. *AIAA J*, 2004. (in press).
- [160] Faller WE, Schreck SJ, Luttgies MW. Neural network prediction and control of three-dimensional unsteady separated flowfields. *J Aircraft*, 1995;32(6):1213–1220.
- [161] Narayanan S, Khibnik AI, Jacobson CA, Kevrekedis Y, Rico-Martinez R, Lust K. Low-dimensional models for active control of flow separation. In: *IEEE Conference on Control Applications - Proceedings*, volume 2, 1999. p. 1151–1156.
- [162] Faller WE, Schreck SJ. Unsteady fluid mechanics applications of neural networks. *J Aircraft*, 1997;34(1):48–55.
- [163] Koumoutsakos P, Moin P. Algorithms for shear flow control and optimization. In: *Proceedings of the IEEE Conference on Decision and Control*, volume 3, 1999. p. 2839–2844.
- [164] Milano M, Koumoutsakos P, Giannakopoulos X, Schmidhuber J. Evolving strategies for active flow control. In: *Proceedings of the IEEE Conference on Evolutionary Computation*, volume 1, 2000. p. 212–218.
- [165] Giunta AA. Use of data sampling, surrogate models, and numerical optimization in engineering design. *AIAA Paper 2002-0538*, 2002.
- [166] Eldred MS, Giunta AA, van Bloemen Waanders BG, Wojkiewicz SF, Hart Jr. WE, All-eva MP. DAKOTA, a multilevel parallel object-oriented framework for design optimization, parameter estimation, uncertainty quantification, and sensitivity analysis. version 3.0 reference manual. Technical Report SAND2001-3796, Sandia National Laboratories, 2002.
- [167] Chapman DR. Status and prospects of computational fluid dynamics. In: *Computational Fluid Dynamics*, volume II. von Karman Institute, 1976. p. 25.
- [168] Joslin RD. Using DNS for active flow control. *AIAA Paper 2001-2544*, 2001.
- [169] Joslin RD. Discussion of DNS: Past, present, and future. In: Liu C, Liu Z, editors. *Advances in DNS/LES*, 1997. p. 1–12.
- [170] Spalart PR. Strategies for turbulence modeling and simulations. In: *4th International Symposium on Engineering Turbulence Modeling and Measurements*, Corsica, France, 1999.
- [171] Israel DM, Fasel HF. Numerical investigation of turbulent separation control using periodic disturbances. *AIAA Paper 2002-0409*, 2002.
- [172] Piomelli U, Balaras E. Wall-layer models for large eddy simulations. *Ann Rev Fluid Mech*, 2002;34:349–374.

- [173] Tennekes H, Lumley JL. A First Course in Turbulence. MIT Press, 1972.
- [174] Canuto VM. Large eddy simulation of turbulence: A subgrid scale model including shear, vorticity, rotation, and buoyancy. *The Astrophysical Journal*, 1994;428:729–752.
- [175] Kral LD. Recent experience with different turbulence models applied to the calculation of flow over aircraft components. *Prog Aero Sci*, 1998;34:481–541.
- [176] Rubinstein R, Rumsey CL, Sala MD, Thomas JL. Turbulence modeling workshop. Technical Report CR-2001-210841, NASA, 2001.
- [177] Slomski JF, Gorski JJ, Miller RW, Marino TA. Numerical simulation of circulation control airfoils as affected by different turbulence models. AIAA Paper 2002-0851, 2002.
- [178] Carpenter MH, Singer BA, Yamaleev N, Vatsa VN, Viken SA, Atkins HL. The current status of unsteady CFD approaches for aerodynamic flow control. AIAA Paper 2002-3346, 2002.
- [179] Piomelli U. Large-eddy simulation: Achievements and challenges. *Prog Aero Sci*, 1999;35:335–362.
- [180] Theofilis V. On steady-state solutions and their nonparallel global linear instability. In: *EUROMECH European Turbulence Conference ETC*, Barcelona, Spain, 2000. p. 35–38.
- [181] Streett CL, Hussaini MY. A numerical simulation of the appearance of chaos in finite-length Taylor-Couette flow. *Appl Num Math*, 1991;7:41–71.
- [182] Joslin RD, Horta LG, Chen FJ. Transitioning active flow control to applications. AIAA Paper 99-3575, 1999.
- [183] Joslin RD. Direct simulation of evolution and control of three-dimensional instabilities in attachment-line boundary layers. *J Fluid Mech*, 1995;291:369–392.
- [184] Joslin RD, Grosch CE. Growth characteristics downstream of a shallow bump: Computation and experiment. *Phys Fluids*, 1995;7(12):3042–3047.
- [185] Kral LD, Donovan JF, Cain AB, Cary AW. Numerical simulation of synthetic jet actuators. AIAA Paper 97-1824, 1997.
- [186] Lee CY, Goldstein DB. Two-dimensional synthetic jet simulation. *AIAA J*, 2002;40(3):510–516.
- [187] Joslin RD, Baker W, Paterson E, Peltier J. Aerodynamic prediction of a NACA0015/flap flow control configuration. AIAA Paper 2002-0410, 2002.
- [188] Joslin RD, Viken SA. Baseline validation of unstructured grids RANS towards active flow control. *J Aircraft*, 2001;38(2):389–392.
- [189] Seifert A, Pack LG. Oscillatory control of separation at high Reynolds numbers. *AIAA J*, 1999;37(9):1062–1071.

- [190] Donovan JF, Kral LD, Cary AW. Active flow control applied to an airfoil. AIAA Paper 98-0210, 1998.
- [191] Ravindran SS. Active control of flow separation over an airfoil. Technical Report TM-1999-209838, NASA, 1999.
- [192] Anderson WK, Bonhaus DL. An implicit upwind algorithm for computing turbulent flows on unstructured grids. *Computers in Fluids*, 1994;23(1):1–21.
- [193] Anderson WK, Rausch RD, Bonhaus DL. Implicit/multigrid algorithms for incompressible turbulent flows on unstructured grids. *J Comp Phys*, 1996;128:391–408.
- [194] Spalart PR, Allmaras SR. A one-equation turbulence model for aerodynamic flows. AIAA Paper 92-0439, 1992.
- [195] Marcum DL. Generation of unstructured grids for viscous flow applications. AIAA Paper 95-0212, 1995.
- [196] Marcum DL, Weatherhill NP. Unstructured grid generation using iterative point insertion and local reconnection. *AIAA J*, 1995;33(9):1619–1625.
- [197] Rumsey CL, Thomas JL, Warren GP, Liu GC. Upwind Navier–Stokes solutions for separated periodic flows. *AIAA J*, 1987;25(4):535–541.
- [198] Baldwin B, Lomax H. Thin layer approximation and algebraic model for separated turbulent flow. AIAA Paper 78-257, 1978.
- [199] Abid R, Rumsey C, Gatski T. Prediction of nonequilibrium turbulent flows with explicit algebraic stress models. *AIAA J*, 1995;33(11):2026–2031.
- [200] McLean JD, Crouch JD, Stoner RC, Sakurai S, Seidel GE, Feifel WM, Rush HM. Study of the application of separation control by unsteady excitation to civil transport aircraft. Technical Report CR-1999-209338, NASA, 1999.
- [201] Pack L, Schaefflet N, Yao CS, Seifert A. Active control of separation from the slat shoulder of a supercritical airfoil. AIAA Paper 2002-3156, 2002.
- [202] Greenblatt ASD, Wagnanski I. A mini UAV controlled and propelled by periodic excitation. Patent Pending, 2002.
- [203] Uturkar R, Mittal R, Rampongoon P, Cattafesta L. Sensitivity of synthetic jets to the design of the jet cavity. AIAA Paper 2002-0124, 2002.
- [204] Seifert A, Eliahu S, Greenblatt D, Wagnanski I. Use of piezoelectric actuators for airfoil separation control. *AIAA J*, 1998;36(8):1535–1537.
- [205] Margalit S, Greenblatt D, Seifert A, Wagnanski I. Active flow control of a delta wing at high incidence using segmented piezoelectric actuators. AIAA Paper 2002-3270, 2002.

- [206] Goldstein ME. The coupling between flow instabilities and incident disturbances at a leading-edge. *J Fluid Mech*, 1981;104:217–246.
- [207] Goldstein ME. The evolution of Tollmien–Schlichting waves near a leading edge. *J Fluid Mech*, 1983;127:59–81.
- [208] Halfon E, Nishri B, Seifert A, Wygnanski I. Effects of elevated free-stream turbulence on active control of a transitional separation bubble. *AIAA Paper 2002-3169*, 2002.
- [209] Nishri B. On the dominant mechanism of active control of flow separation. PhD thesis, Tel-Aviv University, 1995.
- [210] Hein S, Theofilis V. On instability characteristics of isolated vortices and models of trailing-vortex systems. *Computers and Fluids*, 2004;33:741–753.
- [211] Seifert A, Pack LG. Active control of separated flow on a wall-mounted “hump” at high Reynolds numbers. *AIAA J*, 2002;40(7):1363–1372.
- [212] Greenblatt D, Nishri B, Darabi A, Wygnanski I. Some factors affecting stall control with particular emphasis on dynamic stall. *AIAA paper 99-3504*, 1999.
- [213] Zhou MD, Wygnanski I. The response of a mixing layer formed between parallel streams to a concomitant excitation at two frequencies. *J Fluid Mech*, 2001;441:139–168.
- [214] Gad-el-Hak M, editor. *The CRC Handbook of MEMS*. CRC Press, Boca Raton, Florida, 2001.
- [215] Nokhimovitch M, Benima R, Aharonov H, Seifert A. Closed-loop control of a ball position on a beam using piezoelectric fluidic jets. In: *Proceedings of the 42nd ISR Aero Meeting*, 2002.
- [216] Pack LG, Seifert A. Periodic excitation for jet vectoring and enhanced spreading. *J Aircraft*, 2001;38(3):486–495. (also *AIAA Paper 99-0672*).
- [217] Elsberry K, Likhachev O, de Zhou M, Wygnanski I. An experimental and theoretical study of a boundary layer approaching separation. *AIAA paper 97-0867*, 1997.

## List of Tables

1	Status of computational aerodynamics [167] . . . . .	73
2	Multi-block In-Tunnel Grids . . . . .	74

Stage of Approximation	Readiness time period			Limitations	Pacing Items
	2D Airfoils	3D Wings	3D Aircraft		
Inviscid linearized	1930's Used in current aircraft design	1950's	1970's	Slender configurations Small angle of attack Perfect gas No transonic flow No hypersonic flow No flow separation	
Inviscid nonlinear	1971 Development nearly complete	1973	1976	No flow separation	Code development
Viscous time averaged	1975 Early stage of development	1977	1979	Accuracy of turbulence model	Turbulence modeling
Viscous time dependent	Mid 1980's			Accuracy of Navier-Stokes equations	Development of advanced computers

Table 1: Status of computational aerodynamics [167]

Grid	Course		Fine	
	J	K	J	K
1	17	89	17	87
2	63	43	63	42
3	67	43	67	42
4	25	5	25	5
5	89	5	89	5
6	167	47	257	44
7	9	13	9	29
8	9	13	9	29
9	9	13	9	29

Table 2: Multi-block In-Tunnel Grids

## List of Figures

1	Left: spatial structure of the chordwise component of the most unstable stationary BiGlobal eigenmode. Right: a schematic representation of vortex shedding from separation bubbles, on account of BiGlobal instability [52]. . . . .	78
2	Three-dimensionalization of the reattachment zone on account of amplification of a BiGlobal eigenmode, in the absence of KH/TS instability [52]. . . . .	79
3	Regular three-dimensional structures in the wake of a circular cylinder in transitional flow [55]. . . . .	80
4	Magnification of Fig. 3 and sketch of the topological characteristics of an isolated structure. . . . .	81
5	Upper: asymmetric structures in transitional flow over an airfoil. Lower: topological characteristics of these structures [58]. . . . .	82
6	Schematic of the generic flap configuration using in the experiments of Nishri [209].	83
7	Typical closed-loop block diagram. . . . .	84
8	Modern-control block diagram. . . . .	85
9	Drag and turbulent kinetic energy (TKE) histories for LES based terminal turbulent kinetic energy control for different optimization windows $T^+$ at $R_\tau = 100$ [126]. . . . .	86
10	Schematic of optimal DNS control. . . . .	87
11	Drag and TKE histories for LES, DNS, and hybrid LES/DNS based terminal TKE control for optimization interval $T^+ = 30$ at $R_\tau = 100$ [126]. . . . .	88
12	Effect of sensing plane location on drag at different Reynolds numbers [107]. . . . .	89
13	Effect of Reynolds number on power savings ratios: — Actual ration of power saved to power input, --- conservative estimate of power saved to power input. The - - - - line shows the average of the two power savings ratios [107]. . . . .	90
14	Effect of control on the spatial structure of the dominant roll mode : (a) streamwise component, (b) wall-normal component, and (c) spanwise component. — no control; ····· opposition control; - - - - optimal control [151]. . . . .	91
15	Effect of control on the spatial eigenstructure for the dominant roll mode: (a) no control, (b) opposition control, and (c) optimal control. The solid horizontal line denotes the location of the virtual wall [151]. . . . .	92
16	Peak exit velocity with lip thickness [186]. . . . .	93
17	Leading edge and upper surface notch. . . . .	94
18	Lift coefficients versus angle of attack (computed using full simulation pressure distributions). [188]. . . . .	95
19	Lift coefficients with angle of attack, where simulation $C_l$ was computed using the same pressure tap locations as used in the experiment. [188]. . . . .	96
20	Sketch of NACA0015/flap configuration [189]. Upper plot shows flap shoulder slot design. . . . .	97
21	Single-block structured grid. . . . .	98
22	Residual and lift coefficient ( $C_l$ ) versus the number of iterations ( $\alpha = 0^\circ$ ). . . . .	99
23	Pressure coefficient with chordwise location ( $\alpha = -4^\circ$ ). . . . .	100
24	Multi-block grid of NACA0015/flap configuration in wind tunnel. . . . .	101

25	Residual and lift coefficient ( $C_l$ ) with number of iterations ( $R = 17 \times 10^6$ and $28 \times 10^6$ with $\alpha = 0^\circ$ ). Note that the curves at the two different Reynolds numbers are nearly identical. . . . .	102
26	Streamwise ( $u$ ) velocity contours at $R = 8 \times 10^6$ and $\alpha = 0^\circ$ . . . . .	103
27	Pressure coefficient with chordwise location ( $\alpha = 0^\circ$ ; $R = 28 \times 10^6$ ). . . . .	104
28	Unstructured mesh around airfoil/flap configuration with notch discontinuity . . . .	105
29	Streamwise velocity contours ( $R = 8 \times 10^6$ ; $\alpha = 0^\circ$ ). . . . .	106
30	Pressure coefficient versus chordwise location ( $\alpha = -4^\circ$ ). . . . .	107
31	Streamwise velocity contours ( $R = 8 \times 10^6$ ; $\alpha = 0^\circ$ ). . . . .	108
32	Maximum lift coefficient of the IAI Pr8-30 slotted airfoil (shown above) at low Reynolds numbers [7]. . . . .	109
33	Generic Active Flow Control process. . . . .	110
34	Computed actuator output in still air (left) and interacting with boundary layer (right) showing the effect on both, ( $R = 0$ and $R = 1200$ where Reynolds number is based on the displacement thickness of the incoming boundary layers), courtesy Uturkar et al. [203]). . . . .	111
35	The IAI Pr8-SE airfoil with ten Piezo-bender actuators (only two are shown schematically) across the 609mm span of the airfoil [204]. . . . .	112
36	A cross section (upper part) and a top view (lower part) of the Piezo-bender actuators on the Pr8-SE airfoil [204]. . . . .	113
37	RMS velocity fluctuations measured close to the tip of a Piezo-bender actuator in the turbulent boundary layer of the IAI Pr8-SE [204]. . . . .	114
38	Lift to Drag ratio of the IAI Pr8-SE plotted against lift due to the activation of the segmented Piezo benders at 2D and 3D modes [204]. . . . .	115
39	Figure of Merit ( $F.M.$ see Eq. (10)) of the IAI Pr8-SE due to the activation of the segmented Piezo benders at 2D and 3D modes [204]. . . . .	116
40	(a) Experimental setup of the “generic flap” [209]. (b) The effect of actuator type on the frequency response of the reattaching BL, (c) as explained by the ratio of the fundamental to harmonic content of the excitation with variation of the total excitation momentum [209]. . . . .	117
41	The effect of the excitation amplitude on the frequency response of separated flow [209]. . . . .	118
42	The effect of the excitation amplitude on the frequency response of the separated flow about the “generic flap” [6] using zero mass-flux excitation. . . . .	119
43	The combined influence of unsteady and steady excitation for a turbulent boundary layer separation. (a) Sectional side view of the “Hump” model with an excitation slot at $x/c = 0.64$ [211]. (b) Mean and fluctuating model pressures showing the effect of superimposed weak steady mass flux superimposed on the excitation signal. (c) The effect of the added mass flux on the fundamental excitation frequency and its harmonic downstream of the slot. Unsteady $C_\mu = 0.23\%$ , $R_c = 16 \times 10^6$ , $M = 0.25$ , $F^+ = 1.15$ . . . . .	120

44	Effect of forcing frequency for unsteady excitation of a turbulent boundary layer separation. (a) Mean and fluctuating pressures showing the effect of the excitation frequency, and (b) the evolution of the fundamental excitation frequency downstream of the $x/c = 0.64$ slot (vertical dashed line). $C_{\mu}=0.13\%$ , $R_c = 16 \times 10^6$ , $M = 0.25$ [211]. . . . .	121
45	A schematic description of the jet vectoring experimental set-up, side view (a) and front view (b) with the diffuser removed [215] . . . . .	122
46	Baseline jet, Seifert, 1996 unpublished. . . . .	123
47	Deflected jet, excited upper 1/4 circumference. . . . .	124
48	Jet deflection angle as a function of excitation momentum coefficient [98]. . . . .	125
49	Diffuser and actuator cavity mean pressures due to enhanced cavity pressure fluctuations level causing enhanced jet deflection [98]. . . . .	126
50	Jet deflection actuator inputs and outputs. (a) Amplitude modulating signal provided to the signal generator (2.5 out of 90 sec). (b) Actuator's cavity pressure showing the lack of symmetry and the LPF signal, proportional to the jet deflection angle. (c) Hot wire measured velocity signal at $x/D = 1$ and opposite active actuator, showing the jet flow response, indicative of the jet deflection angle [98]. . . . .	127
51	Comparison of oscillatory and steady blowing for post-stall lift-recovery of a NACA 0015 at, $R_c = 300,000$ [7]. . . . .	128

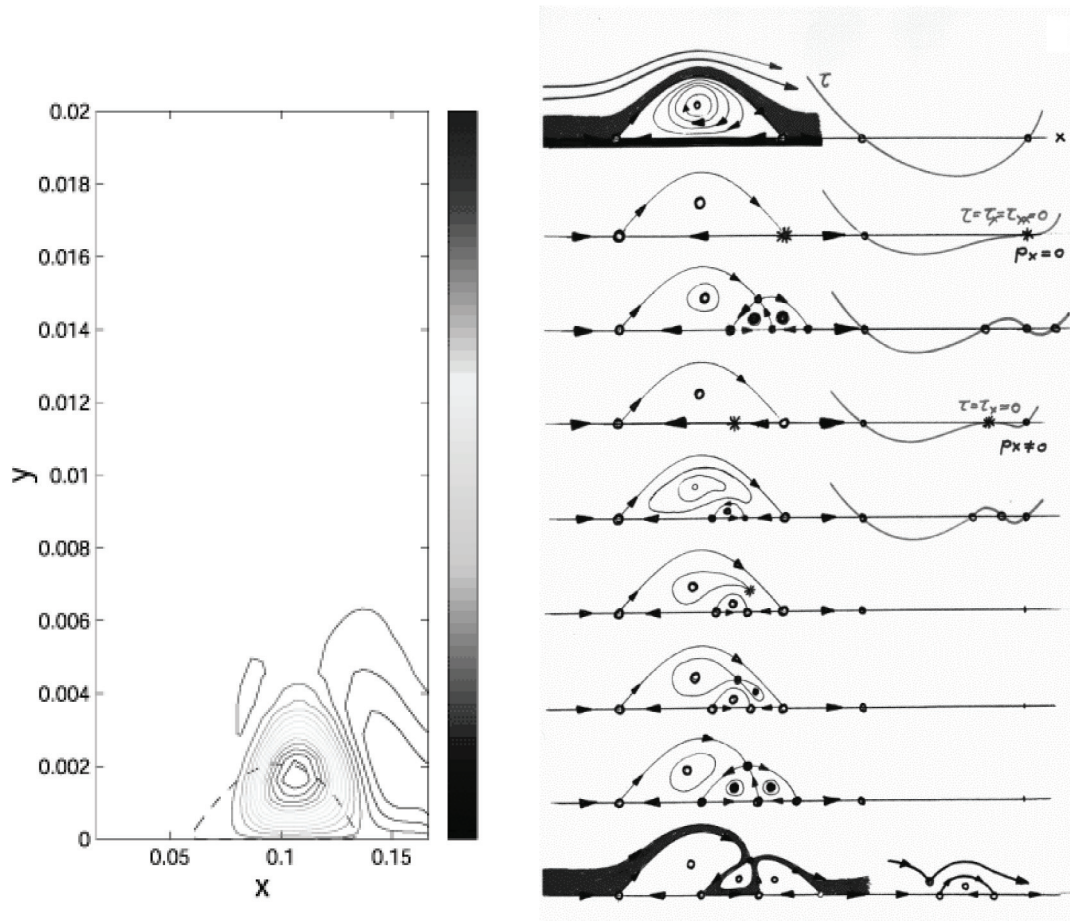


Figure 1: Left: spatial structure of the chordwise component of the most unstable stationary BiGlobal eigenmode. Right: a schematic representation of vortex shedding from separation bubbles, on account of BiGlobal instability [52].

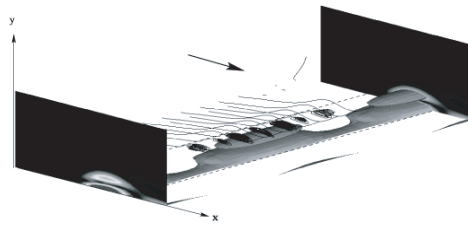


Figure 2: Three-dimensionalization of the reattachment zone on account of amplification of a BiGlobal eigenmode, in the absence of KH/TS instability [52].



Figure 3: Regular three-dimensional structures in the wake of a circular cylinder in transitional flow [55].

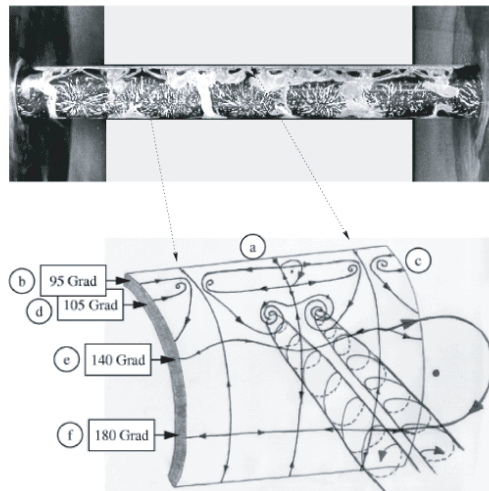


Figure 4: Magnification of Fig. 3 and sketch of the topological characteristics of an isolated structure.

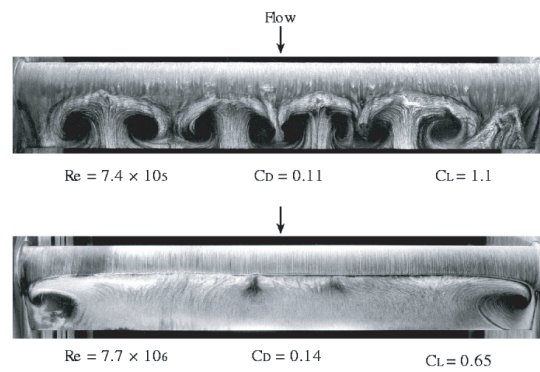


Figure 5: Upper: asymmetric structures in transitional flow over an airfoil. Lower: topological characteristics of these structures [58].

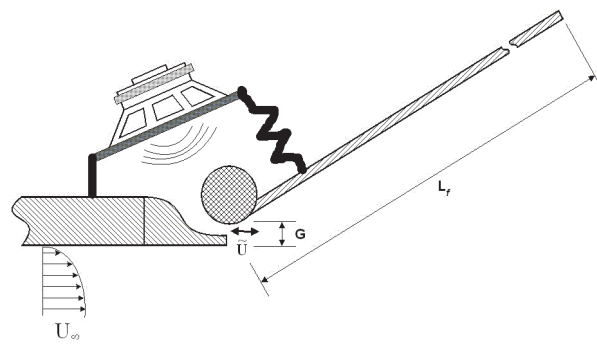


Figure 6: Schematic of the generic flap configuration using in the experiments of Nishri [209].

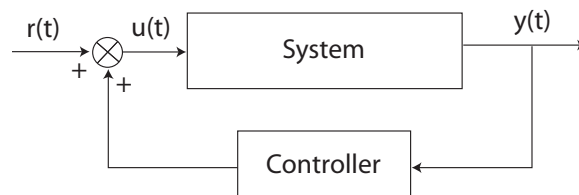


Figure 7: Typical closed-loop block diagram.

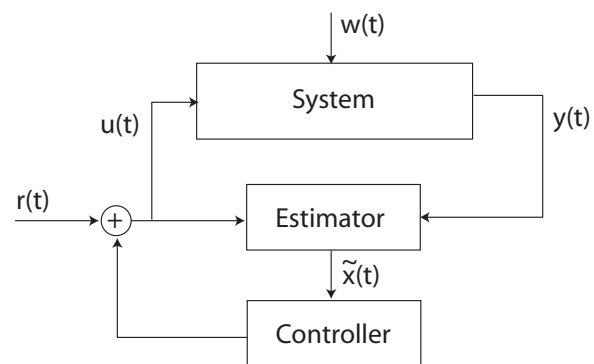


Figure 8: Modern-control block diagram.

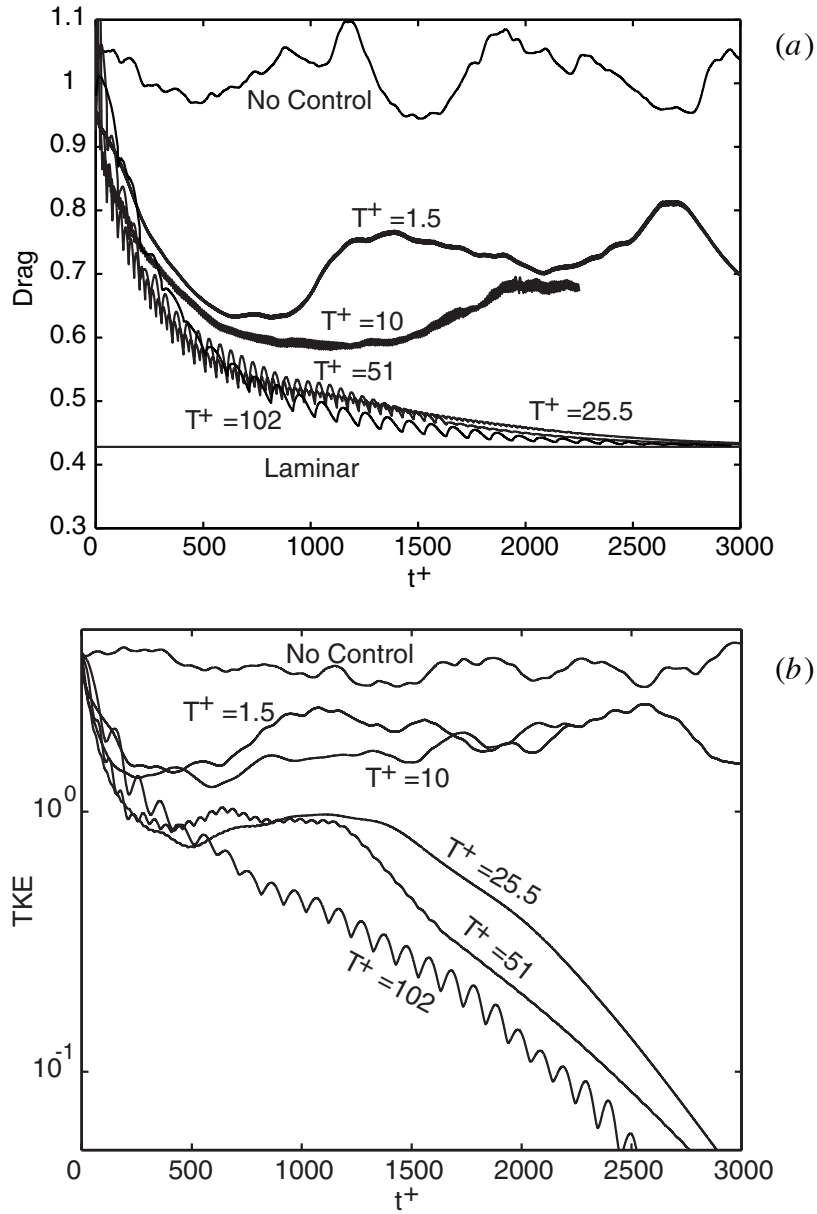


Figure 9: Drag and turbulent kinetic energy (TKE) histories for LES based terminal turbulent kinetic energy control for different optimization windows  $T^+$  at  $R_\tau = 100$  [126].

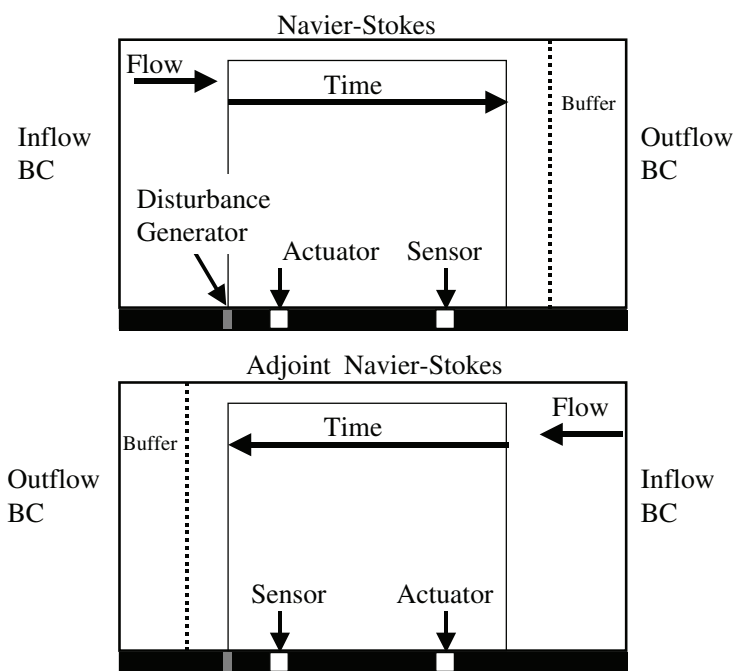


Figure 10: Schematic of optimal DNS control.

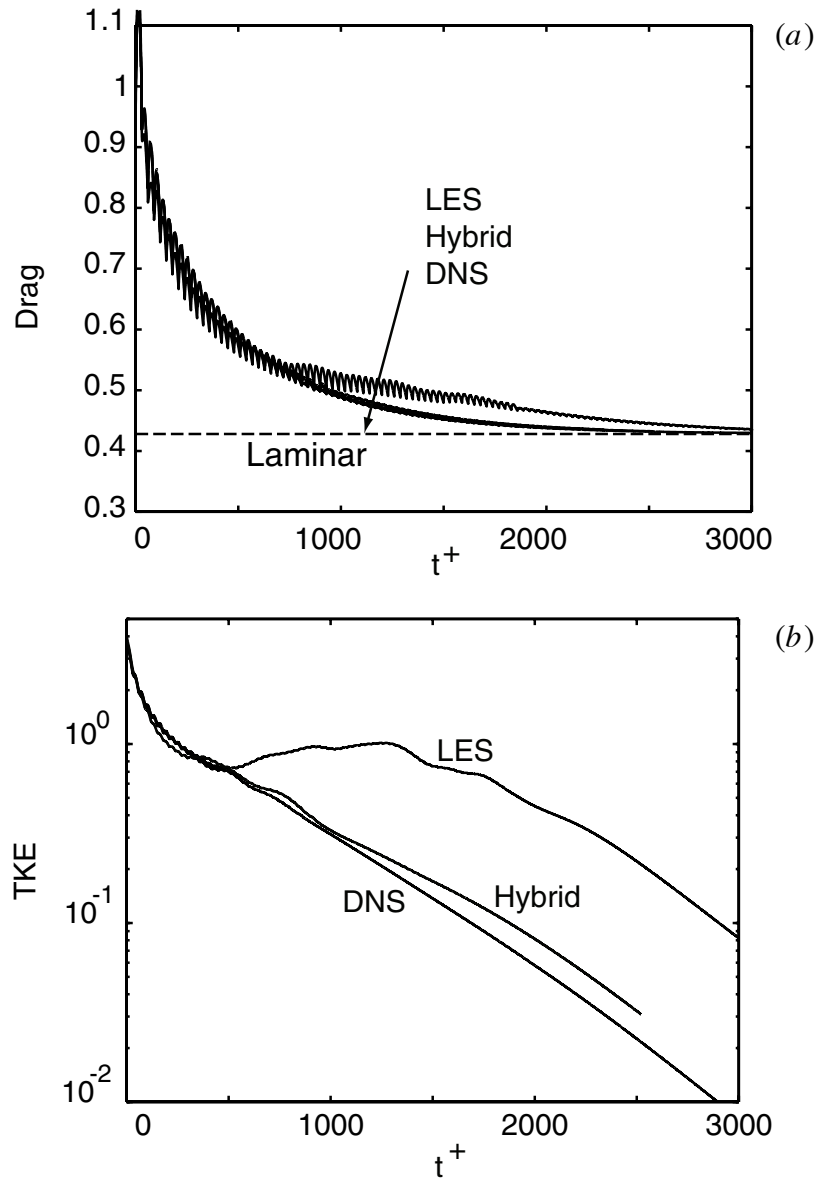


Figure 11: Drag and TKE histories for LES, DNS, and hybrid LES/DNS based terminal TKE control for optimization interval  $T^+ = 30$  at  $R_\tau = 100$  [126].

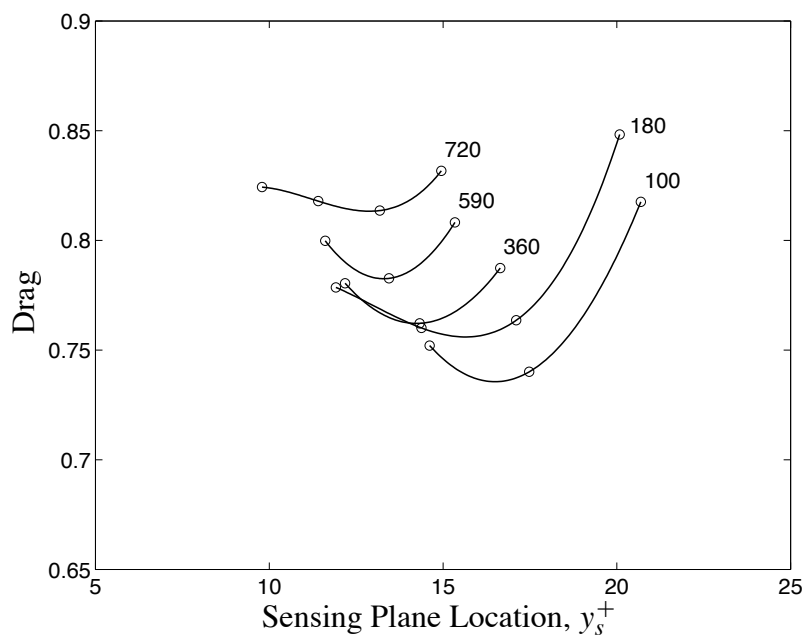


Figure 12: Effect of sensing plane location on drag at different Reynolds numbers [107].

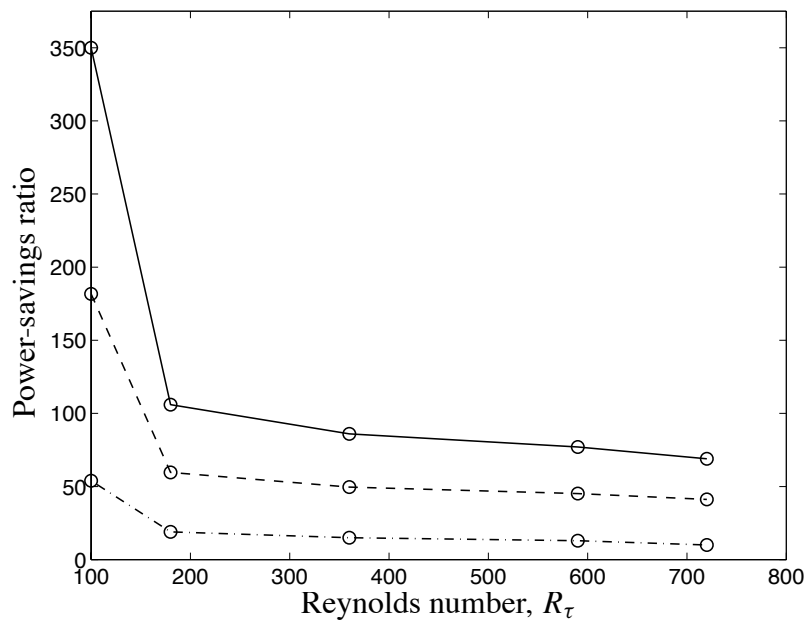


Figure 13: Effect of Reynolds number on power savings ratios: — Actual ration of power saved to power input, --- conservative estimate of power saved to power input. The - - - line shows the average of the two power savings ratios [107].

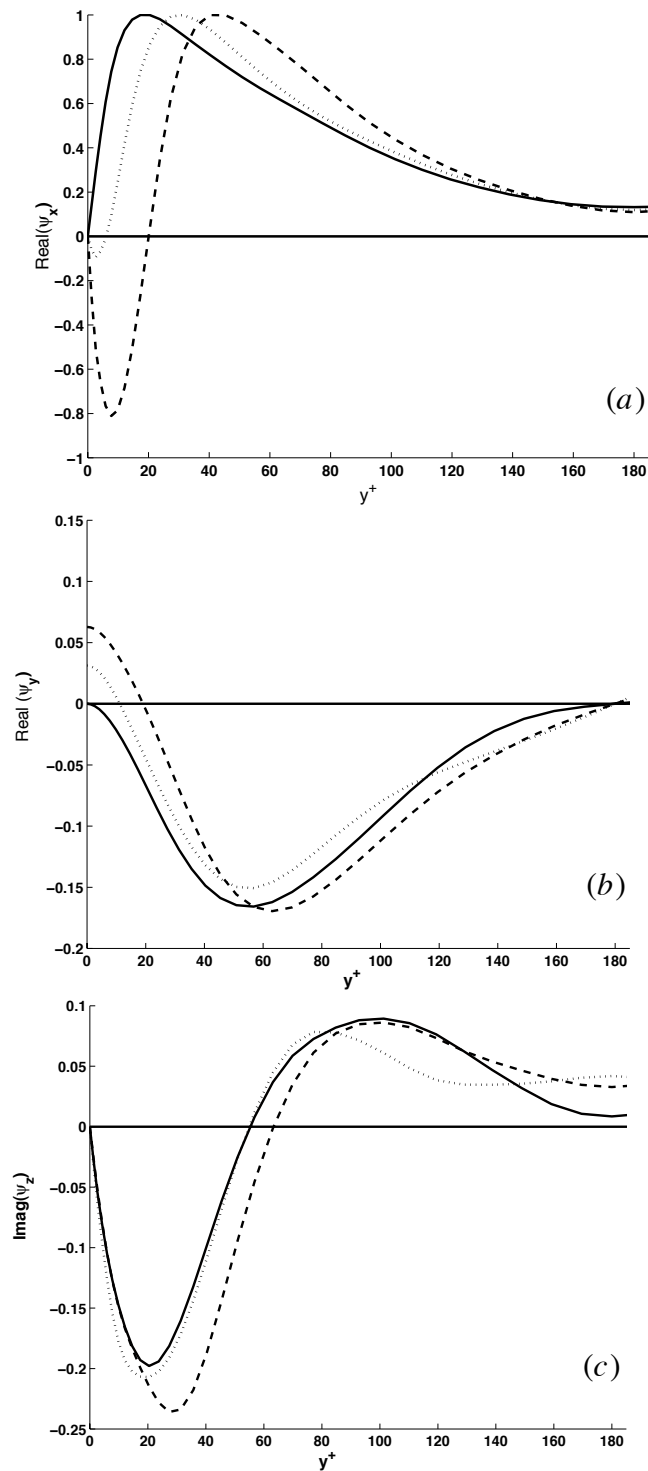


Figure 14: Effect of control on the spatial structure of the dominant roll mode : (a) streamwise component, (b) wall-normal component, and (c) spanwise component. — no control; ..... opposition control; - - - optimal control [151].

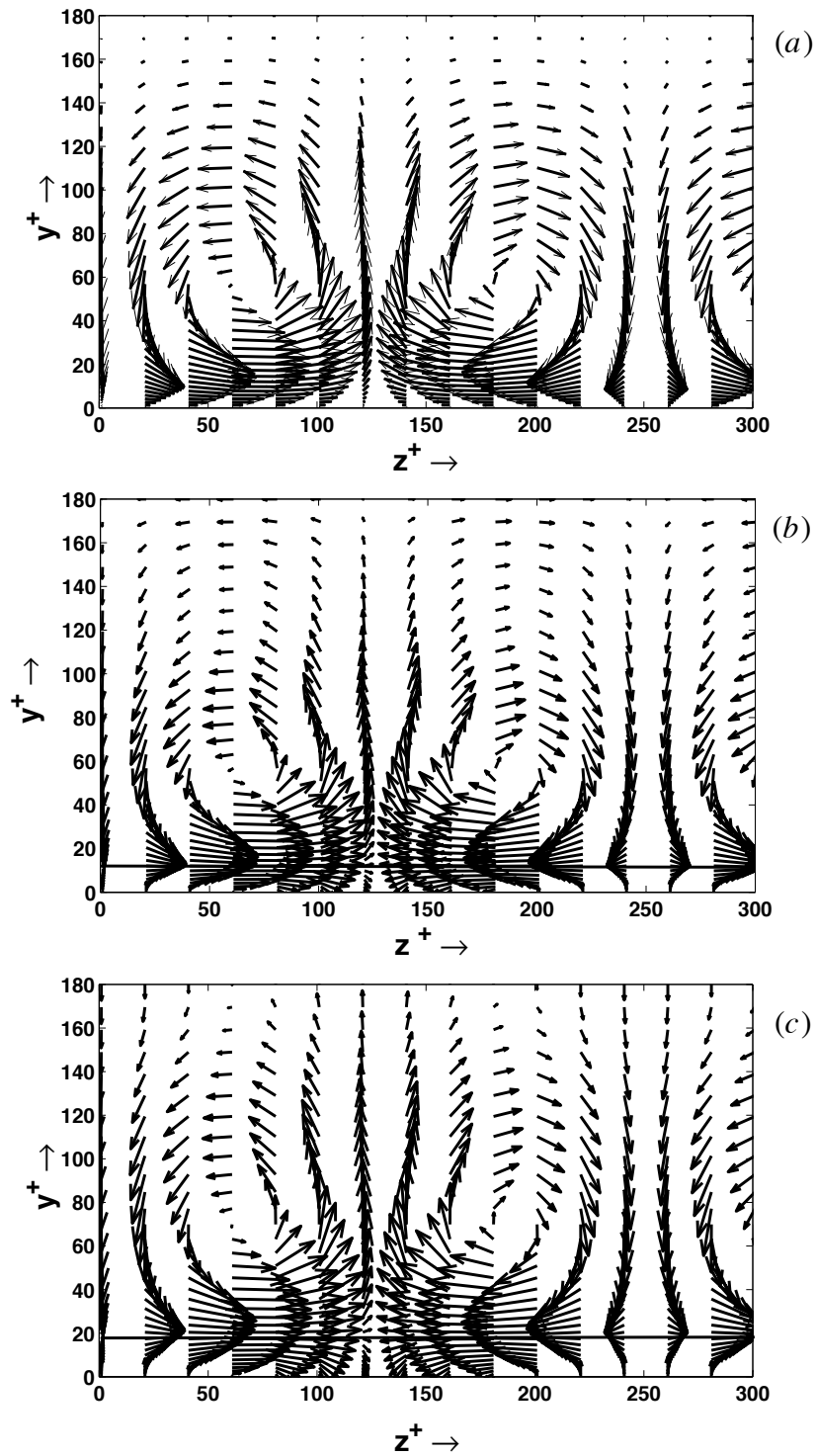


Figure 15: Effect of control on the spatial eigenstructure for the dominant roll mode: (a) no control, (b) opposition control, and (c) optimal control. The solid horizontal line denotes the location of the virtual wall [151].

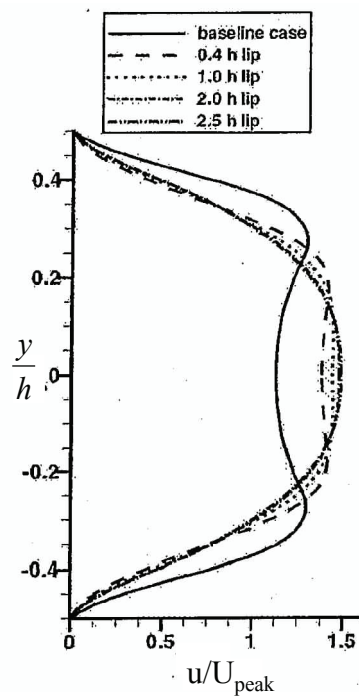


Figure 16: Peak exit velocity with lip thickness [186].

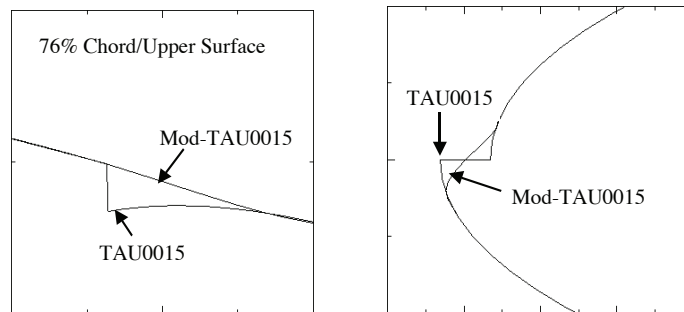


Figure 17: Leading edge and upper surface notch.

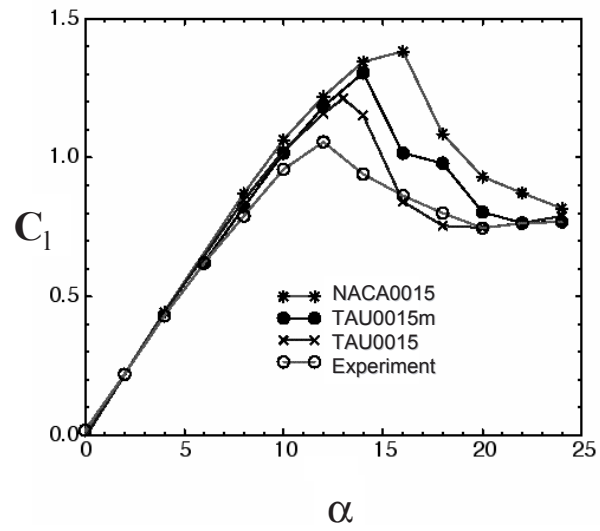


Figure 18: Lift coefficients versus angle of attack (computed using full simulation pressure distributions). [188].

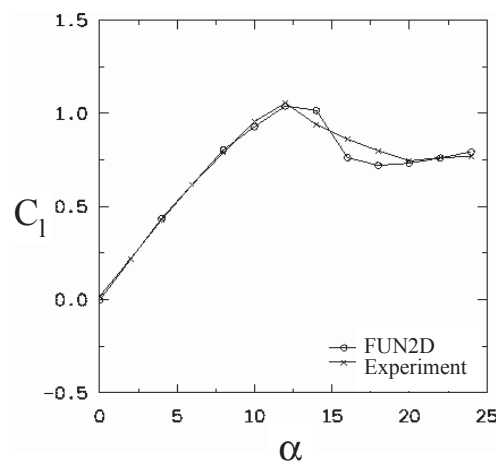


Figure 19: Lift coefficients with angle of attack, where simulation  $C_l$  was computed using the same pressure tap locations as used in the experiment. [188].

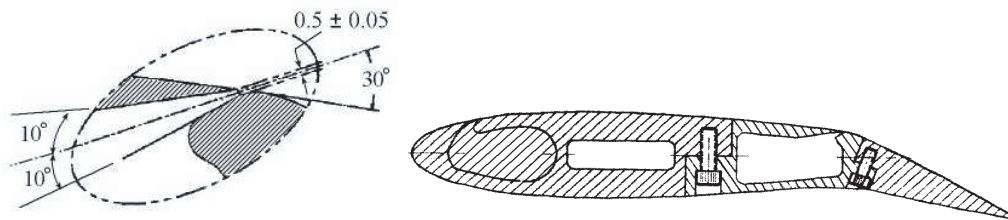


Figure 20: Sketch of NACA0015/flap configuration [189]. Upper plot shows flap shoulder slot design.

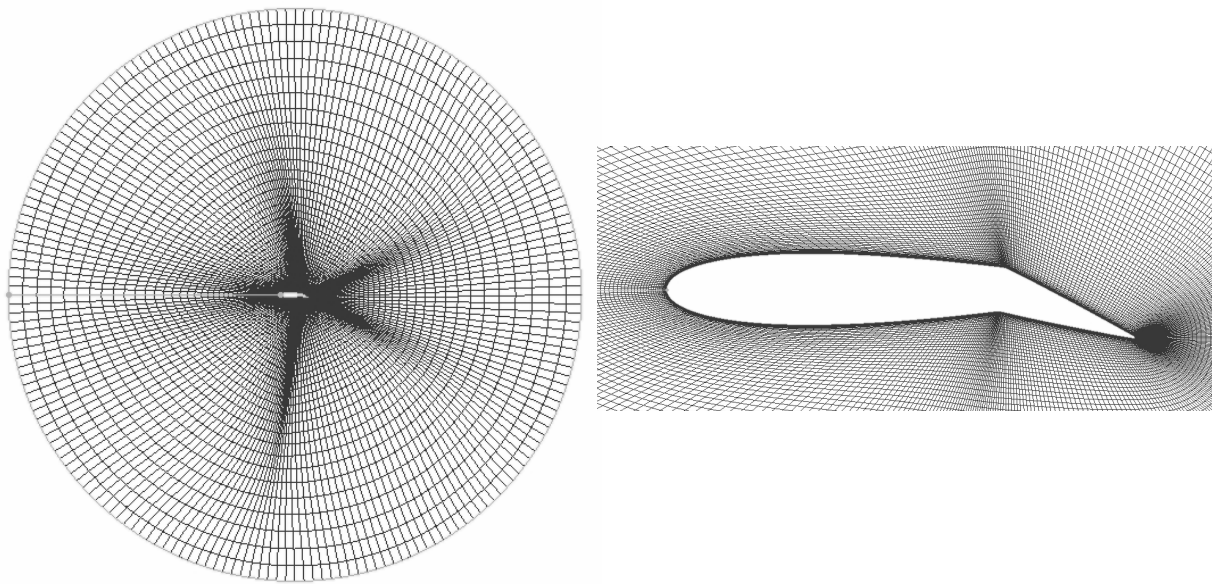


Figure 21: Single-block structured grid.

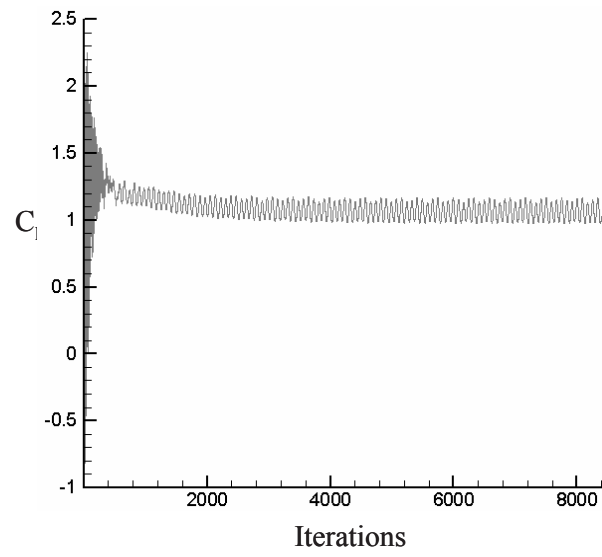


Figure 22: Residual and lift coefficient ( $C_l$ ) versus the number of iterations ( $\alpha = 0^\circ$ ).

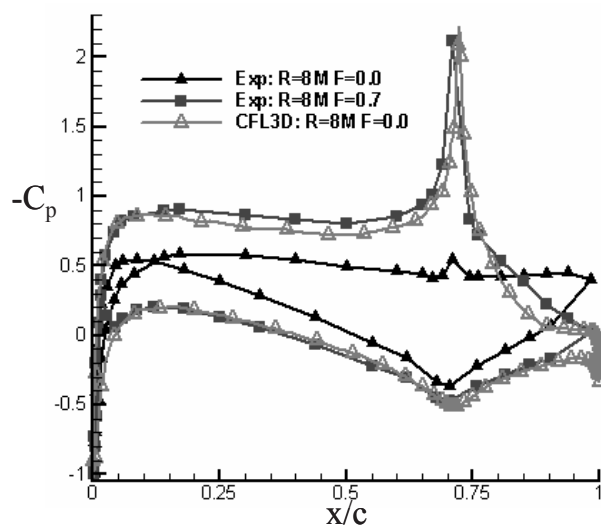


Figure 23: Pressure coefficient with chordwise location ( $\alpha = -4^\circ$ ).

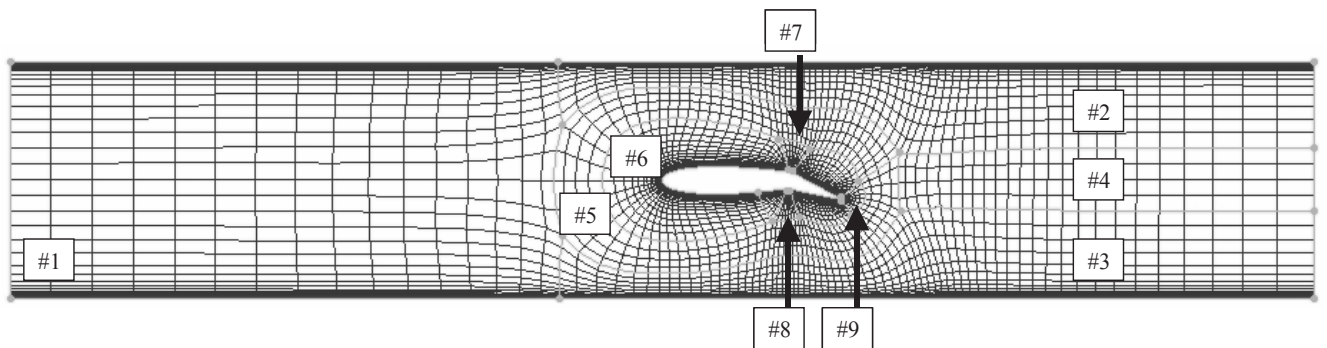


Figure 24: Multi-block grid of NACA0015/flap configuration in wind tunnel.

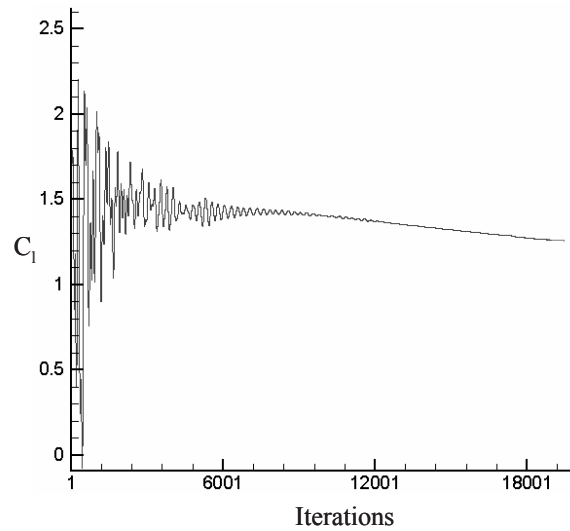
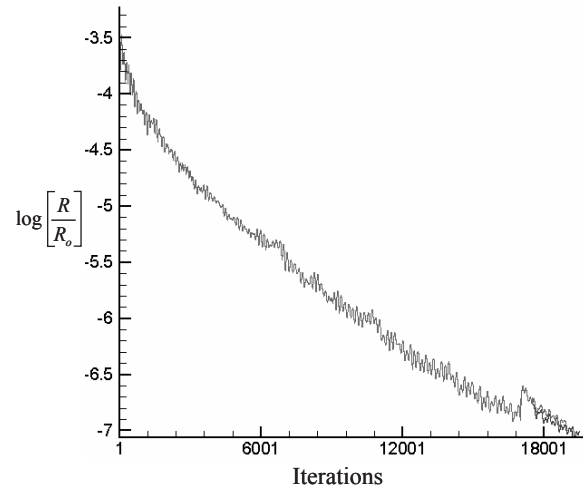


Figure 25: Residual and lift coefficient ( $C_l$ ) with number of iterations ( $R = 17 \times 10^6$  and  $28 \times 10^6$  with  $\alpha = 0^\circ$ ). Note that the curves at the two different Reynolds numbers are nearly identical.

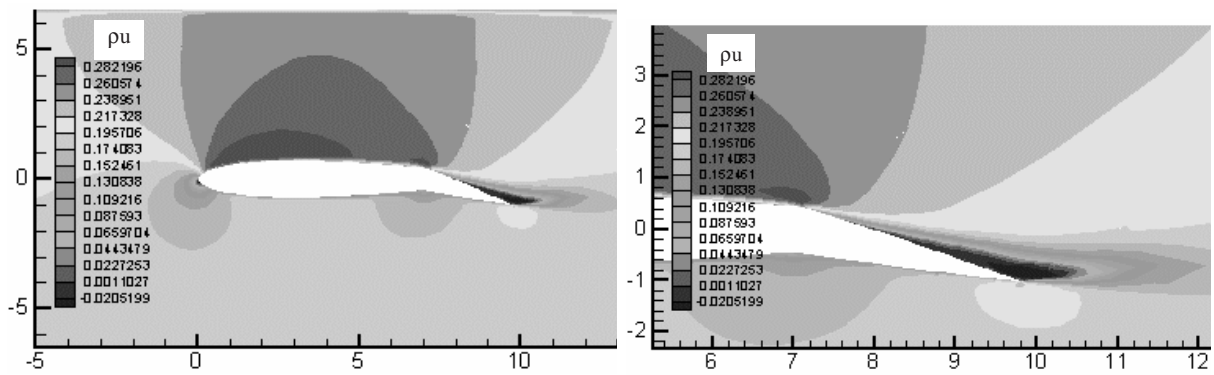


Figure 26: Streamwise ( $u$ ) velocity contours at  $R = 8 \times 10^6$  and  $\alpha = 0^\circ$ .

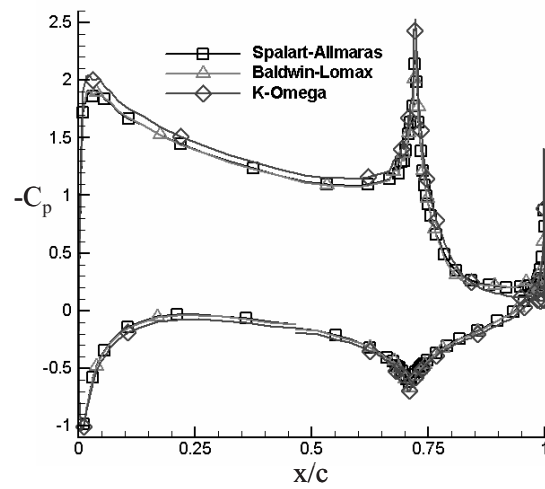


Figure 27: Pressure coefficient with chordwise location ( $\alpha = 0^\circ$ ;  $R = 28 \times 10^6$ ).

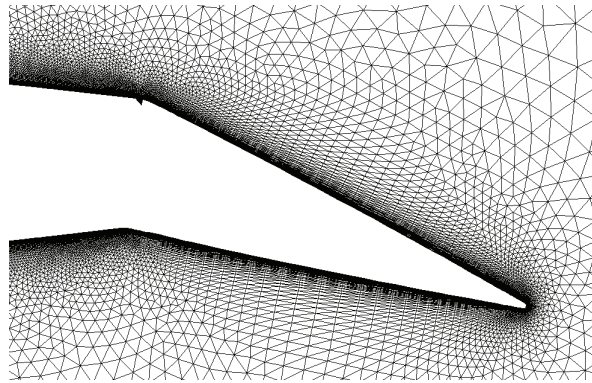


Figure 28: Unstructured mesh around airfoil/flap configuration with notch discontinuity

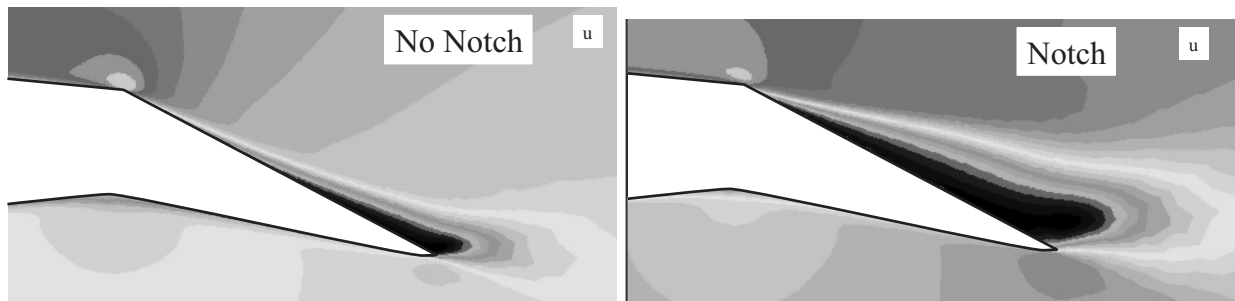


Figure 29: Streamwise velocity contours ( $R = 8 \times 10^6$ ;  $\alpha = 0^\circ$ ).

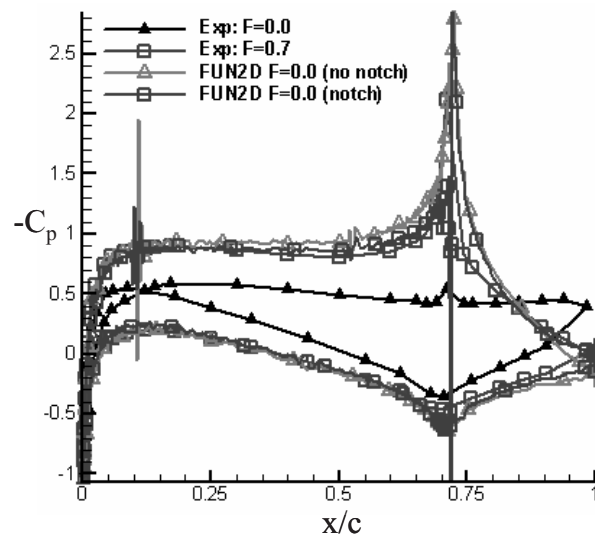


Figure 30: Pressure coefficient versus chordwise location ( $\alpha = -4^\circ$ ).

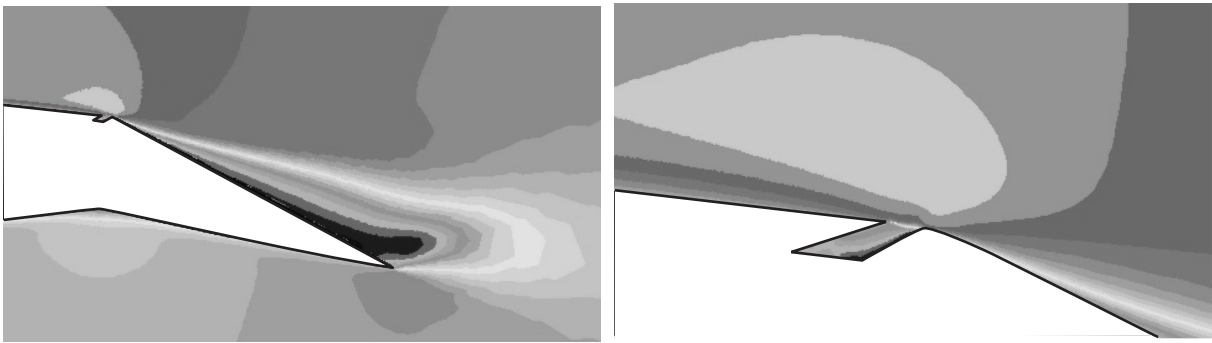


Figure 31: Streamwise velocity contours ( $R = 8 \times 10^6$ ;  $\alpha = 0^\circ$ ).

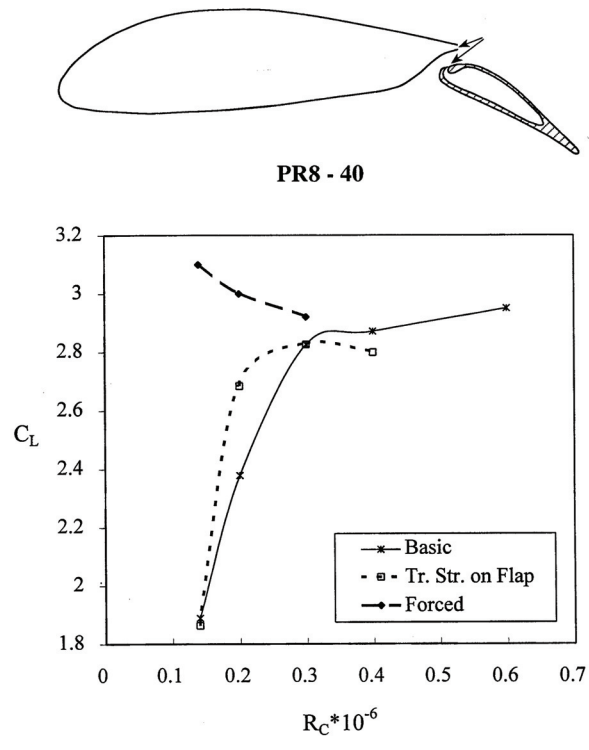


Figure 32: Maximum lift coefficient of the IAI Pr8-30 slotted airfoil (shown above) at low Reynolds numbers [7].

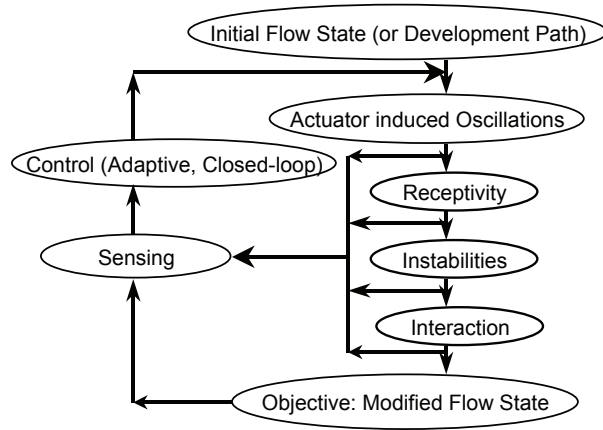


Figure 33: Generic Active Flow Control process.

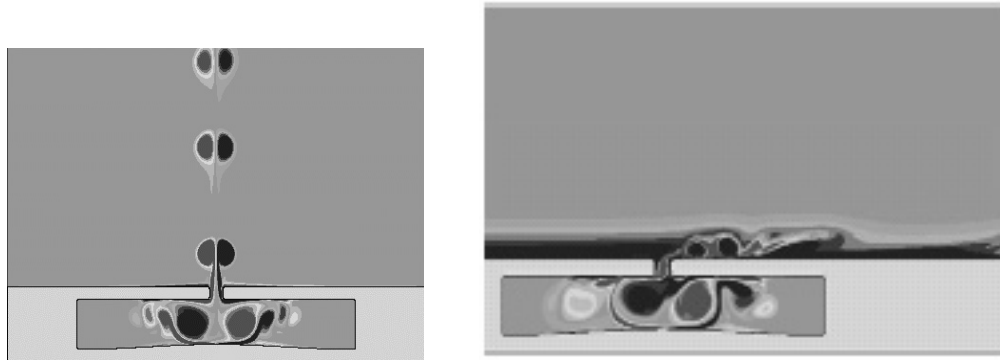


Figure 34: Computed actuator output in still air (left) and interacting with boundary layer (right) showing the effect on both, ( $R = 0$  and  $R = 1200$  where Reynolds number is based on the displacement thickness of the incoming boundary layers), courtesy Uturkar et al. [203]).

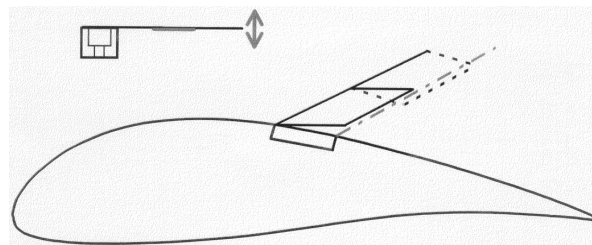


Figure 35: The IAI Pr8-SE airfoil with ten Piezo-bender actuators (only two are shown schematically) across the 609mm span of the airfoil [204].

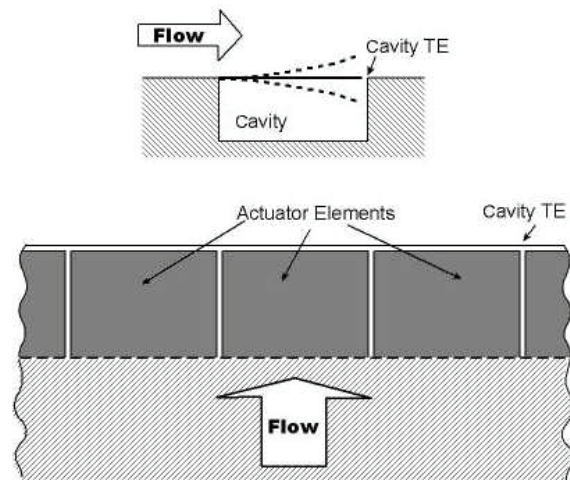


Figure 36: A cross section (upper part) and a top view (lower part) of the Piezo-bender actuators on the Pr8-SE airfoil [204].

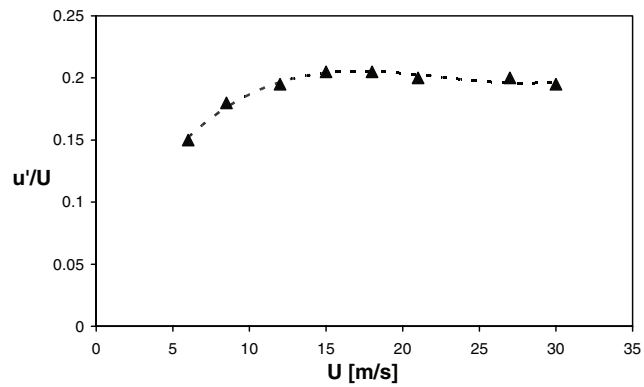


Figure 37: RMS velocity fluctuations measured close to the tip of a Piezo-bender actuator in the turbulent boundary layer of the IAI Pr8-SE [204].

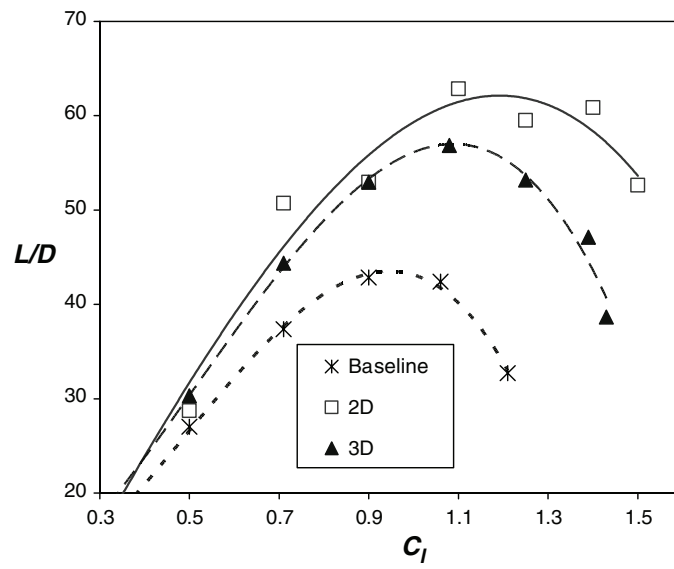


Figure 38: Lift to Drag ratio of the IAI Pr8-SE plotted against lift due to the activation of the segmented Piezo benders at 2D and 3D modes [204].

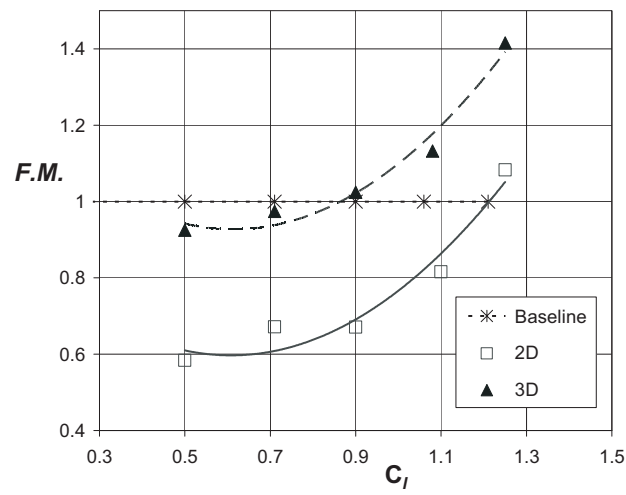


Figure 39: Figure of Merit ( $F.M.$  see Eq. (10)) of the IAI Pr8-SE due to the activation of the segmented Piezo benders at 2D and 3D modes [204].

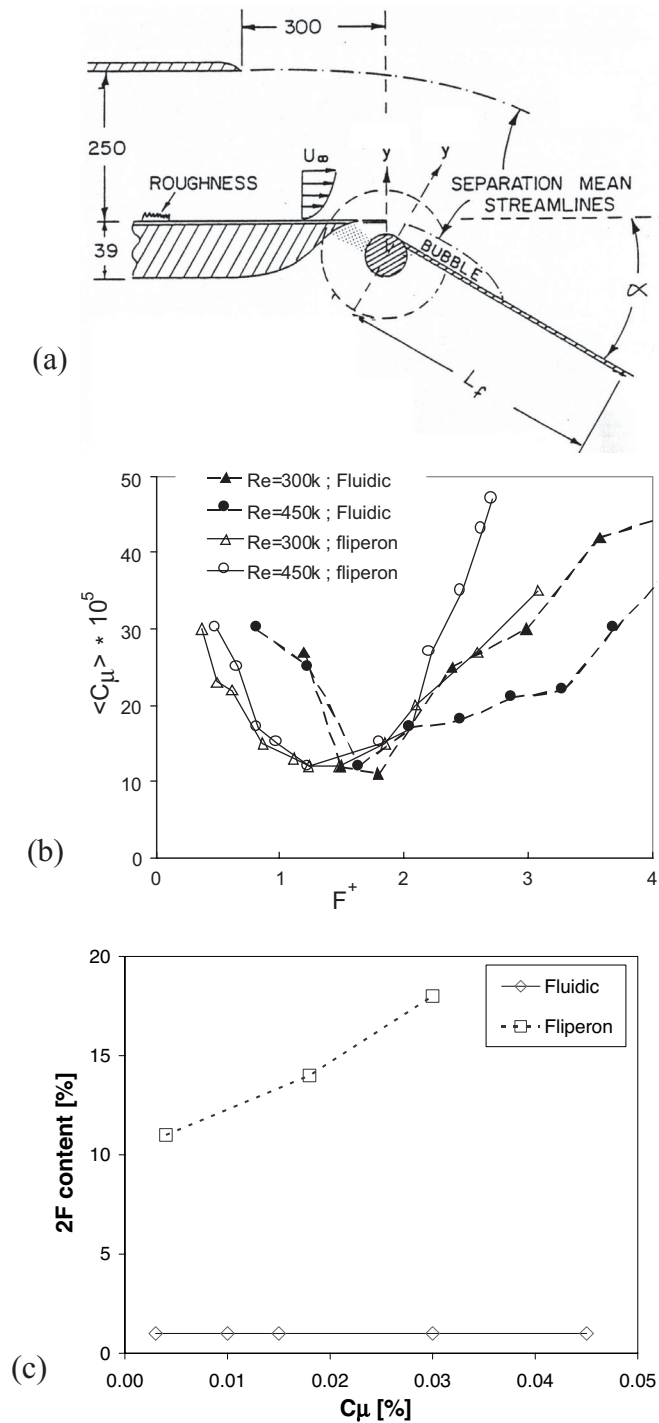


Figure 40: (a) Experimental setup of the “generic flap” [209]. (b) The effect of actuator type on the frequency response of the reattaching BL, (c) as explained by the ratio of the fundamental to harmonic content of the excitation with variation of the total excitation momentum [209].

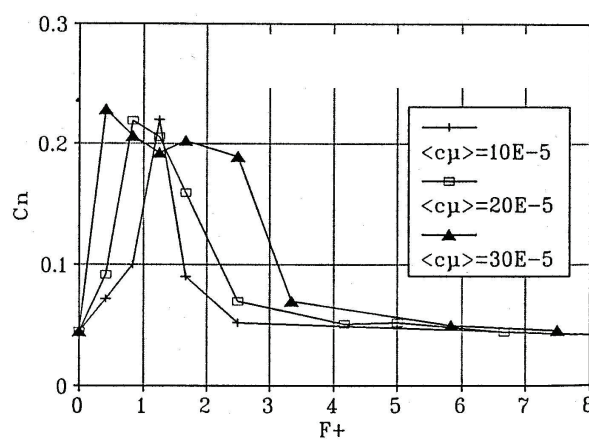


Figure 41: The effect of the excitation amplitude on the frequency response of separated flow [209].

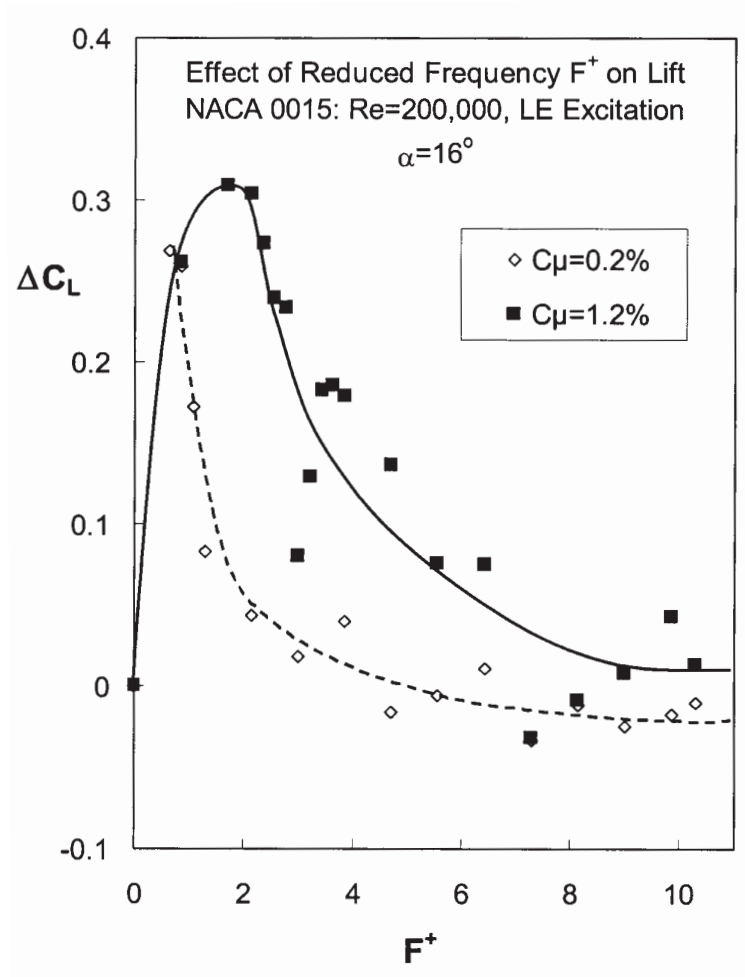
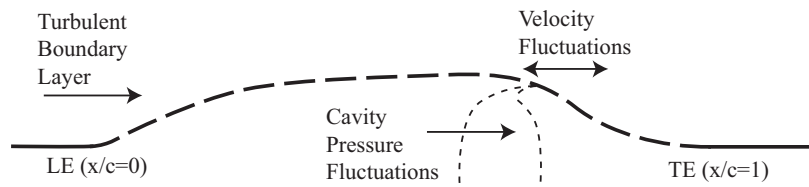
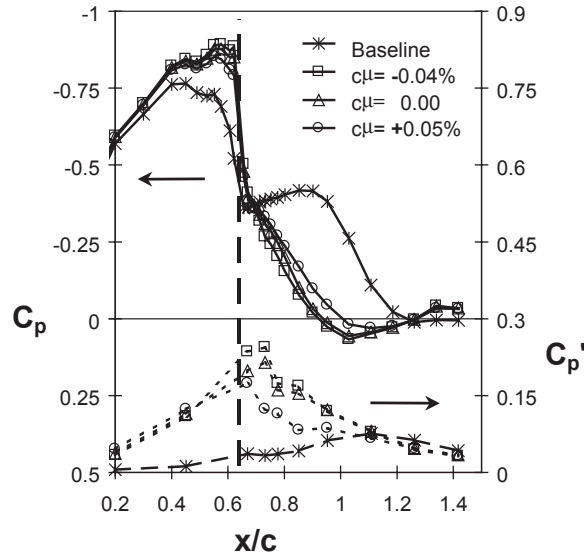


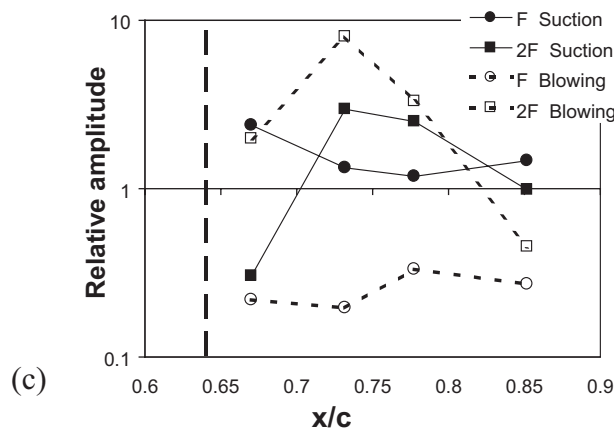
Figure 42: The effect of the excitation amplitude on the frequency response of the separated flow about the “generic flap” [6] using zero mass-flux excitation.



(a)



(b)



(c)

Figure 43: The combined influence of unsteady and steady excitation for a turbulent boundary layer separation. (a) Sectional side view of the “Hump” model with an excitation slot at  $x/c = 0.64$  [211]. (b) Mean and fluctuating model pressures showing the effect of superimposed weak steady mass flux superimposed on the excitation signal. (c) The effect of the added mass flux on the fundamental excitation frequency and its harmonic downstream of the slot. Unsteady  $C_\mu = 0.23\%$ ,  $R_c = 16 \times 10^6$ ,  $M = 0.25$ ,  $F^+ = 1.15$ .

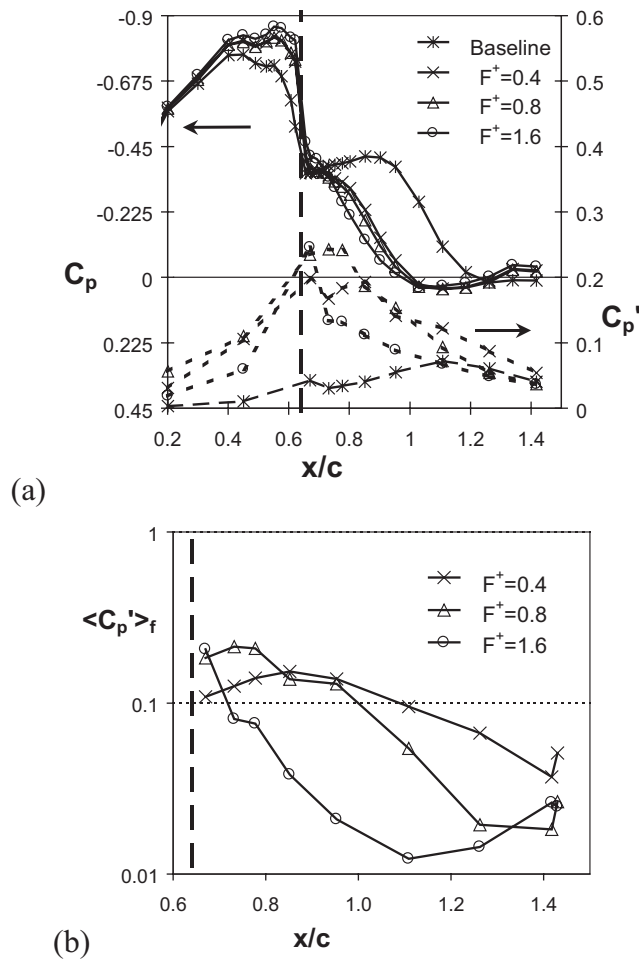


Figure 44: Effect of forcing frequency for unsteady excitation of a turbulent boundary layer separation. (a) Mean and fluctuating pressures showing the effect of the excitation frequency, and (b) the evolution of the fundamental excitation frequency downstream of the  $x/c = 0.64$  slot (vertical dashed line).  $C_\mu=0.13\%$ ,  $R_c = 16 \times 10^6$ ,  $M = 0.25$  [211].

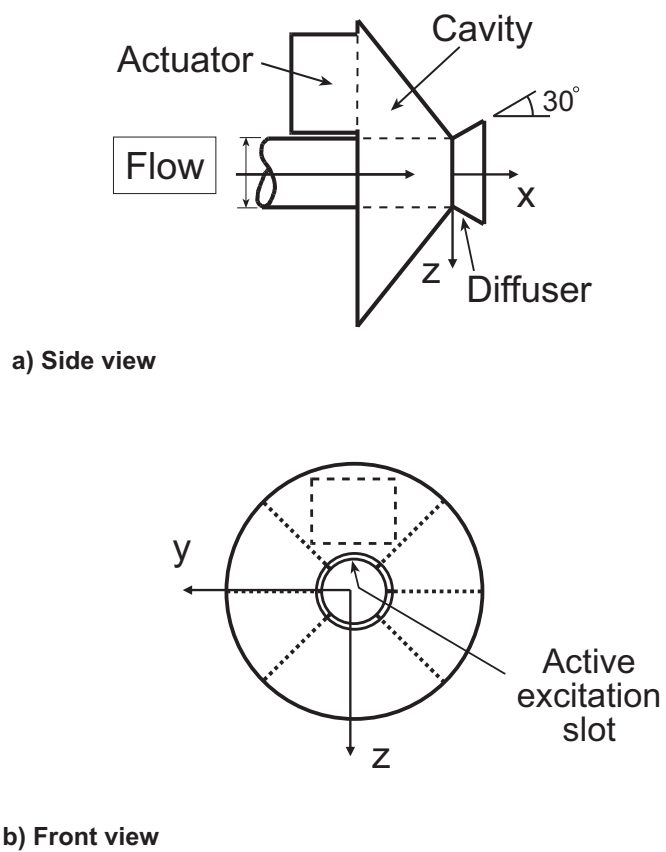


Figure 45: A schematic description of the jet vectoring experimental set-up, side view (a) and front view (b) with the diffuser removed [215]

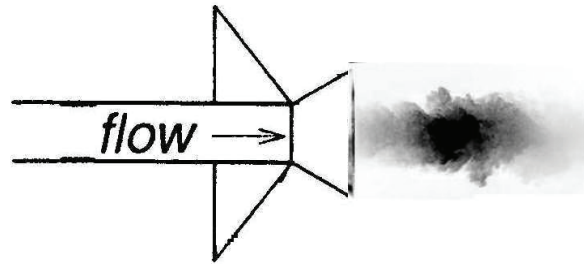


Figure 46: Baseline jet, Seifert, 1996 unpublished.

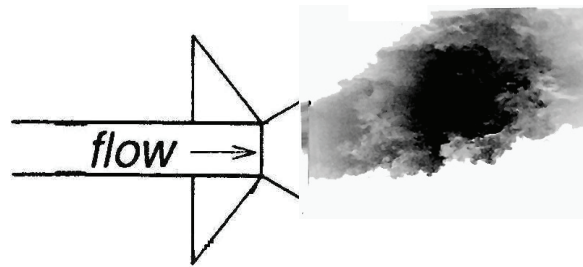


Figure 47: Deflected jet, excited upper 1/4 circumference.

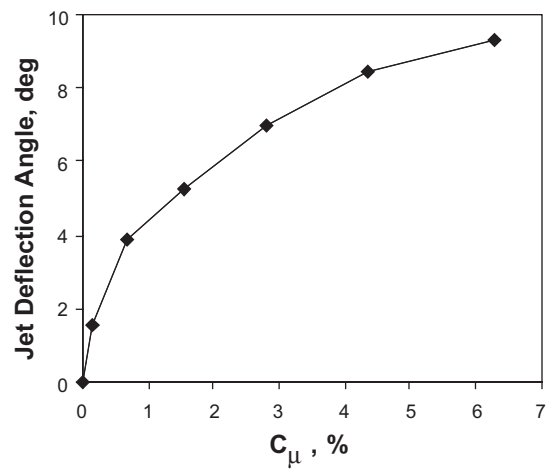


Figure 48: Jet deflection angle as a function of excitation momentum coefficient [98].

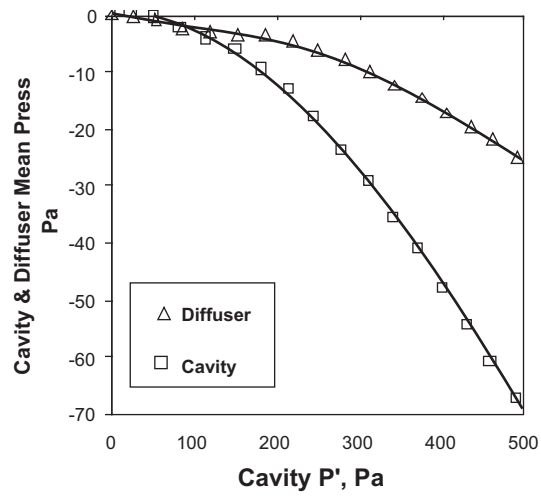


Figure 49: Diffuser and actuator cavity mean pressures due to enhanced cavity pressure fluctuations level causing enhanced jet deflection [98].

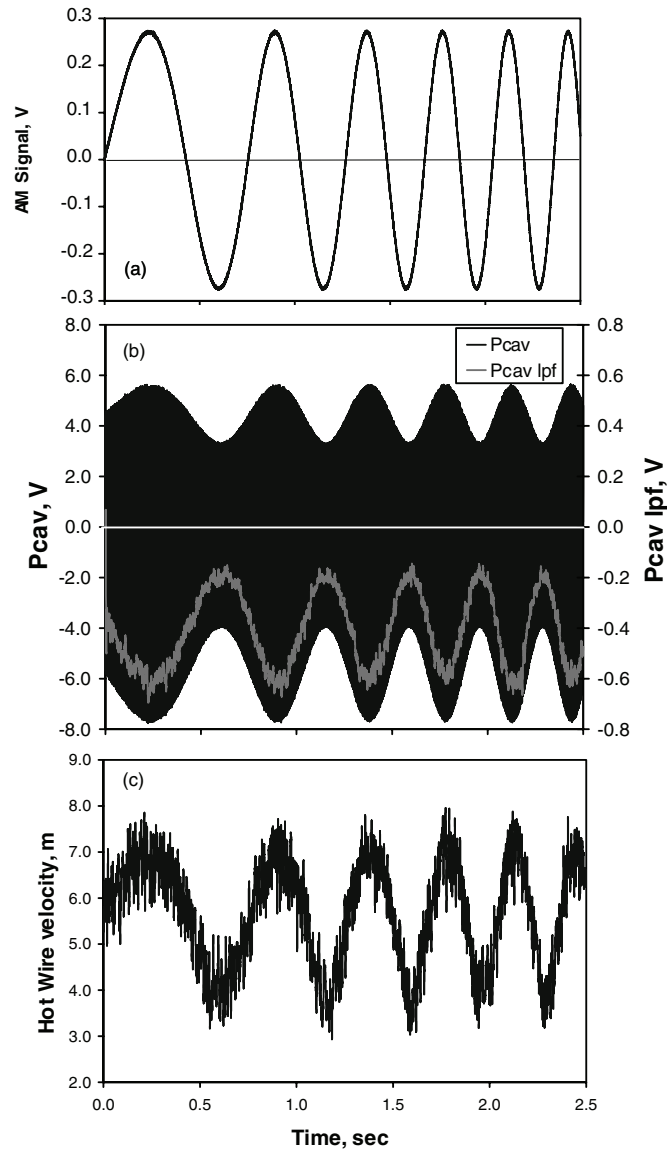


Figure 50: Jet deflection actuator inputs and outputs. (a) Amplitude modulating signal provided to the signal generator (2.5 out of 90 sec). (b) Actuator's cavity pressure showing the lack of symmetry and the LPF signal, proportional to the jet deflection angle. (c) Hot wire measured velocity signal at  $x/D = 1$  and opposite active actuator, showing the jet flow response, indicative of the jet deflection angle [98].

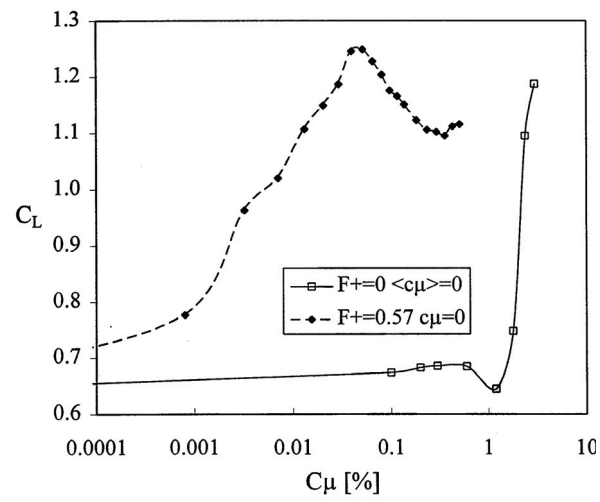


Figure 51: Comparison of oscillatory and steady blowing for post-stall lift-recovery of a NACA 0015 at,  $R_c = 300,000$  [7].